UNIVERSITAT
POLITÈCNICA
DE VALÈNCIA

DEPARTAMENTO
DE INGENIERÍA
HIDRÁULICA
Y MEDIO AMBIENTE

PhD Program in Water and Environmental Engineering

Numerical analysis of air-water flows in hydraulic structures using computational fluid dynamics (CFD)

PhD Thesis

September 15th 2017

Author

Director

Arnau Bayón i Barrachina

Petra Amparo López Jiménez

És més fàcil moure rius i muntanyes
que canviar el caràcter d'una persona.
[Proverbi xinès]

Es más fácil mover ríos y montañas
que cambiar el carácter de una persona.
[Proverbio chino]

It is easier to move rivers and mountains
than to change a person's character.
[Chinese proverb]

A la meua neboda Ona,

a qui esperem prompte amb tota la il·lusió del món.

I a la seua mare Gal·la,

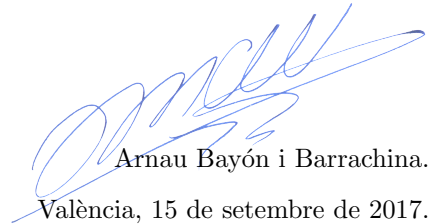que m'ha donat l'alegria més gran de la meua vida.

Agraïments

Vull agrair a totes les persones que han fet possible aquest treball, començant per la meua família: als meus pares, Toni i Maria, pel seu suport incondicional en tots els aspectes de la meua vida i per haver-me educat així (de bé o de malament) i al meu germà Bernat, a qui trobe a faltar cada dia des que se'n va anar (a treballar a l'estranger). També vull agrair als meus oncles, cosins i iaios a banda i banda de l'Ebre. Tindre una família així és un privilegi a l'abast de pocs. En particular, li vull agrair al meu Iaio Antonio la motivació constant que m'ha proporcionat durant aquests anys per a que acabara la tesi, amb el seu recurrent: "A ver si me voy a morir antes de que leas la Tesis...".

D'altra banda, si estic agraït amb les persones que han fet possible aquest treball, és de justícia estar-ho també amb totes les persones que l'han fet impossible. Òbviament, m'estic referint als rosegadors dels meus amics de Benimaclet, els quals han sigut una font constant de dispersió i procrastinació, corrompent-me dia a dia, cap de setmana a cap de setmana, durant aquests anys. I, per això, els estime tant. Una abraçada ben forta a tots: a Carlos, el primer doctor del grup, a Roberto, que serà el pròxim (pel que em deu una paella al Palmar) i al vikinguet (o vikingueta) que prompte ens durà al món, a Macià, per aguantar-me més que ningú i des de fa més anys que ningú, a Xevi, perquè estar al seu costat ens fa parèixer millors persones, a Tamarit, perquè tots ens fem por, a Marco, com és just que siga, a Fede, un gran entre els grans (i a Xip!), a Bert, el meu llaurador belga boig preferit, a Luca i al seu gos sociòpata (que jo sé que, en el fons, m'estima), a Pau, perquè sense ell no sabríem com fer un "cremaet" com Déu mana, i al Sarro, cabanyaler d'origen, benimacleter d'adopció, portuari fins la mèdula, pare de la meua neboda Ona i molt millor cunyat que nadador.

Una abraçada ben forta també als amics i companys per als qui les titulacions universitàries pareix que hagen sigut una mena de maledicció que et condemna a l'exili forçat. Catalunya, Bèlgica, Suïssa, Àustria i Anglaterra poden considerar-se afortunades de comptar amb gent com vosaltres, mal que ens pese als que ens hem quedat a la Terreta.

Per últim, moltes gràcies també als companys del Laboratori d'Hidràulica de la UPV, una vegada més, tant als que han fet aquesta tesi possible, els futurs doctors Bea, Juanfran i Dani (ànim, xavals, que això ja ho teniu fet!), com als que l'han feta impossible, Ximo i Carlos, amb els esmorzars eterns, els dubtes existencials i les batalletes interminables. Per últim, com no podria ser d'altra manera, no podria estar més agraït a Amparo, qui, més que una directora de tesi, ha sigut una mare, i a Paco, el meu director en l'ombra.

Arnau Bayón i Barrachina.

València, 15 de setembre de 2017.

Abstract [English]

The new legal regulations derived from climate change dictate that hydraulic structures must be designed to handle flood events associated with return periods up to 10,000 years. This obviously involves adapting the existing infrastructure to meet such requirements. In order to avoid risks in the restitution of the flow discharged to rivers, such as bank overflows or streambed erosion and scour processes, hydraulic design must be supported by reliable tools capable of reproducing the behavior of hydraulic structures.

In the work presented herein, a fully three-dimensional CFD model to reproduce the behavior of different types of air-water flow in hydraulic structures is presented. The flow is assumed to be turbulent, isotropic and incompressible. Several RANS turbulence models are tested and structured rectangular meshes are employed to discretize the analyzed domain. The presence of two fluids is modeled using different VOF approaches and simulations are run using the PIMPLE algorithm. The model is implemented using the open-source platform OpenFOAM and its performance is compared to the commercial code FLOW-3D. The analysis is conducted separately on two different parts of hydraulic structures, namely: the spillway and the stilling basin. Additionally, a case of practical application, where the model reproduces the flow of a real-life case, is also presented in order to prove the suitability of the model to actual design cases.

Mesh independence and model validation using experimental data are checked in the results of all the case studies. The sensitivity of the presented model to certain parameters is extensively discussed using different indicator variables. Among these parameters are turbulence closure, discretization scheme, surface tracking approach, CFD code or boundary conditions. Pros and contras of each of them are addressed. The analyzed turbulence models are the Standard $k-\varepsilon$, the Realizable $k-\varepsilon$, the RNG $k-\varepsilon$, and the SST $k-\omega$. The discretization schemes under study are: a first-order upwind method, the second-order limited Van Leer method, and a second-order limited central difference method. The VOF approaches analyzed are the Partial VOF, as implemented in OpenFOAM, and the TruVOF, as implemented in FLOW-3D.

In most cases, the Standard $k - \varepsilon$ model provides the most accurate estimations of water free surface profiles, although the rest of variables, with few exceptions, are better predicted by the RNG $k - \varepsilon$. The latter model generally requires slightly longer computation times. The SST $k - \omega$ reproduces correctly the phenomena under study, although it generally turned out to be less accurate than its $k - \varepsilon$ counterparts.

As regards the comparison among VOF approaches and codes, it is impossible to determine which one performs best. E.g. OpenFOAM, using the Partial VOF, managed to reproduce the internal hydraulic jump structure and all derived variables better than FLOW-3D, using the TruVOF, although the latter seems to capture better the momentum transfer and so all derived variables. In the case of flow in stepped spillways, OpenFOAM captures better the velocity profiles, although FLOW-3D is more accurate when estimating the water free surface profile. It is worth remarking that not even their response to certain model parameters is comparable. E.g. FLOW-3D is significantly less sensitive to mesh refinement than OpenFOAM.

Given the result accuracy achieved in all cases, the proposed model is fully applicable to more complex design cases, where stilling basins, stepped spillways and hydraulic structures in general must be investigated.

Abstract [Catalan]

Les noves disposicions legals derivades del canvi climàtic dictaminen que cal que les estructures hidràuliques siguen capaces de funcionar correctament amb esdeveniments d'inundació associats a períodes de retorn de fins a 10,000 anys. Això, òbviament, implica adaptar la infraestrctura existent per satisfer aquests requeriments. A fi d'evitar riscs en la restitució dels cabals vessats al riu, com desbordaments o processos erosius i de socavació, el disseny hidràulic ha de recolzar-se en ferramentes fiables capaces de reproduir el comportament de les estructures hidràuliques.

En aquest treball, es prsenta un model numèric CFD completament tridimensional per a reproduir el comportament de diferents tipus de flux aire-aigua en estructures hidràuliques. S'assumeix que el flux és turbulent, isotròpic i incompressible. Diferents models de turbulència RANS són contrastats i s'empren malles estructurades rectangulars per discretitzar el domini analitzat. La presència de dos fluids és modelada utilitzant diferents enfocaments VOF i les simulacions són executades emprant l'algorisme PIMPLE. El model és implementat mitjançant la plataforma de codi obert OpenFOAM i la seua resposta és comparada amb la del codi comercial FLOW-3D. L'anàlisi es du a terme sobre les diferents parts d'una estructura hidràulica, a saber, sobreeixidors esgraonats i vas esmorteïdor, de forma separada. A més, un cas d'aplicació pràctica, on el model reprodueix el flux a una estructura real, és presentat també a fi de provar l'adequació del model a casos de disseny aplicat.

Es comproven la independència de la malla i la validació amb dades experimentals dels resultats de tots els casos d'estudi. La sensibilitat del model presentat a certs paràmetres és analitzada de forma exhaustiva emprant diferents variables indicadores. Els pros i contres de cadascun d'aquests són plantejats. Els models de turbulència analitzats són l'Standard $k - \varepsilon$, el Realizable $k - \varepsilon$, el RNG $k - \varepsilon$ i l'SST $k - \omega$. Els esquemes de discretització estudiats són: un mètode de primer ordre upwind, un de Van Leer de segon ordre i un esquema de segon ordre limitat de diferències centrades. Els enfocaments VOF analitzats són el Partial VOF, implementat en OpenFOAM, i el TruVOF, implementat en FLOW-3D.

En la majoria de casos, el model Standard $k-\varepsilon$ aporta les estimacions més precises de perfils de làmina lliure d'aigua, tot i que la resta de variables, amb alguna excepció, són millor predites pel RNG $k-\varepsilon$. Aquest model generalment requereix majors temps de càlcul. El $k-\omega$ reprodueix correctament els fenòmens sota estudi, tot i que la seua precisió és generalment més baixa que la dels models $k-\varepsilon$.

Pel que fa la comparació entre enfocaments VOF i codis, és impossible determinar quin és el millor. Per exemple, OpenFOAM, emprant el Partial VOF, aconsegueix reproduir l'estructura interna del ressalt hidràulic i totes les variables derivades millor que FLOW-3D, emprant el TruVOF, tot i que aquest últim pareix capturar millor la transferència de quantitat de moviment i, per tant, totes les variables derivades. En el cas del flux en sobreeixidors esgraonats, OpenFOAM captura millor els perfils de velocitat, tot i que FLOW-3D és més precís en estimar els perfils de làmina lliure d'aigua. Cal deixar palès que ni tan sols la seua resposta a certs paràmetres del model és comparable. Per exemple, FLOW-3D és significativament menys sensible al refinament de malla que OpenFOAM.

En base a la precisió dels resultats obtinguts en tots els casos, el model proposat és completament aplicable a casos de disseny més complexos, on vassos esmorteïdors, sobreeixidors esgraonats i estructures hidràuliques en general han de ser investigades.

Abstract [Spanish]

Las nuevas disposiciones legales derivadas del cambio climático dictaminan que las estructuras hidráulicas sean capaces de funcionar correctamente con eventos de inundación asociados a periodos de retorno de hasta 10,000 años. Esto, obviamente, implica adaptar la infraestructura existente para satisfacer dichos requerimientos. A fin de evitar riesgos en la restitución de los caudales vertidos al río, como desbordamientos o procesos erosivos y de socavación, el diseño hidráulico ha de sustentarse en herramientas fiables capaces de reproducir el comportamiento de las estructuras hidráulicas.

En este trabajo, se presenta un modelo numérico CFD completamente tridimensional para reproducir el comportamiento de diferentes tipos de flujo aire-agua en estructuras hidráulicas. Se asume que el flujo es turbulento, isotrópico e incompresible. Diversos modelos de turbulencia RANS son contrastados y se emplean mallas estructuradas rectanuglares para discretizar el dominio analizado. La presencia de dos fluidos es modelada utilizando diferentes enfoques VOF y las simulaciones son ejecutadas empleando el algoritmo PIMPLE. El modelo es implementado mediante la plataforma de código abierto OpenFOAM y su respuesta es comparada con la del modelo comercial FLOW-3D. El análisis se lleva a cabo sobre dos partes diferentes de una estructura hidráulica, a saber, el aliviadero y el cuenco amortiguador, de forma separada. Además, un caso de aplicación práctica, donde el modelo reproduce el flujo en una estructura real, es presentado también a fin de probar la adecuación del modelo a casos de diseño aplicado.

Se comprueban la independencia de la malla y la validación con datos experimentales de los resultados de todos los casos de estudio. La sensibilidad del modelo presentado a ciertos parámetros es analizada de forma exhaustiva empleando diferentes variables indicadoras. Los pros y contras de cada uno de éstos son planteados. Los modelos de turbulencia analizados son el Standard $k - \varepsilon$, el Realizable $k - \varepsilon$, el RNG $k - \varepsilon$ y el SST $k - \omega$. Los esquemas de discretización estudiados son: un método de primer orden upwind, uno de Van Leer de segundo orden y un esquema de segundo orden limitado de diferencias centradas. Los en-

foques VOF analizados son el Partial VOF, implementado en OpenFOAM, y el TruVOF, implementado en FLOW-3D.

En la mayoría de casos, el modelo $k - \varepsilon$ aporta las estimaciones más precisas de perfiles de lámina libre de agua, pese a que el resto de variables, con alguna excepción, son mejor predichas por el RNG $k-\varepsilon$. Este modelo generalmente requiere mayores tiempos de cálculo. El $k-\omega$ reproduce correctamente los fenómenos bajo estudio, pese a que su precisión es generalmente más baja que la de los modelos $k - \varepsilon$.

En lo que respecta a la comparación entre enfoques VOF y códigos, es imposible determinar cuál es el mejor. Por ejemplo, OpenFOAM, empleando el Partial VOF, logra reproducir la estructura interna del resalto hidráulico y todas las variables derivadas mejor que FLOW-3D, empleando el TruVOF, a pesar de que este último parece capturar mejor la transferencia de cantidad de movimiento y, por tanto, todas las variables derivadas. En el caso del flujo en aliviaderos escalonados, OpenFOAM captura mejor los perfiles de velocidad, pese a que FLOW-3D es más preciso en la estimación de los perfiles de lámina libre de agua. Conviene recalcar que ni tan sólo su respuesta a ciertos parámetros del modelo es comparable. Por ejemplo, FLOW-3D es significativamente menos sensible al refinado de malla que OpenFOAM.

A la luz de la precisión de los resultados obtenidos en todos los casos, el modelo propuesto es completamente aplicable a casos de diseño más complejos, donde cuencos amortiguadores, aliviaderos escalonados y estructuras hidráulicas en general han de ser investigadas.

Contents

List of symbols

Acronyms

AAN	artificial neural network
ACF	auto correlation function
ADR	advection-diffusion-reaction
BSL	baseline
CFD	computational fluid dynamics
DNS	direct numerical simulation
FFT	fast Fourier transform
FVM	finite volume method
GCI	grid convergence index
LES	large eddy simulation
PSD	power spectrum density
RANS	Reynolds-averaged Navier-Stokes
RCC	roller compacted concrete
RNG	re-normalization group
SPH	smoothed particle hydrodynamics
SST	shear stress transport
TKE	turbulent kinetic energy
VOF	volume of fluid
WES	Waterways Experiment Station

Roman symbols (upper case)

C_μ	model parameter
$C_{1\varepsilon}$	model parameter
$C_{2\varepsilon}$	model parameter
$C_{3\varepsilon}$	model parameter
E_i	error in variable-i results
H	hydraulic head
ΔH	energy drop
L_j	length of hydraulic jump
L_r	length of roller
L	distance from the spillway crest in pseudo-bottom
P_b	effect of buoyancy
P_k	production of turbulent kinetic energy
R^2	coefficient of determination
$\overline{S}_{ij}$	strain-rate tensor
S_k	modulus of mean rate-of-strain tensor (k)
S_ε	modulus of mean rate-of-strain tensor (ε)
Q	flow rate
U	normalized velocity
X	normalized longitudinal coordinate
Y	ratio of sequent depths
Y_M	effect of dilatation
Z	normalized vertical coordinate

Roman symbols (lower case)

c	speed of sound in the medium
e_a	approximate relative error
f_b	body forces
f	frequency
g	acceleration of gravity
h	water depth
k	turbulent kinetic energy (TKE)
p'	model apparent order
p	pressure
q	specific flow rate
t	time
u_τ	shear velocity
u_c	compression velocity
u^+	dimensionless velocity
u	freestream velocity
w	channel width
x_0	position of hydraulic jump toe
x_i	Cartesian reference system component
x_j	Cartesian reference system component
x_k	Cartesian reference system component
x_J	position of hydraulic jump end
x_r	position of roller end
Δx	horizontal mesh element size
y^+	dimensionless wall distance
y	distance perpendicular to wall
Δy	vertical mesh element size

Greek symbols (upper case)

Γ dimensionless free-surface profile

Greek symbols (lower case)

α	water fraction in mesh element
δ	boundary layer thickness
ε	dissipation rate of turbulent kinetic energy
γ	TKE decay factor
μ_t	turbulent eddy dynamic viscosity
μ	dynamic viscosity
ν_t	turbulent eddy kinematic viscosity
ν	kinematic viscosity
ω	specific dissipation rate of turbulent kinetic energy
$\overline{\tau}^R$	Reynolds stress tensor
$\overline{\tau}$	molecular deviatoric stress tensor
ρ	fluid density
σ_k , σ_ε	model parameters
σ	TKE threshold
ξ_i	generic flow property of fluid i
η_0, β	model parameter
η	hydraulic jump efficiency

Dimensionless Numbers of Fluid Mechanics

Cr	Courant number
Fr	Froude number
Ma	Mach number
Re	Reynolds number
St	Strouhal number

Sub-indices and super-indices

$\square_1$	subindex relative to supercritical flow
$\square_2$	subindex relative to subcritical flow
$\square_{exp}$	relative to experimental results
$\square_t$	relative to turbulence
$\square_s$	relative to flow recirculation
$\square_w$	relative to water
$\square_a$	relative to air
$\square_{min}$	relative to minimum value
$\square_{max}$	relative to maximum value
$\square_{OF}$	relative to OpenFOAM
$\square_{F3D}$	relative to FLOW-3D
$\square^*$	relative to classical hydraulic jump

List of Figures

List of Tables

Chapter 1

Introduction

Researchers have devoted decades to the study of the climate change and the great effect that it exerts on our daily life. In the field of Hydraulic Engineering, the new unpredictable precipitation patterns are making a good deal of the existing civil infrastructure obsolete. The new hydrological scenarios require adapting the current hydraulic structures to prevent flood episodes and eventual structural failures. To this end, technical legislation and recommendations are currently being modified, becoming more demanding in terms of structural safety and maximum discharge rates. In Spain, e.g., more than 80% of dams where built before 1990, following the criteria established by a law dating from 1967, which only considers a flood event associated with a single return period of 500 years. The new regulations dictate that hydraulic structures must be designed to handle flood events associated with return periods up to 10,000 years, according to the dam type. This new framework will obviously require adapting the existing infrastructure to meet such requirements.

Along with structural safety, the restitution of discharged volumes to the river streambed is the most challenging issue that dam designers have to deal with. Flows containing excessive kinetic energy can lead to dam scour and streambed erosion, so energy dissipation is a matter of paramount importance in hydraulic structure design. As a matter of fact, from an engineering standpoint, energy dissipation is likely the most delicate, complex and costly aspect when adapting dams to new safety requirements.

This concern becomes of outmost importance in semi-arid regions, where flood episodes occur periodically due to the abrupt variability of precipitation regimes. In the Eastern Coast of the Iberian Peninsula, the brutal floods of 1957 made the water level raise up to 5 meters in downtown València and are still part of the local social imaginary (see Fig. 1.1).
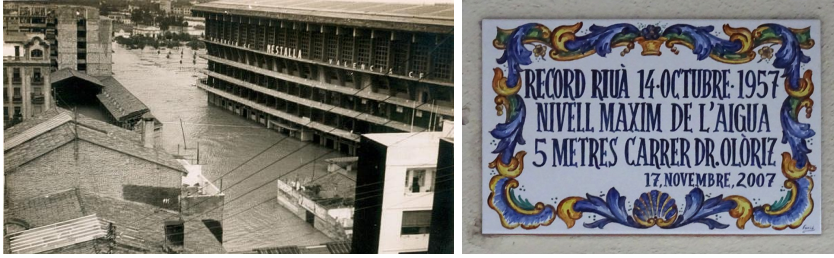
Figure 1.1: Left: Mestalla Football Stadium during the 1957 València flood. Right: example of memorial plaque to the 1957 València Flood (in Catalan: "Memorial to the October 14th 1957 Flood - Maximum water level: 5m in Dr. Olòriz Street").

Ensuring a correct hydraulic structure design, execution and monitoring in flood prevention has repeatedly been proved crucial throughout the last decades. Just to mention two examples, the Tous Dam break in 1982 razed to the ground several Valencian villages causing many casualties; while the recent 2017 Oroville Dam Crisis forced the evacuation of up to 200,000 people in California (see Fig. 1.2).

Figure 1.2: Left: rests of Tous Dam (València) after its failure in 1982. Right: state of the Oroville Dam (California) after the 2017 crisis.

Supercritical flows downstream of dam spillways may contain excessive energy. In order to dissipate it, forcing a hydraulic jump in a stilling basin is the most common strategy [Chow, 1959]. Hydraulic jumps occur in the transition from supercritical to subcritical flows (see Fig. 1.3). They are characterized by a highly chaotic behavior, where large turbulent fluctuations of velocity and pressure, air entrainment and energy dissipation occur. The most relevant parameter to describe hydraulic jumps is their approaching Froude number (Fr_1) which, in horizontal rectangular channels, is computed as follows:

$$Fr = \frac{u_1}{\sqrt{g \ h_1}} \tag{1.1}$$

where u_1 is supercritical mean velocity, y_1 is supercritical flow depth, and g is the acceleration of gravity. It is commonly accepted that approaching Froude numbers between 4.5 and 9.0 yield steady hydraulic jumps, whose behavior is more predictable and show low dependence on tailwater variations [Hager, 1992, Peterka, 1984]. Lower values of Fr_1 lead to undular or transition jumps, characterized by lower dissipation efficiencies and formation of waves of irregular period [Chanson and Montes, 1995, Chow, 1959, Fawer, 1937]. Higher values of Fr_1 produce choppy jumps, where flow detachment and bubble and spray formation are frequent. For these reasons, the U.S. Bureau of Reclamation [Peterka, 1984] recommends designing energy dissipation structures so that only steady hydraulic jumps occur.
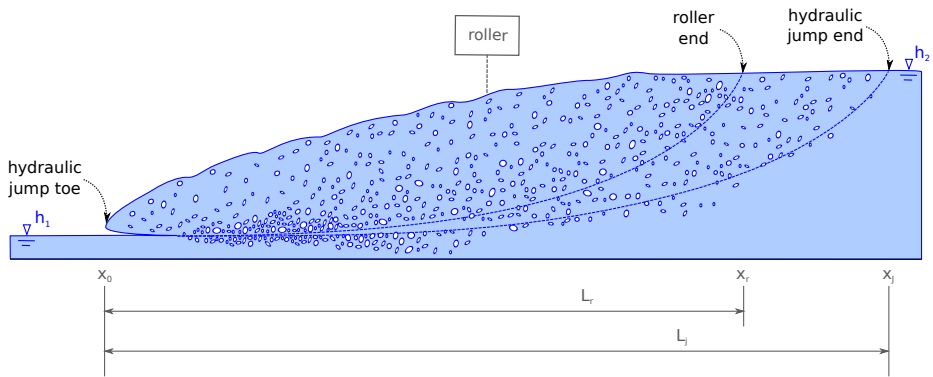
Figure 1.3: Flow in hydraulic jumps. Adapted from Bayon et al. [2016].

Soil erosion on streambeds occurs when the shear stress produced by a flow on a solid surface exceeds a certain threshold, which is characteristic of several variables, such as soil type, granulometry or temperature [Moody et al., 2005]. In hydraulic structures, the most severe effects generally occur in the vicinity of hydraulic jumps, and its magnitude is highly correlated with the Froude number [Oliveto et al., 2011]. For this reason, hydraulic jumps are forced to occur within stilling basins built with more resistent materials.

Despite the fact that hydraulic jumps are essentially chaotic, steady hydraulic jumps show a series of identifiable morphologic features, such as the roller: the region right downstream of the jump toe, where the flow detaches from the channel bottom, circulates backwards and most of the air entrainment occurs. The analysis and characterization of hydraulic jumps, as well as the state of the art of their study, is discussed in depth in Chap. 2.

In dams designed to discharge by overtopping, great attention is also paid to the energy dissipation throughout the spillway, before the flow reaches the stilling basin. Flat spillways are generally the most simple option in terms of design

and execution, but not necessarily the best choice from a hydraulic standpoint. As discussed below, an appropriate spillway design can help, not only to dissipate more energy, but also to force flow aeration throughout the chute, exerting a series of mostly favorable effects on the flow behavior.

During centuries, stepped spillways have been used in the design of hydraulic structures. Nevertheless, this responded to structural requirements rather than hydraulic design criteria. It was not until last century that, thanks to the spreading of more resistant materials, such as roller compacted concrete (RCC), stepped spillways became appealing for their hydraulic behavior [Chanson, 2002].

Obstacles on the chute, such as aerators or steps, which act as macro-roughness elements and make the turbulent boundary layer development faster, thus displacing upstream the section where the boundary layer encounters the water free surface and eddies possess enough energy to distort it, the so-called inception point of air entrainment [Meireles et al., 2014]. This phenomenon leads to a sudden increase of surface turbulent kinetic energy that, in turn, triggers a sudden and abrupt flow aeration process (see Fig. 1.4).
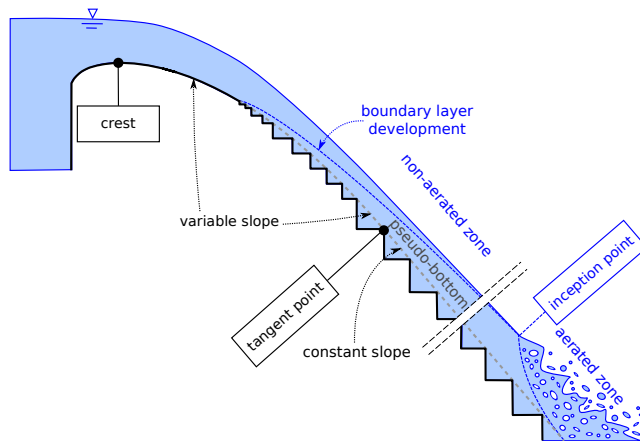
Figure 1.4: Flow in stepped spillways. Adapted from Bayon et al. [2015a].

This forced aeration process causes flow emulsification, which modifies its volume, depth, density and compressibility [Carvalho, 2002], thus affecting the momentum transfer. When it comes to energy dissipation, aeration exerts antagonistic effects on flows. On the one hand, flow aeration reduces the friction with the spillway solid contours [Wood, 1985, 1991, Chanson, 1994, 1996, 2002, Matos, 1999, Matos and Meireles, 2014], thus increasing the flow velocity and reducing the energy dissipation. On the other hand, water free surface breakage and air transfer through it causes an additional drag force that decreases the flow velocity [Valles-Moran

et al., 2015b]. Also, the emulsified flow stratification leads to eddy formation, and so to larger energy dissipation rates [Yih, 1980].

Another important phenomenon on which aeration plays a paramount role is cavitation. The high velocities occurred on very steep spillways can make the pressure drop to such an extent that water vaporizes at ambient temperature, forming small vapor bubbles. When these bubbles reach higher pressure regions, they collapse in such a virulent way that, in relatively short times, they can erode metal and concrete surfaces, so jeopardizing the integrity of hydraulic structures and machinery (see Fig. 1.5). In this regard, the presence of significant amounts of air in the flow can help to reduce cavitation damage by buffering its erosive effect [Chanson, 2002, 2014, Frizell et al., 2012, 2015, Pfister and Hager, 2011].

Figure 1.5: Effects of cavitation on hydraulic structures. Left: Nagarjuna Sagar Dam, India [Giridhar et al., 2014]. Right: Hoover Dam, USA [Warnock, 1945].

For all the reasons exposed above, the number of studies on the area of hydraulic structure design has multiplied during the last decades. Given the complexity of the flow processes occurring in such structures, analytical approaches with severe simplifying assumptions are not generally viable to achieve a thorough description of the flow and the use of numerical or experimental models becomes necessary. Further discussion on the topic can be found in Chap. 2.

Chapter 2

State of the art

The work presented herein deals with the numerical analysis of hydraulic structures. However, this analysis is conducted separately on spillways and stilling basins, as depicted in Fig. 2.1. Coherently, the review of the topic state of the art is also conducted separately.
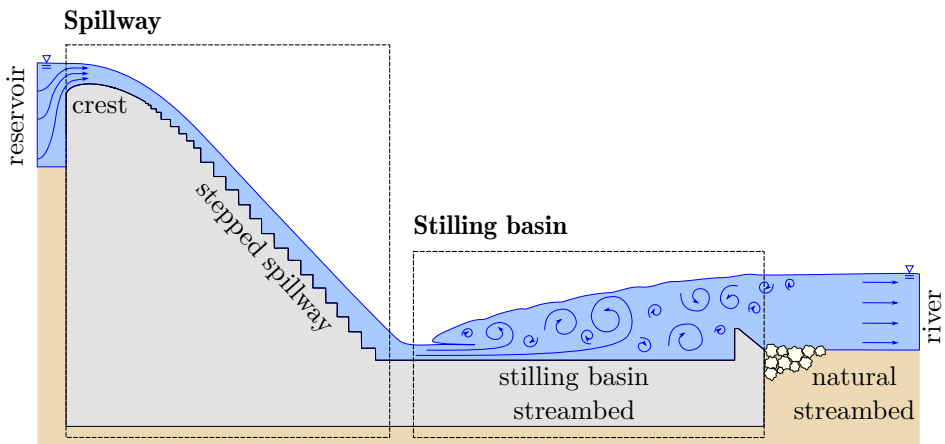
Figure 2.1: General scheme of dam spillway and stilling basin.

2.1 Stepped spillways

As discussed in Chap. 1, the energy dissipation processes occurring in stilling basins are strongly conditioned by what happens upstream, especially, when spillways contain macro-roughness elements, such as steps. Given the complexity of the flow processes characteristic of these type of structures, analytical approaches with simplifying assumptions are not viable to achieve a thorough description of the flow.

So far, most of the studies on stepped spillways in the literature are based on experimental modeling [Amador, 2005, Andre, 2004, Andre and Schleiss, 2004, Boes and Hager, 2003, Chamani and Rajaratnam, 1999, Chanson, 2001, 2002, Chanson et al., 2015, Gomes, 2006, Gonzalez, 2005, Matos, 1999, Matos and Meireles, 2014, Meireles, 2004, Ohtsu et al., 2004, Renna, 2004, Sanchez-Juny, 2001, Takahashi and Ohtsu, 2012]. These works focus mostly on skimming flows and provide a clear insight into many of the flow processes occurred within them, such as boundary layer development or air transfer through the air-water interface, and other related variables, such as air concentration distribution, pressure distribution, velocity profiles or distance to the inception point of air entrainment [Bayon et al., 2015a].

Especially during the last five years, the amount of studies on stepped spillway has increased significantly, using both approaches: experimental [Bung, 2013, Pfister and Hager, 2011, Hunt and Kadavy, 2010, 2014, Meireles et al., 2014, Munta and Otun, 2014, Pfister and Hager, 2011, Pfister, 2011, Wu et al., 2013] and numerical [Attarian et al., 2014, Bayon et al., 2015a, 2017, Bombardelli et al., 2011, Chinnarasri and Wongwises, 2006, Husain et al., 2014, Toro et al., 2016]. It is also important to remark that some studies are focusing on other solutions, such as pooled stepped spillways [Felder and Chanson, 2013] or gabion stepped spillways [Zhang and Chanson, 2016c], although most of the literature is still devoted to structures of flat steps.

Despite studies using numerical models to describe the flow in stepped spillways are overwhelmingly outnumbered by experimental approaches, the number of mathematical models in the field is also growing. Most of these works approach the problem using Eulerian Computational Fluid Dynamics (CFD) to achieve a full description of the flow behavior [Arantes, 2007, Bayon et al., 2015a, 2017, Bombardelli et al., 2011, Carvalho and Amador, 2009, Chen et al., 2002, Cheng et al., 2004b,a, Tabbara et al., 2005, Toro et al., 2016]. However, different Lagrangian techniques are also used, such as Smoothed Particle Hydrodynamics – SPH [Husain et al., 2014] or even non-deterministic models based on artificial neural networks – ANN [Roushangar et al., 2014].

The number of works dealing with the non-aerated part of the flow is relatively scarce [Amador, 2005, Amador et al., 2006, Bayon et al., 2015a, 2017, Bombardelli

et al., 2011, Carvalho and Amador, 2009, Hunt and Kadavy, 2010, Meireles and Matos, 2009, Toro et al., 2016, Zhang and Chanson, 2016a,b]. This fact is, to a certain extent, justified, as on most prototype applications, self-aeration would occur in a considerable portion of the chute, for the design discharge. Nevertheless, in some real-life cases, especially in small structures at large discharges, the non-aerated flow can dominate most of the flow [Bombardelli et al., 2011, Meireles et al., 2014]. Also, the non-aerated portion of the flow is where cavitation problems are most likely to occur, for high discharges [Chanson, 2014, Frizell et al., 2015]. In addition, an accurate description of the non-aerated region is crucial to understand what happens downstream of the inception point.

Recent numerical works focused on the non-aerated region have provided good predictions of time-averaged velocities, water depths, development of the boundary layer and turbulence statistics [Bayon et al., 2015a, 2017, Bombardelli et al., 2011, Meireles, 2011b, Toro et al., 2016]. However, relatively little emphasis has been put into the influence of the turbulence closure and the discretization schemes on the numerical results. There is the natural question as to whether these variables exert significant differences in the main flow properties in such region.

A more thorough analysis on the state of the art of stepped spillway models using numerical methods can be found in Bayon et al. [2017], also available in Appx. C.

2.2   Stilling basins

Since first known studies on hydraulic jumps [Belanger, 1841, Bidone, 1819], a wealth of studies on this topic has been conducted. The first known study reporting turbulence quantities in hydraulic jumps was conducted by Rouse et al. [1959] and was later completed by Rajaratnam [1965] and Long et al. [1991]. On the flow structure description, Resch and Leutheusser [1972] also reported turbulence quantities and pointed out dependence on the inlet flow conditions. Gualtieri and Chanson [2007, 2010] further analyzed the inlet sensitivity conditions and Liu et al. [2004] provided a complete turbulence description for low Froude numbers. Additionally, Chanson and Brattberg [2000], Murzyn et al. [2005], Chanson and Gualtieri [2008], and Zhang et al. [2014] focused on the flow aeration properties. Recently, Chanson [2007], Wang et al. [2014a], Zhang et al. [2013], Chachereau and Chanson [2011], Murzyn et al. [2007], and Chanson [2007] reported turbulent integral length and time scales, which might contribute to a better validation and understanding of numerical models.

So far, the experimental works overwhelmingly outnumber the studies using a numerical approach. Most of the studies performed up until today focused on the analysis of easily-measurable external macroscopic variables using an experimental approach. This can partially be explained by the difficulty of measuring certain

variables using non-intrusive acoustic and optical methods in highly aerated flows [Ma et al., 2011]. However, since the 1970s, coinciding with the emergence of computational fluid dynamics (CFD), more and more studies on the hydraulic jump are conducted by means of numerical methods. In this regard, computational techniques brought a brand new approach to water engineering modeling. This implied a whole paradigm shift in the field.

Computational Fluid Dynamics (CFD) can supplement and assist in the design of energy dissipation structures [Bombardelli, 2012, Chanson and Carvalho, 2015, Meireles et al., 2014]. Nevertheless, mathematical models still present accuracy issues when modeling some hydraulic phenomena [Blocken and Gualtieri, 2012, Murzyn and Chanson, 2009b], to which the lack of validation is usually pointed out [Chanson, 2013, Chanson and Lubin, 2010]. Murzyn and Chanson [2009b] state that mathematical models still have problems to reproduce the physics of certain hydraulic phenomena, although they can contribute to their better comprehension. As Romagnoli et al. [2009] remark, an entire comprehension of the hydraulic jump internal flow features and turbulence structures has not been achieved so far. For Murzyn and Chanson [2009b], the main features of hydraulic jumps that have not been fully understood are the following: fluid mixing, bubble break-up and coalescence, free surface turbulent interactions and wave formation and breaking processes. Improving numerical models to reproduce the behavior of hydraulic structures is therefore an ongoing task and constitutes a very active research topic.

Several authors, such as Carvalho et al. [2008] and Ma et al. [2011], among others, recently managed to reproduce the hydraulic jump structure using different CFD approaches. Caisley et al. [1999] accurately modeled a hydraulic jump using FLOW-3D. Bayon and Lopez-Jimenez [2015], Bayon et al. [2016], Romagnoli et al. [2009], and Witt et al. [2015] used OpenFOAM to model hydraulic jumps also with success.

Numerical approaches different from CFD have also been used to model hydraulic jumps, such as Smoothed Particle Hydrodynamics [De Padova et al., 2013] or Artificial Neural Networks [Omid et al., 2005]. Other authors preferred one-dimensional and two-dimensional models to study the hydraulic behavior of rivers or stilling basins and erosion-sedimentation phenomena [Hartanto et al., 2011, Dewals et al., 2004, Juez et al., 2013]. Nevertheless, flows occurring in hydraulic structures tend to be highly three-dimensional [Ahmed and Rajaratnam, 1997, Chanson and Montes, 1995]. For this reason, the use of three-dimensional models, such as that proposed in this paper, becomes a must in most cases.

A more in-depth discussion on the state of the art of the modeling of hydraulic jumps using numerical methods can be found in Bayon and Lopez-Jimenez [2015] and Bayon et al. [2016], also available in Appx. A and B.

2.3   Practical application case

The attempts to reproduce the behavior of all kinds of hydraulic structures are numerous, although their typology, geometry and flow characteristics are extremely variable, so analytical approaches are rarely feasible. One- and two-dimensional models of spillways, stilling basins and channels have been the traditional approach to this problem [Valles-Moran et al., 2011]. Nevertheless, these techniques become obsolete when attempting to reproduce very complex geometries, where flow patterns are highly tridimensional. For this reason, and coinciding with the increase of computational power, the number of tridimensional numerical models applied to the analysis of hydraulic structure behavior has gained use during the last years [Caisley et al., 1999, Meireles et al., 2012].

A close observation of the literature shows that one of the phenomena most difficult to address is the hydraulic jump [Romagnoli et al., 2009, Carvalho, 2002]. The literature treating this feature is vast and so is the number of approaches used: CFD [Witt et al., 2015], smooth particle hydrodynamics [De Padova et al., 2013], experimental [Chanson, 2013] or a combination of several of them [Bombardelli et al., 2011].

Nevertheless, most of the studies are rather theoretical and focus on the so-called classical hydraulic jump, i.e. the hydraulic jump occurring in a flat rectangular prismatic channel of smooth walls [Hager, 1992]. The number of real life cases of structures involving hydraulic jumps is small compared to the total amount of publications in this field. Besides, many of them use an experimental approach, as numerical models still fail to reproduce certain aspects of this phenomenon, as discussed above in this chapter. However, numerical approaches provide a clean non-intrusive way to measure some features of hydraulic jumps [Murzyn and Chanson, 2009a].

A more in-depth discussion on the state of the art of the modeling of hydraulic structures using numerical methods can be found in Appx. A, B, C and D.

Chapter 3

Objective and justification

The importance of developing reliable methods to characterize the flow in hydraulic structures has been extensively discussed in Chap. 1. With this aim in mind, on the one hand, the work presented herein focuses on the analysis of the capabilites of CFD models to reproduce air-water flows in hydraulic structures. On the other hand, a fully three-dimensional CFD-based method to model hydraulic structures is developed and reported. This involves discussing the different methods to track the water free surface in air-water flows, as well as using an appropriate meshing approach and a computationally cost-efective turbulence model, among others. To this end, a model is proposed and several case studies are conducted, where different variables of interest are computed and compared to analytical and experimental studies for validation purposes. The mesh convergence, as well as the sensitivity of the model to certain parameters, such as turbulence model, discretization scheme or boundary conditions, is assessed and the most recommendable choice in each case is discussed.

As discussed in Chap. 2, other CFD models have previously been developed also reproducing the hydraulic behavior of hydraulic structures using both commercial and open source codes, as discussed in Chap. 2. Nevertheless, to the best of the Author's knowledge, the use of an open source code to reproduce in such detail the behavior of entire hydraulic structures has not been reported so far.

It is important to point out the importance of the development of open source numerical models in Engineering as it allows a continuous community-based improvement of the code. In addition, open source software, where users can directly modify the code to fit their needs, allows a greater versatility compared to the stiffness of their commercial counterparts and avoid having to pay for costly software licenses.

Another specific goal of the work presented herein is to establish a systematic comparison among several model parameters, such as turbulence model or meshing method, whose choice may be a tedious and confusing task for CFD modelers. To this end, a sensitivity analysis to the most decisive parameters is performed which, to the best of the Author's knowledge, has not been conducted so far in this field.

Choosing the most suitable numerical code among the available software also requires a systematic comparison among the possible options. For this reason, this work pays close attention to the differences in performance between different CFD codes. In particular, the proposed model is systematically compared to one of the most widely used CFD codes in hydraulic engineering applications: the commercial software FLOW-3D. Differences in accuracy and sensitivity to certain model parameters between both codes is assessed as well.

As discussed below, going through a reliable validation process, the model presented herein is fully applicable to more complex design cases of stilling basins, stepped spillways or hydraulic structures in general. Indeed, a real-life application case is reported, where the proposed model was successfully applied to model a hydraulic structure containing a channel stretch, a weir and a stilling basin with macro-roughness elements for energy dissipation.

The content of this document is distributed as follows: the first three chapters provide a short introduction on the topic (Chap. 1), followed by a survey of the state of the art (Chap. 2) and a discussion on the work's goals (Chap. 3). The next three chapters deal with the material and methods used in this work (Chap. 4), a thorough analysis of the results (Chap. 5) and some final conclusions (Chap. 6). As this is a PhD thesis dissertation based on a collection of publications, more in-depth information on the content discussed in the main body is available in the publications, which appear as Appendices A, B, C and D.

Chapter 4

Materials and Methods

4.1 Numerical model

The following sections describe the overall characteristics of the proposed numerical model regarding its definition and implementation. Specific minor aspects may vary from one case study to another, as discussed more in depth in Appx. A, B, C and D.

4.1.1 Flow equations

The water level of open channel flows can be accurately estimated using shallow wave approaches, such as Saint-Venant [1871] or Boussinesq [1871]. 1D and 2D methods provide good estimates of this variable for many common civil engineering applications. However, these methods fail to model complex geometries or highly three-dimensional flows involving breaking surfaces, as they assign a single water depth value to each point on the streambed. In cases where a more detailed description of the flow characteristics is necessary, resolving the Navier-Stokes Equations becomes a must.

Eq. 4.1 and 4.2 are the Navier-Stokes Equations for mass and momentum conservation in their incompressible form. In their general form, these equations, derived from the Mass Conservation Principle and Newton's Laws of Motion, govern the motion of fluids. Unfortunately, their complete analytical resolution has not been reached so far. In fact, it constitutes one of the seven Millenium Problems whose resolution would be rewarded with US$1,000,000 by the Clay Mathematics Institute. In the meanwhile, numerical methods are necessary to approximate a solution to problems involving viscous fluid motion.

$$\nabla \vec{u} = 0 \tag{4.1}$$

$$\frac{\partial \vec{u}}{\partial t} + \vec{u} \cdot \nabla \vec{u} = -\frac{1}{\rho}\nabla p + \upsilon \nabla^2 \vec{u} + \vec{f_b} \tag{4.2}$$

Where u is velocity, p, pressure, t, time, ρ, density, υ, kinematic viscosity, and f_b, body forces (gravity and surface tension). In all the cases discussed herein, the flow is assumed to be incompressible in order to save computational resources and so density varying terms have been neglected. This assumption can be done in most hydraulic engineering applications given the low compressibilty of liquid water. As regards the air phase, incompressibility can be assumed when Mach numbers (ratio of the flow velocity, u, to the speed of sound, c) remain below the widely accepted threshold of $Ma < 0.3$ [Young et al., 2010], as is the case.

$$Ma = \frac{u}{c} \tag{4.3}$$

A wealth of algorithms has been developed to approximate numerically the Navier-Stokes Equations during the last decades. Nevertheless, none of them constitutes a perfect solution as their efficiency in performance is highly case specific. Indeed, this is a topic extensively discussed in the literature [Barton, 1998, Jang et al., 1986]. It is important to remark that algorithm performances are generally assessed in terms of computation requirements and stability as, eventually, all algorithms should converge to a similar solution. The most widely used algorithm to solve the linear pressure-velocity coupling in stationary simulations in CFD is the SIMPLE algorithm [Patankar and Spalding, 1972]. Several improvements to its original implementation, such as SIMPLER or SIMPLEC, have been made since the model was developed. One of the most used variations is the PISO algorithm [Issa, 1985]. However, problems may arise when dealing with multiphase flows where phase changes are abrupt or the density differences are large (Brennan, 2001). In order to overcome this issue, an algorithm was developed combining the best features of SIMPLE and PISO; the so-called PIMPLE algorithm [Open-FOAM User Guide, 2011]. This algorithm merges the outer-correction tools of SIMPLE with the inner-corrector loop of PISO in order to achieve a more robust and generalizable pressure-velocity coupling [Rodrigues et al., 2011].

Hence, the PIMPLE algorithm is used in the proposed model as it constitutes a good compromise between computation requirements and stability. This algorithm is implemented in OpenFOAM, a freely available open source platform constituted by all sort of C++ applications and libraries to solve all kinds of continuum mechanics problems [Weller et al., 1998]. This code uses a tensorial approach and object-oriented programming techniques following the widely known Finite Vol-

ume Method (FVM), first used by McDonald [1971]. An in-depth explanation of the algortihm implementation can be found in the PhD Thesis of Jasak [1996], Ubbink [1997] and Rusche [2002].

4.1.2   Geometry and mesh

In order to discretize the geometrical domain occupied by the air-water flow, two big categories of approaches are normally used, namely: unstructured and structured meshing. As always, none can be considered the best method as their performance is highly case specific.

Unstructured meshes are generally better suited for a selective refinement, so preventing the over-refinement of regions where no large gradients are expected [Kim and Boysan, 1999]. Besides, this kind of meshes fit better into complex geometries, show less closure issues and their arbitrary topology makes automatizing the meshing process easier [Biswas and Strawn, 1998].

Some authors state that mesh non-orthogonality does not affect results as long as the skewness of its elements is kept low enough [Huang and Prosperetti, 1994]. Nevertheless, structured meshes tend to be more accurate than their unstructured counterparts caeteris paribus [Biswas and Strawn, 1998]. Besides, structured meshing algorithms are generally more straightforward to implement and faster to execute. According to Keyes et al. [2000], structured meshing algorithms present a more regular access to memory, which significantly reduces its latency. Also, as discussed in Sec. 4.1.3, in multiphase flows, topologically orthogonal meshes with their axis aligned with the fluid interface tend to show less numerical problems. For all these reasons, a static structured rectangular hexahedral mesh is considered the best choice for the cases discussed in this text.

In some cases, meshes can be slightly refined in the vicinity of solid boundaries for accurately resolving the flow features in boundary layers, where larger gradients occur. This may result in the formation of highly skewed elements, although this is not a real issue as long as orthogonality between the mesh axes and solid boundaries is ensured [Hirsch, 2007]. This additional refinement becomes a must when using low-Reynolds-number models, as discussed in Sec. C.3.4 and A.2.7.

The geometries analyzed in the present work show different degrees of complexity. In the hydraulic jump model, the analyzed geometry is rather simple: the domain consists of a prismatic rectangular channel (see Fig. 4.1). However, in the case of stepped spillways and the practical application case, flow domains are geometrically more complex and so are their meshing requirements (see Fig. 4.2). In these cases, a structured mesh of rectangular elements is also employed but, unlike the hydraulic jump case, in order to fit the mesh to the modeled geometry singularities, OpenFOAM employs snappyHexMesh to collapse the elements intersecting

Stepped spillway
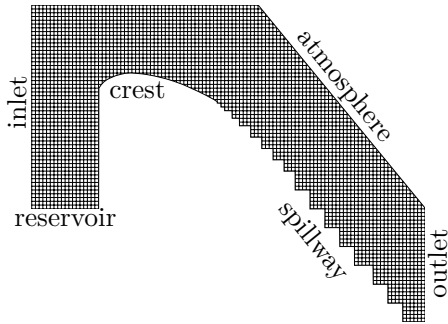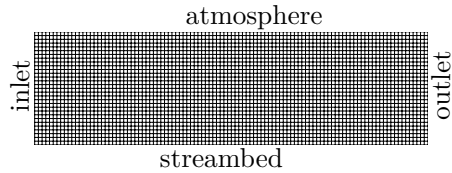
Figure 4.1: Schematic of the mesh used in the stepped spillway and stilling basin models.

solid boundaries, whose use in similar applications has yielded good results [Bayon et al., 2017, Sweeney, 2014]. In the case of FLOW-3D, a different method to adapt to complex solid surfaces is used: the porosity-based FAVOR method, which also yields accurate results [Carvalho et al., 2008, Bombardelli et al., 2011]. All details regarding the geometry of the practical application case are reported in Bayon et al. [2015b] and Appx. D.

Practical application case
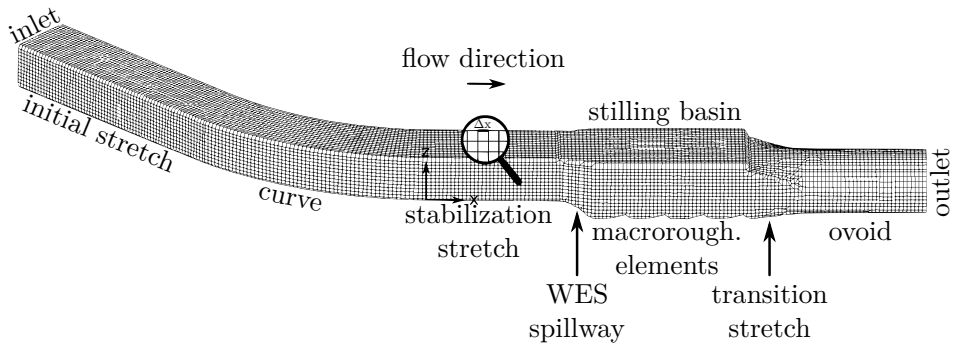
Figure 4.2: Schematic of the mesh used in the practical application case model.

The optimum mesh element size cannot be determined a priori as it is strongly case-specific, so mesh convergence analyses must be conducted on simulations of a single case run with different mesh sizes. The specific characteristics of the tested meshes are discussed in Sec. A.2.1, B.2.1, C.4.1 and D.2.1. In all cases, a mesh

convergence analysis is conducted to check that the results are mesh-independent, as reported in Sec. 5.1.

4.1.3 Free surface modeling

The coexistence and interaction of several fluids and the way that the interface among them is defined is of paramount importance in numerical modeling of multiphase flows. Complex algorithms must be developed to model this phenomenon, whose stability and accuracy have a strong influence on the model final results [Hyman, 1984]. Surface tracking methods fall into two families of approaches, namely: the surface methods and the volume methods. On the one hand, surface methods explicitly define the free interface either using a Lagrangian approach, i.e. tracking a set of surface marker particles [Daly, 1969], or using an Eulerian approach, i.e. defining functions that determine the free surface position [Osher and Sethian, 1988]. These methods present topology issues when dealing with highly deformed flows and breaking surfaces. For this reason, they are not considered appropriate to model hydraulic structures of complex geometry.

On the other hand, volume methods adapt better to this kind of phenomena, but do not define a neat flow interface explicitly. Instead, a surface tracking method has to be implemented in the model. Some models use an Eulerian-Lagrangian approach (particles on fluid methods) combining an Eulerian flow resolution with particle tracking [Harlow and Welch, 1965]. However, in three-dimensional models, the large number of necessary particles makes the computational cost of this approach unaffordable. For this reason, an entirely Eulerian approach is used in the present model. This kind of methods proved to be more computationally efficient as they only have to deal with a single variable value per mesh element [Ubbink, 1997]. This variable is an indicator property (α) expressing the proportion of one fluid or another that every mesh element contains. Its distribution throughout the domain is modeled by approximating an additional convection transport equation (Eq. 4.4). This implies considering both fluids, A and B, as a single multiphase fluid, whose properties are treated as weighted averages according to the fraction occupied by one fluid or another in each mesh element (see Eq. 4.5). This results in a set of α values between 0 and 1 distributed throughout the entire modeled domain, but no clear water-air interface is defined.

$$\frac{\partial \alpha}{\partial t} + \nabla \cdot (\vec{u}\alpha) = 0 \tag{4.4}$$

$$\xi = \xi_a \alpha + \xi_b(1 - \alpha) \tag{4.5}$$

Where α is fluid fraction, u, velocity, t, time, and ξ represents a flow generic property. As regards the method used to clean up the misty zones and so define a neat

interface between both fluids, a wealth of approaches has been developed during the last decades. The traditional line techniques, such as SLIC [Noh and Woodward, 1976], PLIC [Youngs, 1984] or FLAIR [Ashgriz and Poo, 1991], provided the first viable solutions to the surface definition issue in volume methods. However, they present problems of generalization when used on unstructured meshes. The donor-acceptor methods, such as the original implementation of the VOF [Hirt and Nichols, 1981], have been widely used in the past, but they are prone to show false interface deformation issues.

In the present model, an interface compression algorithm is implemented in order to overcome the aforementioned issues. This method adds an extra term in the left hand side of Eq. 4.4: $\nabla \cdot (\vec{u}_c \alpha [1 - \alpha])$, where $\vec{u}_c$ is a compression velocity with normal direction to the fluid interface. Multiplying $\vec{u}_c$ by $\alpha[1 - \alpha]$ ensures that it will only affect those regions where the flow fraction is close to 0.5 [Rusche, 2002]. The compression velocity term is computed according to a method based on the theory of two-phase flow [Berberovic et al., 2009]:

$$\vec{u}_c = |\vec{u}| \frac{\nabla \alpha}{|\nabla \alpha|} \tag{4.6}$$

4.1.4 Flow aeration

In air-water flows, aeration induces volume bulking, increases flow depth, adds compressibility to the flow and modifies its macroscopic density [Chanson, 2013, Falvey, 1980], thus affecting momentum distribution of the carrier phase. Flow aeration also bounds scour phenomena caused by cavitation [Bung and Schlenkhoff, 2010, Wood, 1991, Pfister, 2011] and shear stresses on the channel boundaries [Chanson, 1994]. The use of a stable and accurate method to treat this phenomenon is critical when dealing with potentially erosive flows, such as bores, breaking waves or hydraulic jumps. Unfortunately, no method per se can accurately reproduce phenomena with a characteristic length scales smaller than mesh elements, e.g. bubbles or droplets [Valero and Bung, 2015, Lobosco et al., 2011, Toge, 2012].

Subscale air-entrainment models can be implemented in order to overcome this issue [Valero and Garcia-Bartual, 2016, Ma et al., 2011]. In low-aerated flows, Eulerian-Lagrangian approaches are a good choice. These methods consist of the approximation of the Navier-Stokes Equations, while air bubbles are treated as flow-driven discrete particles. However, this approach becomes computationally unaffordable in highly aerated flows. In these cases, Eulerian-Eulerian methods arise as an efficient approach, despite they require finer meshes. An entirely Eulerian method has been used in the present study, allowing both fluids to mix in the same cell but locating the free surface where $\alpha = 0.5$. Using this approach,

no additional equation needs to be employed for bubble and droplet dynamics. However, as no additional aeration model is implemented, phenomena of characteristic scales below the mesh element size cannot be captured by the model. This implies that small bubbles or droplets are "filtered out" from the simulations. A detailed discussion on more advanced methods can be found in Balachandar and Eaton [2010].

4.1.5 Turbulence modeling

One of the key aspects of CFD models is the way turbulence is treated. Velocity and pressure fluctuations can be numerically resolved down to their lowest scales (Direct Numerical Simulation or DNS) as long as the mesh is accordingly fine [Pope, 2000, Hirsch, 2007]. However, this approach is still unaffordable in terms of computational cost for engineering applications. The use of DNS in multiphase flows has been reported in the literature [Borue et al., 1995, Nagosa, 1999, Prosperetti and Tryggvason, 2009], although in engineering applications turbulence is dealth with using coupled models.

Large Eddy Simulation (LES) methods offer accurate multiphase flow simulations at lower computational costs, being however still unaffordable for most engineering applications [Spalart, 2000]. Thus, the most widely used approach in engineering applications is the Reynolds Averaged Navier-Stokes (RANS). The models of this kind are based on averaging the flow equations yielding the Reynolds Averaged Navier-Stokes (RANS) equations. Mathematical closure to the Navier Stokes Equations is achieved by adding transport equations to reproduce the behavior of flow turbulence and then relate the turbulence scales to a turbulent viscosity (μ_t), which is introduced in the flow equations aiming to account for the so-called Reynolds stresses. The first complete models are the two equation models; they are able to provide a full description in turbulence in terms of length and time scales, thus they could reproduce a wide variety of flows [Pope, 2000]. An extended description of RANS equations and turbulence closures can be found in Pope [2000] and Wilcox et al. [1998].

Among the available models, the performance of some of the most used is here studied. The assessed models are the Standard $k - \varepsilon$ [Launder and Sharma, 1974], the RNG $k - \varepsilon$ [Yakhot et al., 1992], the Realizable $k - \varepsilon$ [Shih et al., 1995] and the SST $k - \omega$ [Menter, 1993]. Their effect on the model outcome is assessed in order to determine their adequacy to each case.

The Standard $k - \varepsilon$ model has been widely used in this kind of applications [Lopez and Garcia, 2001]. Its formulation is depicted in Eq. 4.7 and 4.8:

$$\frac{\partial}{\partial t}\left(\rho k\right) + \frac{\partial}{\partial x_i}\left(\rho k u_i\right) =$$

$$= \frac{\partial}{\partial x_j}\left[\left(\mu + \frac{\mu_t}{\sigma_k}\right)\frac{\partial k}{\partial x_j}\right] + P_k + P_b - \rho\varepsilon - Y_M + S_k \tag{4.7}$$

$$\frac{\partial}{\partial t}\left(\rho\varepsilon\right) + \frac{\partial}{\partial x_i}\left(\rho\varepsilon u_i\right) =$$

$$= \frac{\partial}{\partial x_j}\left[\left(\mu + \frac{\mu_t}{\sigma_\varepsilon}\right)\frac{\partial\varepsilon}{\partial x_j}\right] + C_{1\varepsilon}\frac{\varepsilon}{k}\left(P_k + C_{3\varepsilon}P_b\right) - C_{2\varepsilon}\rho\frac{\varepsilon^2}{k} + S_\varepsilon \tag{4.8}$$

Where k is turbulence kinetic energy, ε, dissipation rate of k, t, time, ρ, density, x_i, coordinate in the i axis, μ, dynamic viscosity, μ_t, turbulent dynamic viscosity, P_k, production of turbulent kinetic energy, P_b, buoyancy effect, Y_M, dilatation effect, and S_k and S_ε, modulus of mean rate-of-strain tensor. The rest of terms, $(C_\mu, C_{1\varepsilon}, C_{2\varepsilon}, C_{3\varepsilon}, \sigma_k,$ and $\sigma_\varepsilon)$ are model parameters that, in the Standard $k - \varepsilon$ model, are 0.09, 1.44, 1.92, -0.33, 1.0, and 1.3, respectively.

Several authors claim that $k - \varepsilon$ models are not suitable to model large adverse-pressure gradient flows [Menter, 1993, Wilcox et al., 1998]. In order to overcome this issue, $k - \omega$ models were first introduced by [Wilcox et al., 1998]. Their implementation is significantly different from that of $k - \varepsilon$, as the dissipation rate of turbulence kinetic energy (ε) is not modeled. Instead, a transport equation for its relative value ($\omega = \varepsilon/k$) is implemented. Among them, the SST $k - \omega$ [Menter, 1993] proved to perform better than the Standard and the BSL $k - \omega$.

The suitability of one model or another is highly case specific and differences from using one model or another are normally remarkable. Hence, in order to determine which model performs best at a reasonable computational cost, a sensitivity analysis is conducted. To do so, simulations are run using the RANS models discussed above caeteris paribus.

As regards the RNG $k - \varepsilon$ [Yakhot et al., 1992] model, its formulation mainly differs from that of the Standard $k - \varepsilon$ in the values of the aforementioned parameters, which are deduced from renormalization techniques. These changes seem to improve the model results to such an extent that, according to Bradshaw [1996], the RNG $k - \varepsilon$ is the most used model in hydraulic applications. Also other authors claim that this model provides better performance for swirling flows than the standard $k - \varepsilon$ model [Bombardelli et al., 2011, Bradshaw, 1996, Kim and Baik, 2004, Pope, 2000, Speziale and Thangam, 1992].

The transport of k and ε in the RNG $k - \varepsilon$ model is computed according to the following advection-diffusion-reaction (ADR) equations:

$$\frac{\partial}{\partial t}(\rho k) + \nabla \cdot (\rho k \vec{u}) = \nabla \cdot [(\mu + \frac{\mu_t}{\sigma_k})\nabla k] + P_k + \rho \varepsilon \tag{4.9}$$

$$\frac{\partial}{\partial t}(\rho \varepsilon) + \nabla \cdot (\rho \varepsilon \vec{u}) = \nabla \cdot [(\mu + \frac{\mu_t}{\sigma_\varepsilon})\nabla \varepsilon] + (C_{1\varepsilon} - M)\,\frac{\varepsilon}{k}\,P_k - C_{2\varepsilon}\rho\frac{\varepsilon^2}{k} \tag{4.10}$$

$$M = \eta(-\frac{\eta}{\eta_0} + 1)\,/\,(\beta\eta^3 + 1); \quad \eta = S\frac{k}{\varepsilon}; \quad S = (2\overline{S}_{ij}\overline{S}_{ij})^{\frac{1}{2}} \tag{4.11}$$

The formulation constants are, in this case, $\sigma_k = 0.7194$, $\sigma_\varepsilon = 0.7194$, $c_{1\varepsilon} = 1.42$, $c_{2\varepsilon} = 1.68$, $C_\mu = 0.0845$, $\eta_0 = 4.38$, and $\beta = 0.012$. The eddy viscosity is computed as:

$$\upsilon_t = \frac{\mu_t}{\rho} = C_\mu \frac{k^2}{\varepsilon} \tag{4.12}$$

4.1.6 Boundary conditions

The boundary conditions imposed to the analyzed model slightly differ from one case to another. This variations are due to differences in the inlet/outlet flow regime, as depicted in Fig. 4.3. Velocity in subcritical and supercritical inlets are both defined by a Dirichlet boundary condition given by their Froude numbers. Pressure is set to a null Von Neumann condition, thus developing a hydrostatic profile: $p = \rho g y$.

Supercritical otulets are essentially free outlets as a null Dirichlet condition is imposed to pressure (i.e. atmospheric pressure), thus letting the velocity profile to develop. However, as regards subcritical outlets, most of the cases modeled with OpenFOAM found in the bibliography, such as Romagnoli et al. [2009] or Witt et al. [2015], use an additional stretch of channel with an obstacle to raise the water level, followed by a conventional free outlet. In this study, subcritical outlets are forced by imposing a velocity profile such that the desired outlet water level is reached. This is obviously an iterative process, but it proved to save up to 30% of computaitonal resources, exerting no effect on the model outcome [Bayon and Lopez-Jimenez, 2015].

The rest of boundary conditions do not differ from one case to another and are summarized in Tab. 4.1. A no-slip condition is imposed to walls, so velocity is set to zero whereas a null Von Neumann condition is imposed to pressure. As discussed in Sec. 4.1.7, a wall function is imposed in $k - \varepsilon$ simulations, so velocity and the turbulence model variables (k and ε) are calculated according to the the wall function formulation. The latter variables cannot be directly set at the inlet

Stepped spillway
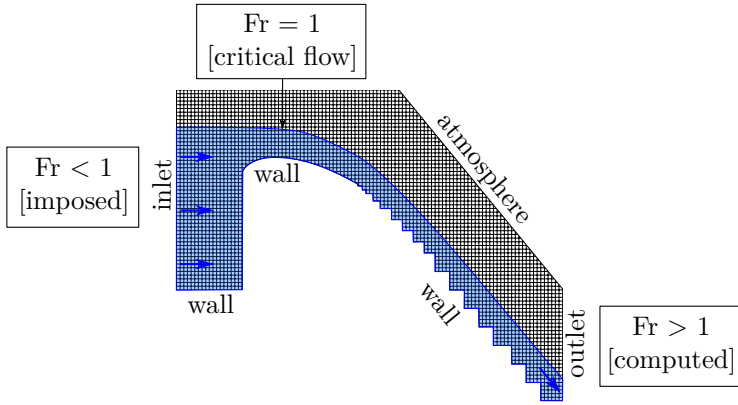
Stilling basin
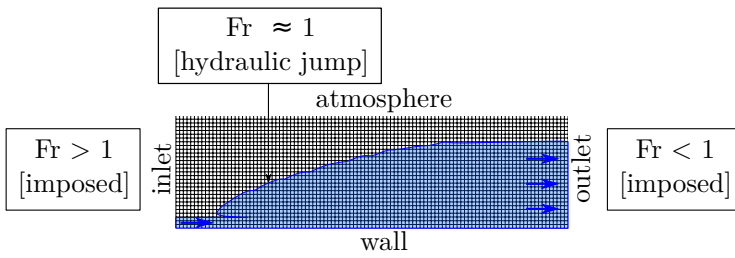
Practical application case
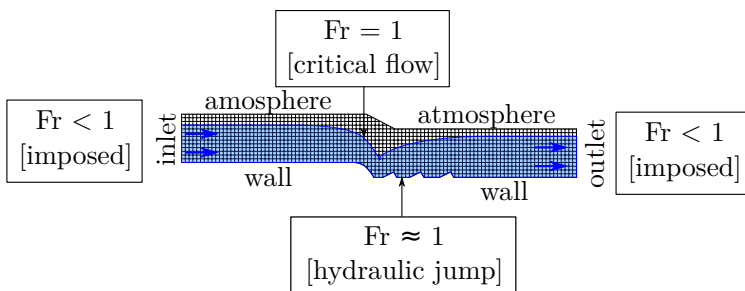
Figure 4.3: Flow regime boundary conditions according to case study.

according to the available experimental data. Instead, they are set to an arbitrary low value and a short initial stretch of channel is added in order for the flow to develop while approaching the zone of interest.

Inlet	Outlet
$u = u_1$	*
$\frac{dp}{dx} = 0$	
$k = k_1$	$\frac{dk}{dx} = 0$
$\varepsilon = \varepsilon_1$	$\frac{d\varepsilon}{dx} = 0$

Atmosphere	Walls
$\frac{du}{dx} = 0$	$u = 0$
$p = 0$	$\frac{dp}{dx} = 0$
$\frac{dk}{dx} = 0$	$k = f(y)$
$\frac{d\varepsilon}{dx} = 0$	$\varepsilon = f(y)$

* Subcritical outlets: $\quad u = f(y) \; ; \quad \frac{dp}{dx} = 0$

Supercritical outlets: $\frac{du}{dx} = 0 \; ; \quad p = \rho g y$

Table 4.1: Boundary condition configuration.

The atmospheric boundary conditions impose atmospheric pressure through a null Dirichlet condition and allow velocity, k and ε to be computed by the model, as free outlets do. However, this boundary condition allows air to enter the domain under negative pressures.

4.1.7 Wall treatment

The way the boundary layer is treated is of paramount importance in fluid modeling. Von Karman [1930] established a universal law of the wall which defines the flow velocity profiles in the boundary layer. Velocity (u) and distance to wall (y) are respectively adimensionalized using shear velocity (u_τ) and viscosity (v):

$$y^+ = y\frac{u_\tau}{v} \tag{4.13}$$

$$u^+ = \frac{u}{u_\tau} \tag{4.14}$$

The lowest-y^+ regions, the so-called viscous sub-layer [Schlichting and Gersten, 2000], are characterized by large gradients of velocity and turbulence properties and the predominance of viscous effects, being the velocity profile: $u^+ = y^+$. The upper layer, the so-called logarithmic layer, describes a logarithmic velocity profile, whereas the profile in between both regions, the so-called buffer sub-layer, does not show a clearly predictable behavior. In order to avoid having to resolve the lowest regions of boundary layers, wall functions are often used in CFD models. These functions are imposed as boundary conditions on solid patches to avoid the use of excessively fine meshes, with the subsequent saving of computational resources. As a consequence, the model mesh has to be refined so that the y^+ coordinate of the center of all mesh elements in touch with solid walls be somewhere between the buffer and the logarithmic sub-layers, i.e. $y^+ \in [15, 300]$. This condition has been met in all the simulations conducted in this research.

It is also important not to over-refine meshes when using wall functions. If this happened, wall functions could be modeling the behavior of the viscous sub-layer, whereas the model itself would be resolving the flow in this region, causing an accuracy drop. This controversy may cause that finer meshes yield less accurate results.

In terms of accuracy, the best choice would be using a low-Reynolds-number model with no wall function at all, as the SST $k - \omega$ model. However, as the this implies that the center of the first mesh element must meet the condition $y^+ < 15$, meshes must be refined to such an extent that the computational cost may become unaffordable in some cases.

There is vast literature on improvements to the original implementation of wall functions, such as Johnson and Launder [1982], but most of the proposed solutions have not been adopted by most of CFD codes. This is due to the fact that, despite these approaches are valid from a theoretical point of view, many of them may cause stability issues [Blocken et al., 2007].

In this research, a high-Reynolds-number wall function for RANS models and smooth solid surfaces are implemented, except for the cases where the SST $k - \omega$ model is employed. Despite boundary layers can often be slightly skewed [Taylor, 1959], as the flow mainstream direction is completely longitudinal in all the cases analyzed herein, a bi-dimensional wall function is used for the sake of simplicity.

4.1.8   Discretization schemes

As regards the discretization schemes used to make the CFD model partial differential equations numerically approximable, the best choice must be a good compromise between accuracy and stability. In spatial discretization, upwind models are generally preferred to downwind approaches as the latter tend to show severe stability issues. Compared to central differencing schemes, upwind approaches are slower, but also less diffusive and so more accurate. The problem is that, when abrupt property gradients occur, the latter schemes may require limiters in order to prevent spurious oscillations [Blazek, 2005]. Once limited, upwind schemes, such as Van Leer [1977], are very appealing to discretize abruptly-varied properties. The only drawback is that, when limited, these schemes become first order accurate.

Different discretization approaches are employed according to the case, as discussed in Appx. A, B, C and D. In particular, special attention is paid to the following schemes in the approximatation of the advection terms: first-order upwind methods, the second-order limited Van Leer [1977] method, and second-order limited central difference methods. A sensitivity analysis to the numerical discretization scheme is conducted along with the rest of model parameters.

The diffusive terms of the equations are discretized using a second-order accurate Gauss linear corrected scheme in all cases. Also, in order to ensure stability of simulations, time steps are automatically modified so that Courant numbers always remain below a given threshold, which is strongly case specific.

4.2   Experimental data

In order to validate the model presented herein, several study cases are conducted and the numerical results are compared to experimental data. Part of this data are obtained ad hoc, whereas others are obtained from previous studies. Despite the numerical model implementation is fairly similar in all cases, the nature of the study cases is very different, so they are discussed in separate sections.

In the numerical model, the most relevant mechanical properties of water, density and kinematic viscosity, are set to $\rho_w = 1000 kg/m^3$ and $\upsilon_w = 10^{-6} m/s^2$, respec-

tively. For air, the employed values are $\rho_a = 1.20 kg/m^3$ and $v_a = 10^{-3} m/s^2$. Surface tension is set to $\sigma = 0.07 N/m$.

4.2.1 Stepped spillways

The experimental stepped spillway model used for validation of the numerical model presented herein was built at the National Laboratory of Civil Engineering (LNEC), in Lisbon, Portugal. The experimental results have been already published elsewhere [Bombardelli et al., 2011, Matos, 1999, Meireles, 2004, 2011b, Meireles et al., 2012, Renna, 2004], so only a brief summary is provided in Bayon et al. [2017].

The facilities consisted of a reservoir, and a smooth crest following the profile of the Waterways Experimental Station (WES). The first steps downstream of the crest had variable size for their tips to fit the WES profile. A tangent point was defined downstream, where the WES profile met the 1V:0.75H constant slope steps.

Measurements were taken using a conductivity probe and a back-flushing Pitot tube held in such way that measurements could be taken perpendicularly to the spillway pseudo-bottom (see Fig. 4.4). A more thorough discussion on the experimental setup is available in Sec. C.2 or in Matos [1999], Meireles [2004, 2011b], Bombardelli et al. [2011], and Meireles and Matos [2009], Meireles et al. [2014].
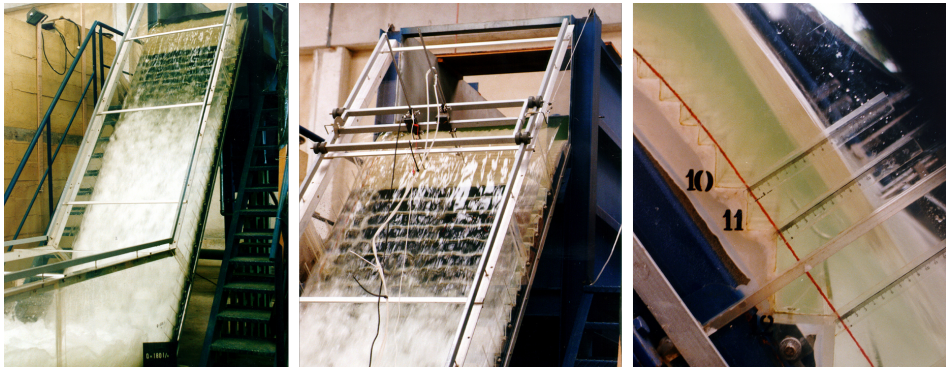
Figure 4.4: Stepped spillway experimental model at the National Laboratory of Civil Engineering (LNEC) in Lisbon, Portugal [Bombardelli et al., 2011, Matos, 1999, Meireles, 2004, 2011b, Meireles et al., 2012, Renna, 2004].

4.2.2 Stilling basins

Hydraulic jump experimental data from a small scale open channel installed at the Hydraulics Laboratory of the Universitat Politècnica de València (UPV), Spain, is used (see Fig. 4.5). The device consists of methacrylate walls and a PVC streambed, a recirculation tank and a water pump is employed to provide the desired flow rate. The facility characteristics is discussed in depth in Sec. B.4. Flow depth measurements are conducted by means of digital image processing using videos of the hydraulic jump profile recorded at $50Hz$ and $1280 \times 720px$ $(4.1 \cdot 10^{-4}m/px$ in average, before perspective effect correction). Flow depth is automatically determined using edge detection tools to track the sudden changes of light intensity that an air-water interfaces cause. Filtering algorithms are applied to raw results to remove the bias caused by reflections, droplets, etc.

Given the reduced channel dimensions, Froude numbers around $Fr_1 \approx 6$ can be obtained. A case study of approaching Froude number (Fr_1) between 6 and 7 is suitable for model validation as it is exactly in the middle of the Fr_1 value span recommended by the U.S. Bureau of Reclamation for stilling basin design [Peterka, 1953]. Therefore, this Fr_1 value is considered representative of the behavior of all steady hydraulic jumps within this range. However, Reynolds numbers remain relatively low $(Re_1 \approx 30,000)$, thus making the extrapolation of these results to real life scales controversial. For this reason, the model is also validated using non-dimensional empirical expressions obtained by other authors in larger facilities. In this case, a similar Froude number value is used $(Fr_1 \approx 6)$, but the Reynolds number is significantly larger: $Re_1 = 3.54 \cdot 10^5$. The details of this larger-scale case study are discussed in Sec. A.2.10.
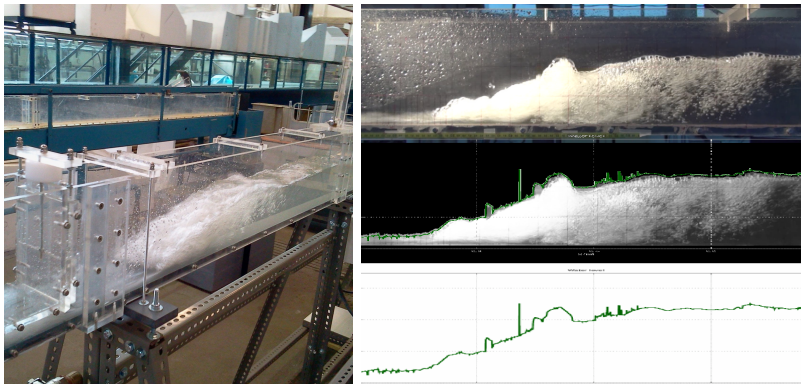
Figure 4.5: Hydraulic jump experimental model at the the Universitat Politècnica de València (UPV), Spain [Valles-Moran et al., 2015a].

4.2.3 Practical application case

The experimental data to validate the numerical model of the South Valencia Sewage Collection System (SCS) were obtained from a scale model also built at the Hydraulics Laboratory of the Universitat Politècnica de València (UPV), Spain (see Fig. 4.6). The flow under study was likely to be highly tridimensional, so a geometrically distorted model was no viable. The water depths imposed have to be those maintaining geometric proportionality with the channel size. The scale 1/20 was found to be the most unfavorable fulfilling the Russell and Chow criterion, which ensures the rough turbulent behavior of the scaled flow.

instant water level
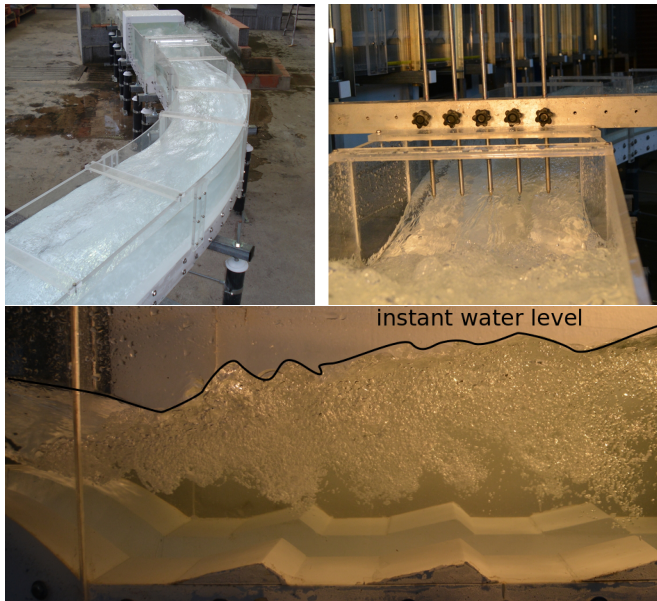
Figure 4.6: South Valencia Sewage Collection System experimental model at the Universitat Politècnica de València (UPV), Spain [Bayon et al., 2015b].

The size of the flow features that play the most important role in a case like this, such as eddy formation and flow detachment, maintains proportionality with flow external dimensions, such as water depth. This allows to scale the model within a certain range without using fluids of different properties, i.e. not fulfilling Reynolds similarity. Nevertheless, given that the flow is essentially driven by gravity, Froude similarity must be strictly respected. This criterion is therefore used to determine the inlet velocity and so the inlet flow rate.

A single case study was analyzed corresponding to the most demanding conditions expectable in the structure, i.e. $100m^3/s$, which is equivalent to $55.9 \cdot 10^{-3}m^3/s$ in the scaled model.

Water depth measurements were conducted using a multipoint gauge to capture the flow deviation caused by curves and so characterize the risk of channel bank overflow. The hydraulic jump free surface profile was measured employing digital image treatment. Further details concerning the SCS experimental apparatus can be found in Sec. D.2.7.

Chapter 5

Analysis of results

5.1 Mesh convergence

As discussed above, in all the cases analyzed herein, a mesh convergence analysis is conducted to ensure that all results are mesh-independent. To do so, all the simulations are run varying their cell sizes using a series of variables as convergence indicators and following the methodology proposed by Roache [2009] and discussed in Celik et al. [2008]. According to these sources, the number of meshes in every study must be of at least three, being the minimum recommended size ratio between the coarsest and finest of them of 1.3 [Celik et al., 2008]. This condition is fulfilled in all the case sudies.

In the case of the stepped spillway simulations, the apparent order (p'), the approximate relative error (e_a) and the grid convergence index (GCI) computed following the methodology proposed by Celik et al. [2008] are presented in Fig. 5.1. The apparent order reaches a values of approximately $p' = 0.9$ for mesh size $h' = 1.73mm$. This value is close to the model formal order, so indicating that the asymptotic range has been reached.

The same analysis indicates that the average approximate relative error (e_a) was below 4% and the grid convergence index (GCI) was below 5% in all cases, revealing that numerical uncertainty remains within an acceptable range. None of the indicator variables of the mesh convergence analysis shows significant improvement at sizes below the aforementioned size of mesh, while the computational costs increase dramatically. For these reasons, all subsequent analysis on the stepped spillway model is conducted on this case results.
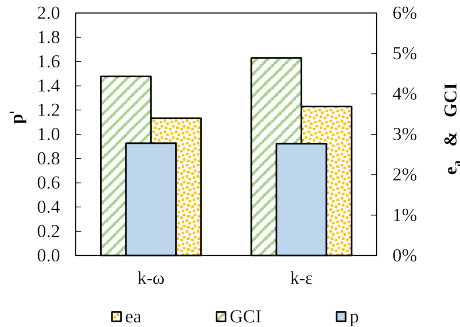
Figure 5.1: Mesh sensitivity analysis of stepped spillway model. Model apparent order (p'), grid convergence index (GCI) and approximate relative error, using water depths (h) at 6 different locations as indicators and computed according to Celik et al. [2008]. Adapted from Bayon et al. [2017].

In the case of the hydraulic jump simulations, as discussed in more depth in Appx. B, the mesh of size $h' = 3.00mm$ reached convergence and was in the asymptotic range, as the model apparent order approached the model formal order. For this reason, all subsequent considerations regarding the quantitative analysis of results of this model were exclusively referred to that mesh size. In this case, the model grid convergence index remained close to 6.0%, also showing an acceptable numerical uncertainty.

Regardless of the model, both codes, OpenFOAM and FLOW-3D, respond differently to mesh size reduction, which is a fact that has already been observed in different types of flows by Bombardelli [2009]. More specifically, it appears that OpenFOAM tends to be more sensitive to this parameter than FLOW-3D [Bayon et al., 2016, 2017]. Turbulence models also respond differently to mesh refinement, as observed in Fig. 5.1, although in this case a pattern for this response cannot be observed.

5.2   Model validation

5.2.1   Stepped Spillways

This analysis on the stepped spillway model was exclusively conducted using Open-FOAM results, as FLOW-3D results have already been analyzed in Bombardelli et al. [2011].

Sensitivity analysis

First of all, it was observed that the differences in the model outcome are small among different second-order discretization schemes, as depicted in Fig. 5.2. Differences between first- and second-order methods are small when predicting the mean flow velocities (4%), although they reach large values when predicting other variables, such as maximum TKE on step edges. Both second-order limited central-difference and limited Van Leer discretization schemes yield very similar results, with differences in estimations below 4% for all the analyzed variables. Nevertheless, the limited central-difference scheme seems to systematically achieve accuracies between 5% and 10% higher employing approximately 30% smaller computational times than the Van Leer scheme.

With regard to turbulence models, it is shown in Fig. 5.3 that the RNG $k - \varepsilon$, the Standard $k - \varepsilon$ and the Realizable $k - \varepsilon$ models yield virtually the same results (differences are on average below 1%). A slightly better performance can be attributed to the RNG $k - \varepsilon$ model in the prediction of certain variables, such as water depths or the profiles within the boundary layer, but yet this difference is not significant. As depicted in Fig. 5.3, the SST $k - \omega$ model tends to overestimate water depths (4%) with a consistent underestimation of velocities slightly above the RNG $k - \varepsilon$ (2% overestimation of water depths).
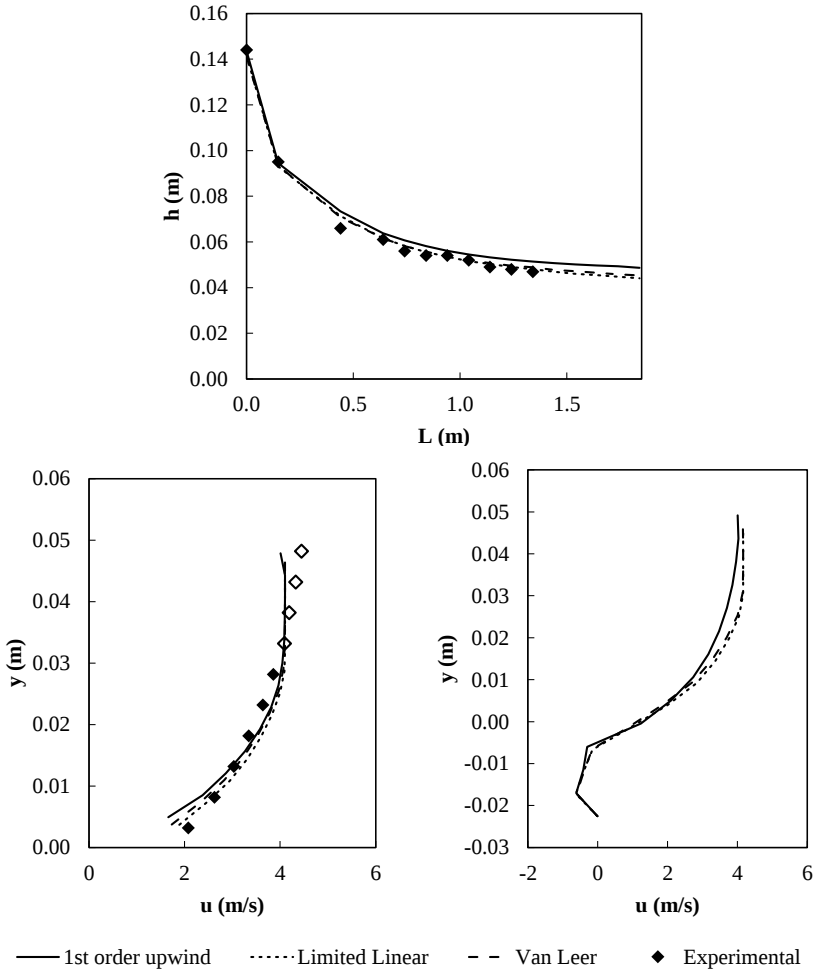
Figure 5.2: Numerical results using RNG $k-\varepsilon$ model and diverse discretization schemes, with a converged mesh size of $\Delta x = 1.5mm$. a) Water free surface profiles; b) Velocity profile at step 23 ($L = 1.04m$); c) Velocity profile within the cavity at $L = 1.072m$. For the experimental data, unfilled symbols indicate measurements affected by either the fluctuations of the free surface or the location of the inception point.
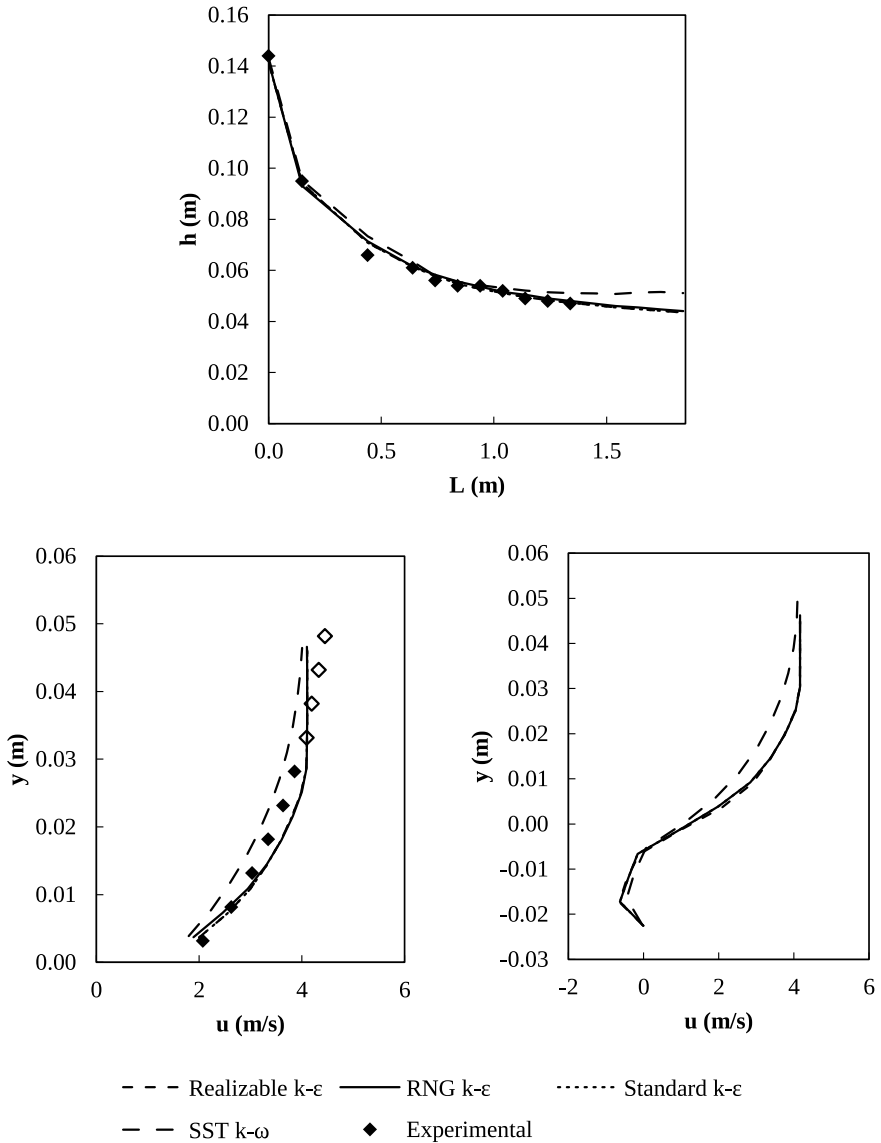
Figure 5.3: Numerical results using a limited central-difference discretization scheme and diverse turbulence models, with a converged mesh size of $\Delta x = 1.5mm$. a) Water free surface profiles; b) Velocity profile at step 23 ($L = 1.04m$); c) Velocity profile within the cavity at $L = 1.072m$. For the experimental data, unfilled symbols indicate measurements affected by either the fluctuations of the free surface or the location of the inception point.

When comparing the Partial VOF (OpenFOAM) and the TruVOF (FLOW-3D), the flow depth throughout the stepped spillway is very well predicted by both approaches (see Fig. 5.4). The first reach located over the smooth region near the spillway crest is reproduced with a root mean square error (RMSE) below 1%. In the last steps, all approaches seem to overestimate the experimental results, although results with TruVOF are slightly closer to the experimental data. The RMSE in the water profile estimation for the TruVOF method is 4.2%, slightly below the 6.2% attained by teh Partial VOF.
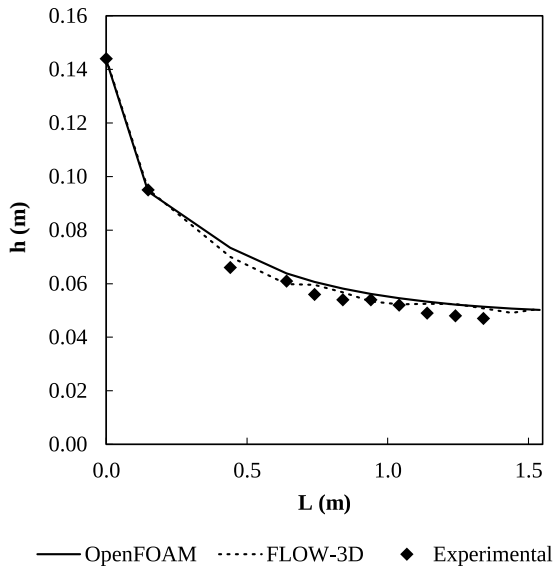
Figure 5.4: Water free surface profile using RNG $k - \varepsilon$ model and first-order upwind discretization scheme and a converged mesh size of $\Delta x = 1.5mm$ according to type of VOF method: Partial VOF (OpenFOAM) and TruVOF (FLOW-3D).

With regards to velocity profiles, the formation of a boundary layer is accurately captured by both methodologies (see Fig. 5.5). Although both codes tend to underestimate velocities, OpenFOAM (Partial VOF) achieves a smaller difference with the experimental data than FLOW-3D (TruVOF). Looking at the normalized velocity profiles on Fig. 5.6, it can be observed that also the velocity profile shape within the boundary layer is better captured by OpenFOAM than by FLOW-3D. These differences may be due, among other causes, to the fact that the TruVOF does not account for free-surface tangential stresses, whereas the Partial VOF does.

Figure 5.5: Velocity profiles using RNG $k - \varepsilon$ model and a first-order upwind discretization scheme and a converged mesh size of $\Delta x = 1.5mm$ according to type of VOF method: Partial VOF (OpenFOAM) and TruVOF (FLOW-3D).
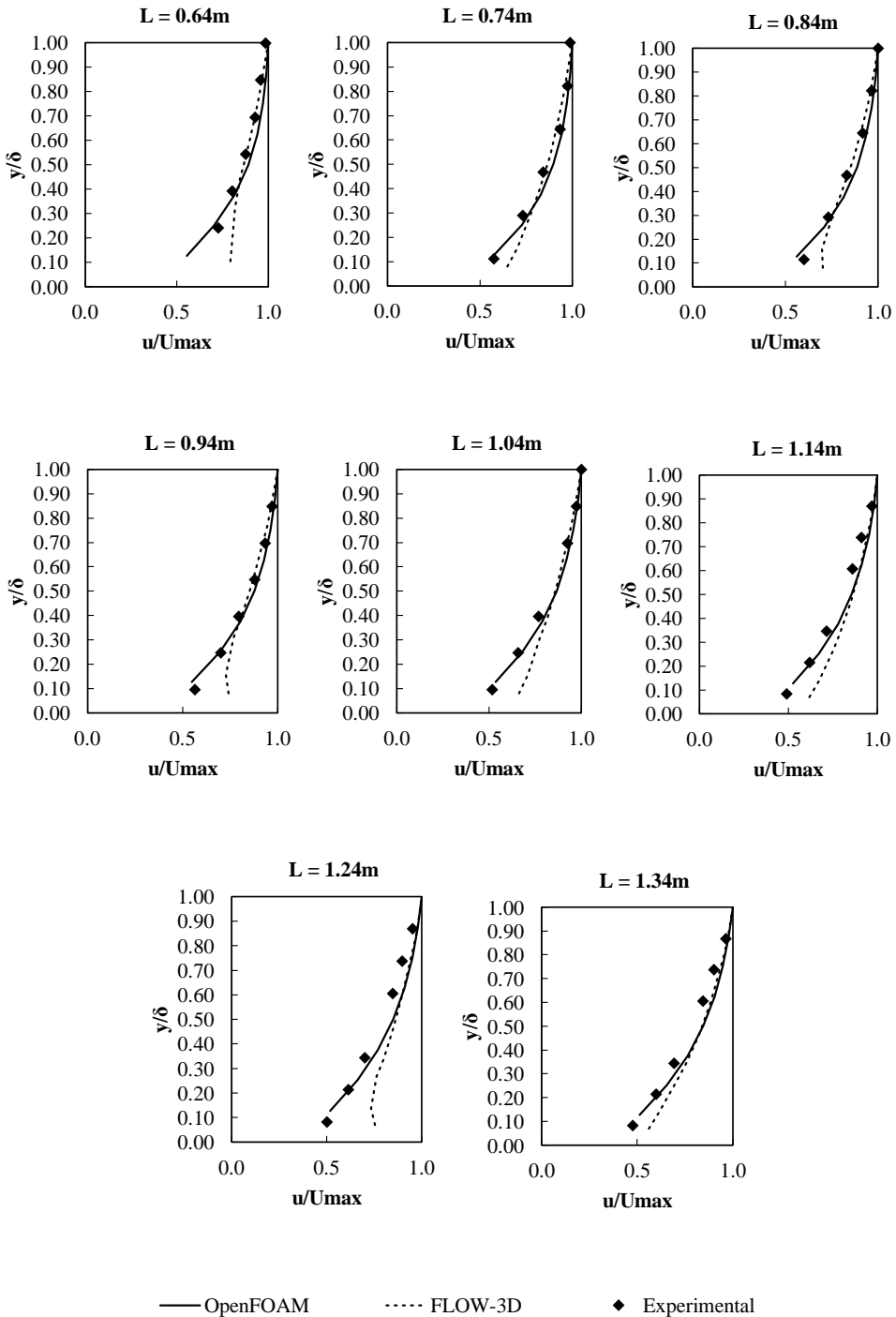
Figure 5.6: Normalized velocity profiles using RNG $k-\varepsilon$ model and a first-order upwind discretization scheme and a converged mesh size of $\Delta x = 1.5mm$ according to type of VOF method: Partial VOF (OpenFOAM) and TruVOF (FLOW-3D).

As regards the evolution of flow depths and boundary-layer development, Open-FOAM tends to yield more developed velocity profiles near the spillway crest than FLOW-3D. By extrapolating their trending curves, the approximate location of the air inception point can be estimated. According to this extrapolation, Partial VOF and TruVOF overestimated this variable by 14% and 30%, respectively. Compared to the measurements reported by Chanson [2002], the results of Partial VOF and TruVOF differ with experiments in 2% and 7%, respectively. It bears emphasis that the experimental data have uncertainties on its own given the difficulty of determining the precise location of the inception point due to unsteadiness.

Additionally, a recent experimental work [Zhang and Chanson, 2016a] state that the inception point occurs where the boundary layer thickness reaches 80% of the water depth. Using this criterion, OpenFOAM and FLOW-3D underestimate distances to the inception point of by 8% and 11.5%, respectively.

A more in-depth comparative analysis on the differences of performance between OpenFOAM and FLOW-3D in the modeling of stepped spillways can be found in Bayon et al. [2017], also available in Appx. C.

Self-similarity analysis

Meireles [2011a] and Toro et al. [2016] proposed and corroborated self-similarity of turbulence statistics in stepped spillways, an unprecedented result. Similarly, Felder and Chanson [2011] discussed self-similarity of the integral time scales in terms of similar trends in the flow distributions along the cavity. However, there was no clear description of the self-similarity in the flow velocity within the cavity, as no negative velocities were recorded in the recirculation region. Previously, in Gonzalez and Chanson [2004], similar trends of the flow velocity within the cavity were presented; in that study, non-dimensional velocities were obtained by using the velocity at which half of the freestream velocity is reached. For a description of a self-preserving boundary layer, the reader is referred to the experimental work by Gonzalez and Chanson [2004], one of the pioneer studies of the flow over rough walls.

In the case presented herein, the results show the occurrence of a certain pattern in the velocity and TKE distributions throughout the spillway. Using a suitable normalization, most of flow variables present self-similar behavior throughout the spillway. This fact was investigated by using exclusively OpenFOAM data and the results indicate approximate flow self-similarity.

Fig. 5.7 shows the normalized profiles of velocity, TKE, dissipation rate and pressure at different step edges compared with the results reported in previous works for the velocities. These profiles show an important degree of overlapping. Additionally, it was observed that the highest pressures always occur close to the pseudo-bottom at approximately $0.32cm$ upstream of the step edges (cf. also with Toro et al. [2016]).

A self-similar behavior can also be observed in the step cavities, as depicted in Fig. 5.8. The velocity profiles predicted by the model in the recirculation zone attain an accuracy of 93.3%, compared to data by Amador et al. [2006]. The same authors state that the maximum recirculation velocity is 15% of u_{max}, which is confirmed by the results presented herein. With regards to pressure profiles, it can be observed how this variable drastically drops below the hydrostatic profile in the recirculation region, as reported in Toro et al. [2016].

Concerning the TKE and dissipation rate of TKE profiles, a peak can be neatly identified near the pseudo-bottom, so corroborating that the flow in the pseudo-bottom vicinity is responsible for the highest dissipation rates of TKE [Toro et al., 2016]. It was also observed that the dissipation rate profiles perfectly reproduce the shape of the integral turbulent length scale profiles reported in Amador et al. [2006].

**Figure 5.7:** Normalized velocity profiles, turbulent kinetic energy (TKE), dissipation rate of TKE and pressure at different step ed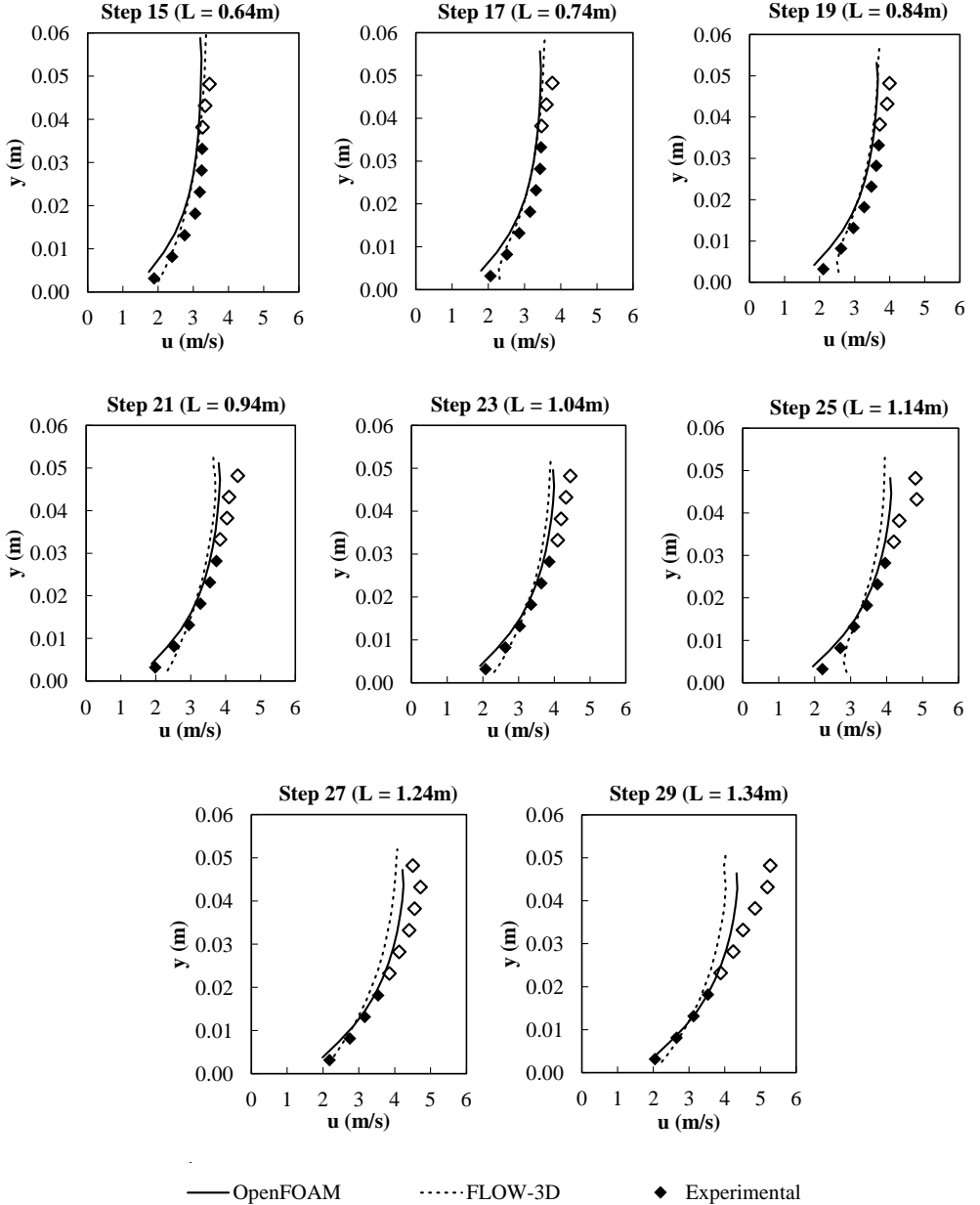ges using RNG $k - \varepsilon$ model and a first-order upwind discretization scheme and a converged mesh size of $\Delta x = 1.5mm$. In the pressure plot, unfilled symbols correspond to pressure profiles $0.32cm$ upstream of step edges, where maximum pressure occurs, and the dashed line represents the hydrostatic profile.
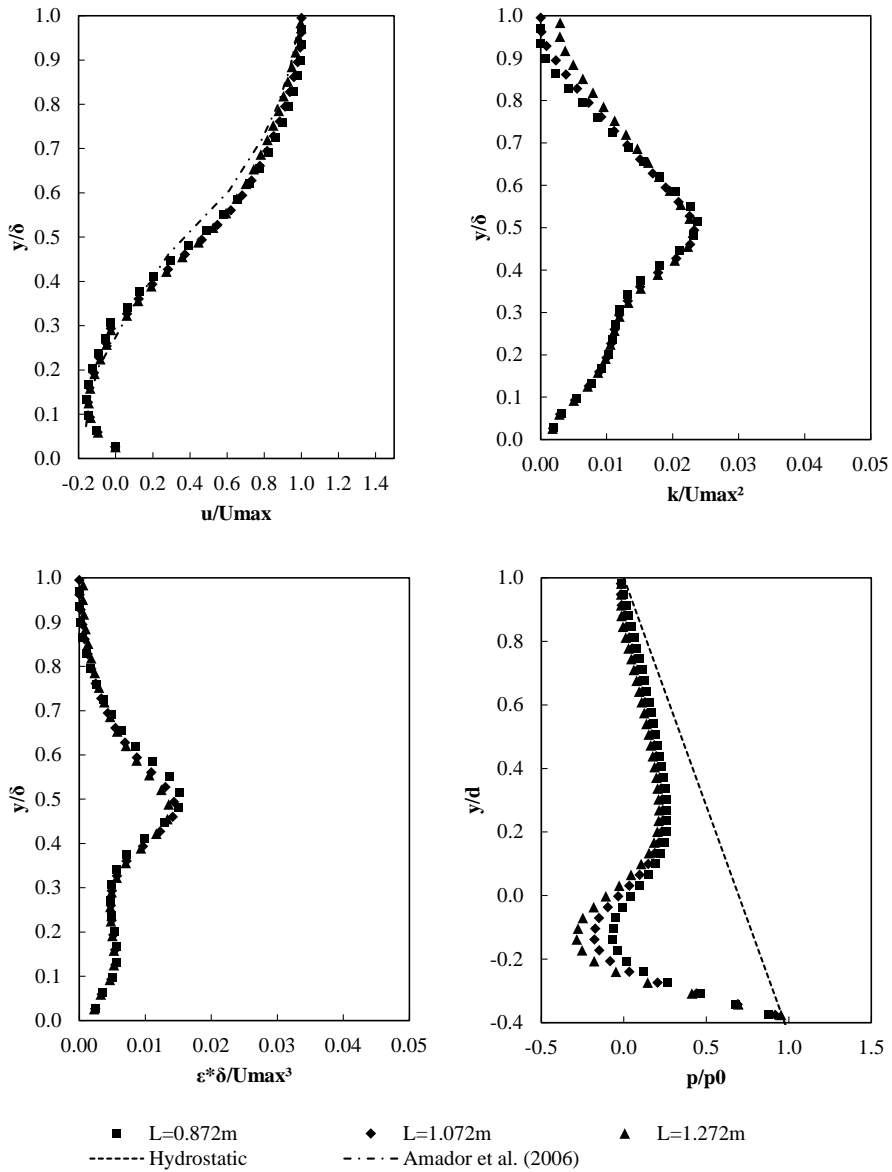
Figure 5.8: Normalized velocity profiles, turbulent kinetic energy (TKE), dissipation rate of TKE and pressure at different step gaps using RNG $k - \varepsilon$ model and a first-order upwind discretization scheme and a converged mesh size of $\Delta x = 1.5mm$.

5.2.2   Stilling basins

Time analysis

Unlike the case of flow in stepped spillways, where variables show a quite uniform time variation of very short period, hydraulic jump behave in a more chaotic way and all variables show, in a best case scenario, a statistically-stationary behavior. Hence, it is of paramount importance to extend the simulation time sufficiently and then average the variables in order to avoid bias in the model outcome. In order to ensure that the time-averaging window size does not affect results significantly, a sensitivity analysis is also conducted. Some oscillating variables are carefully observed, namely: jump toe position (x_0), roller end position (x_r) and subcritical flow depth (h_2). As a conclusion, it can be stated that the sampling period chosen of $10s$ captures several characteristic oscillation periods of these variables, so avoiding bias in the averaging process [Bayon et al., 2016].

During this analysis, certain quasi-periodicity in the variables is observed (i.e. patterns can eventually be detected, although their characteristic period seems not to be constant). The autocorrelation function (ACF) is computed to investigate whether the monitored variables show periodic behavior or not, and if so, what is the characteristic time scale of their oscillations. Indeed, the autocorrelation function of all variables tested shows an attenuation trend comparable to that of a sine wave with a characteristic time scale way smaller than the averaging window size. In order to further infer this phenomenon, the same three variables are analyzed in the frequency domain using the Fast Fourier Transform (FFT). Fig. 5.9 (a, b and c) show the normalized power spectrum density (PSD) of these three variables according to the code used and the experimental data, respectively.

The analysis shows that the observed quasi-periodic oscillations have well defined periods. In fact, for the variables considered in the analysis of numerical results, a peak in each spectrum can be observed at a frequency around $1.0Hz$. The three variables analyzed oscillate at approximately the same frequency regardless of the numerical code used. In the case of OpenFOAM, the dominant frequency is $0.90Hz$ (period of $1.11s$), whereas in FLOW-3D, the dominant frequency is $1.10Hz$ (period of $0.91s$), with an uncertainty of $0.1Hz$. The experimental data PSD (Fig. 5.9 c) depicts slightly higher dominant frequencies for x_0 ($1.6Hz$) and h_2 ($2.9Hz$).

Despite of that, all these results compare well to previous works in terms of Strouhal number (St), showing certain correlation to Reynolds number (see Fig. 5.9 d). It should be remarked that the similar dominant frequency found using both modeling approaches, not far from those experimentally determined, suggests that the regularity of the oscillating phenomena can be well described as a non-random and orderly process, which is superimposed on a background of turbulent
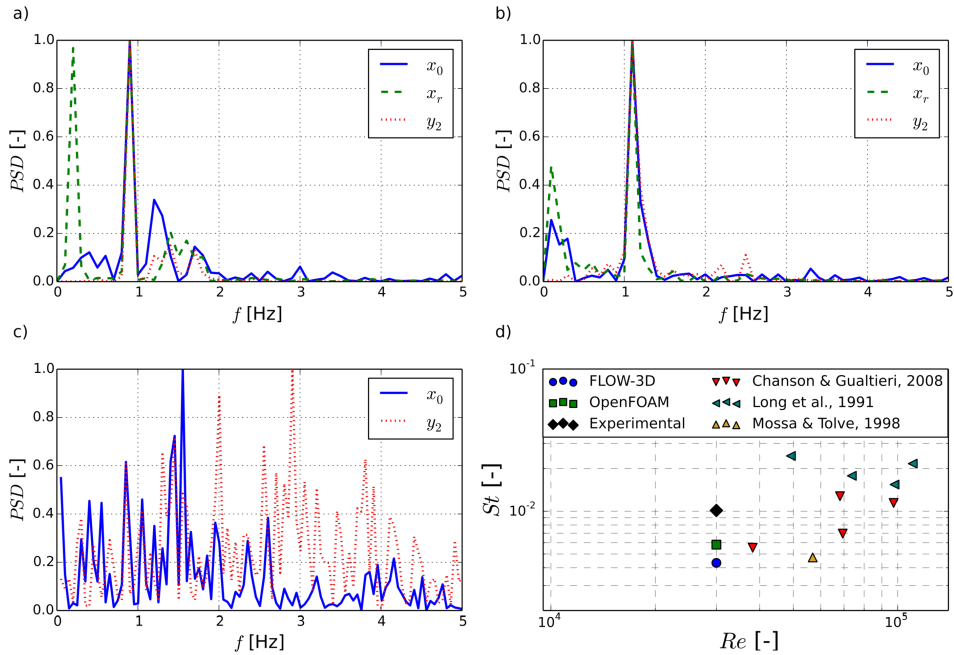
Figure 5.9: Power spectrum density (PSD) of hydraulic jump toe location (x_0), roller end location (x_r) and subcritical depth (h_2): a) OpenFOAM; b) FLOW-3D; c) Experimental results; d) Comparison of resulting Strouhal numbers (St) to previous studies.

random motion [Mossa, 1999]. This fact obviously results from the complex relationship among vortex structures, internal features of the hydraulic jump and observable external variables.

Sensitivity analysis

As discussed in Sec. 4.1.6, a new approach for the outlet boundary condition is used, so avoiding having to introduing an additional channel stretch with an obstacle to force subtrical flow to occur. Fig. 5.10 shows examples of hydraulic jumps simulated using both approaches. A closer comparison between them shows no significant effect on the model outcome accuracy. No undesirable effects, such as wave formation, occur despite the new approach implies bringing the boundary conditions significantly closer to the phenomenon under study. The domain reduction achieves computation times up to 30% shorter in some cases.

The three tested turbulence models show small influence on the sequent depth (Y) estimations. The most accurate model is the RNG $k-\varepsilon$, followed by the SST $k-\omega$ and the Standard $k-\varepsilon$, although all errors are below 4%. The inflexion point in the
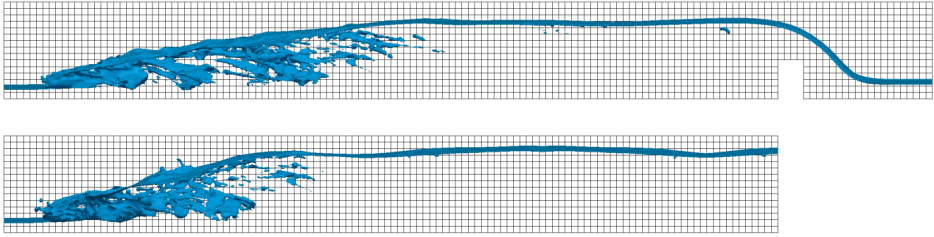
Figure 5.10: Instant comparison of hydraulic jumps simulated using two different outlet boundary conditions: the traditional approach (top) and a new approach (bottom).

accuracy of the all models can be clearly observed at a mesh size of $7.50mm$, thus being the RNG $k - \varepsilon$ model with $7.50mm$ size mesh the most accurate approach. Compared to Hager and Bremen [1989], the mismatch of FLOW-3D is slightly above 5%. Compared to experimental results, OpenFOAM and FLOW-3D attain average errors of of 2.0% and 2.2%, respectively.

Another important variable in the analysis of hydraulic jumps is the roller length (L_r), as that is the region where the largest shear stresses on the streambed occur and so needs to be carefully protected in hydraulic structures. This variable is easier to determine as a flow stagnation region, where streamwise velocity tends to zero, can always be identified. Murzyn and Chanson [2009a] define the roller as the stretch of hydraulic jumps where the flow depth increases monotonically. Nevertheless, the stagnation point is used as criterion in the present work for it is easier to identify in CFD modeling.

The SST $k - \omega$ model appears not to be able to capture accurately this variable. The Standard $k - \varepsilon$ model shows a reasonable accuracy (all errors are below 6%) and low sensitivity to mesh size, which is a desirable characteristic. However, RNG $k - \varepsilon$ is even more accurate and shows a perfect monotonically decreasing trend in errors, although the model is also highly sensitive to mesh size variations.

When comparing between both CFD codes, FLOW-3D appears to be less accurate when estimating the roller length: this model achieved an accuracy of 80.5%, whereas OpenFOAM reached 98.9%, both compared to Hager [1992]. Compared to Wang and Chanson [2015a], the accuracy decreased to 77.4% and 91.5% respectively. This variable shows the largest sensitivity to model parameters, such as mesh element size.

The prediction of the hydraulic jump efficiency achieves the highest accuracy values, being the error of all models below 2%. The Standard $k-\varepsilon$ is the most accurate (0.1%) but the sensitivity of this variable to the model parameters is extremely low. In the study case where OpenFOAM results are compared to FLOW-3D, the

accuracy of both model in the prediction of hydraulic jump efficiency is slightly lower: 97.1% and 94.6%, respectively.

The comparison of water surfaces to previous studies [Bakhmeteff and Matzke, 1936] proves that the most accurate RANS model is the Standard $k - \varepsilon$ ($R^2 = 0.996$), followed by the RNG $k - \varepsilon$ ($R^2 = 0.992$) and the SST $k - \omega$ ($R^2 = 0.985$). This demonstrates that, in the case presented herein, turbulence models exert very little effect on the water free surface definition in average terms (see Fig. 5.11). Nevertheless, an instant observation of the evolution of this variable shows that SST $k - \omega$ models produce a more unstable and bursting water surface with high bubble and spray production.
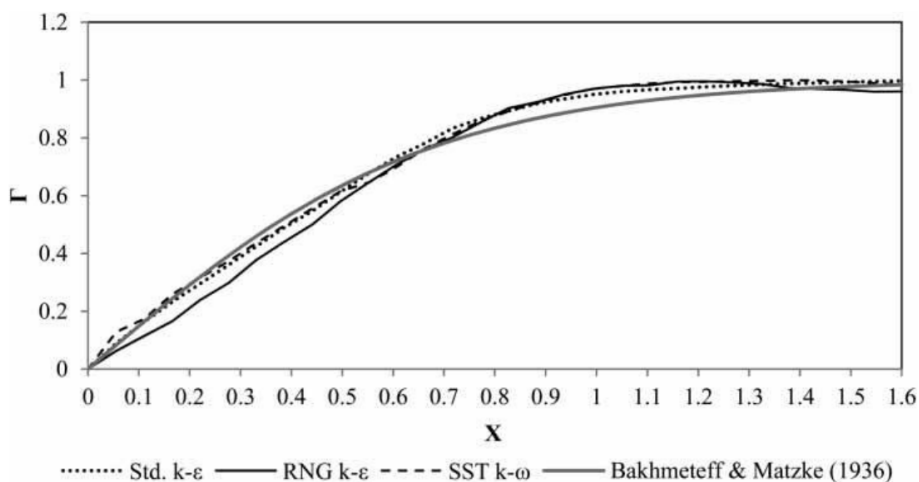
Figure 5.11: Water free surface level according to turbulence model used compared to Bakhmeteff and Matzke [1936] obtained with OpenFOAM [Bayon and Lopez-Jimenez, 2015].

When comparing among CFD codes, FLOW-3D achieves a coefficient of determination of $R^2 = 0.988$ compared to Bakhmeteff and Matzke [1936] and $R^2 = 0.952$ compared to Chanson [2015], respectively. Compared to experimental results, OpenFOAM and FLOW-3D yield accuracies of $R^2 = 0.982$ and $R^2 = 0.966$, respectively. Fig. 5.12 shows the dimensionless free surface profile obtained by both codes compared to Bakhmeteff and Matzke [1936], Chanson [2015], and experimental results. The sudden increase of water level in experimental results near $X \approx 0.7$ comes from the bias caused by the large bubbles being expelled from the flow, which cannot be filtered out by the employed surface detection algorithm.

Concerning flow velocity distributions, as discussed in Appx. B, the maximum differences with values reported by Hager [1992] occur for backward velocities (U_s).
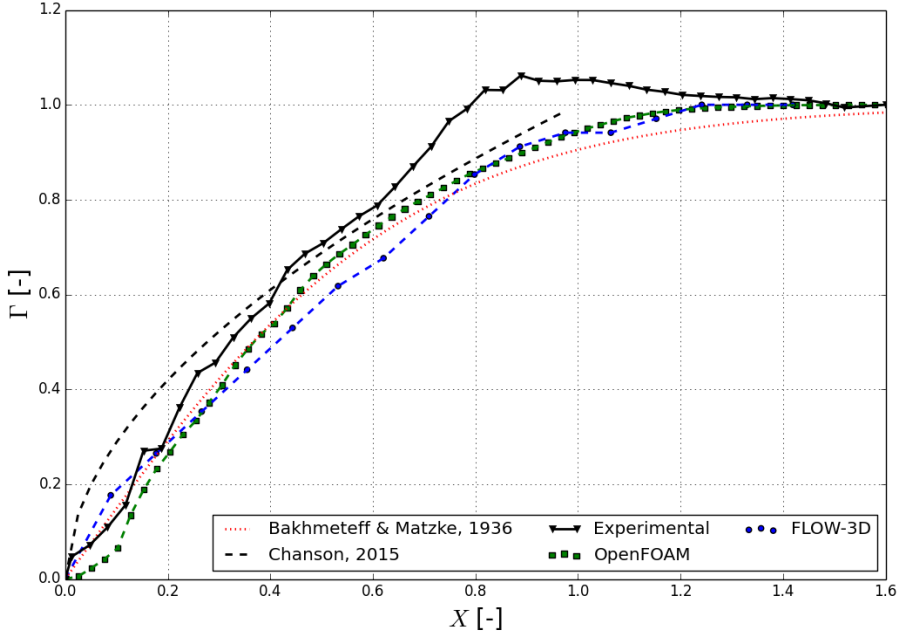
Figure 5.12: Dimensionless free surface profile computed with OpenFOAM and FLOW-3D compared to Bakhmeteff and Matzke [1936], Chanson [2015], and experimental results.

The flow processes in this region of hydraulic jumps are particularly complex. It is therefore expectable that the maximum errors take place in the swirling region, where turbulence models are most prone to fail in reproducing the flow behavior [Wilcox et al., 1998]. Better accuracy can be expected for the rest of the analyzed flow variables. For the maximum velocity decay, FLOW-3D achieves higher degree of accuracy (99.7%) than OpenFOAM (99.5%). However, OpenFOAM yields better results than FLOW-3D in the estimation of backward velocities (88.2% and 83.7%) and vertical velocity profiles (97.6% and 90.3%), respectively. Anyway, these differences are rather small as both numerical codes reproduce the shape and main features fairly well as reported in the literature.

Unlike the roller end position, which can be easily defined, determining the end of the hyraulic jump is a complex task. A measureable variable is proposed to this end in Bayon et al. [2016]: the TKE decay (σ). To obtain this variable, the values of TKE provided by the CFD models are estimated along the channel longitudinal axis, starting at the jump toe, where maximum values of TKE occur. An exponential decay for the TKE throughout the hydraulic jump is assumed out of mere observation of the variable evolution (see Fig. 5.13).
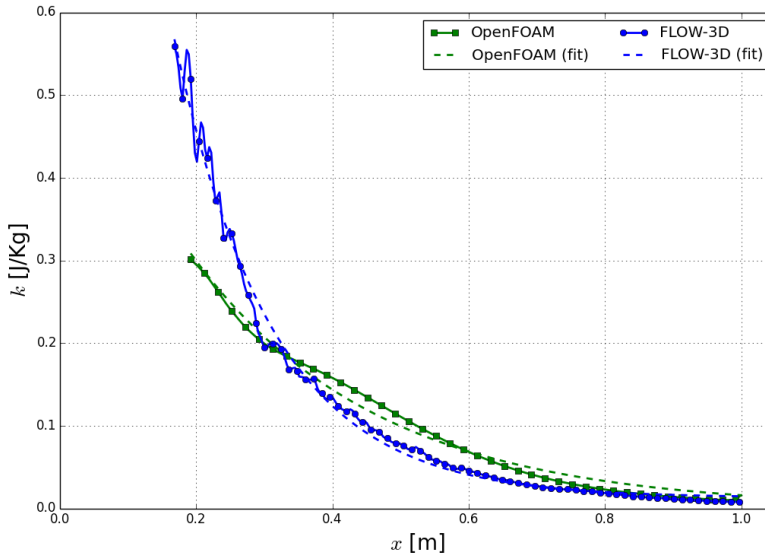
Figure 5.13: TKE decay within the hydraulic jump along the longitudinal axis.

The TKE decay threshold that makes hydraulic jump length (L_j) match with the expression by Bradley [1945] is $\sigma_{OF} = 98.3\%$ and $\sigma_{F3D} = 96.6\%$ for OpenFOAM and FLOW-3D, respectively. Thus, a 95% decay of the maximum TKE could be established as an approximate threshold to define the jump end location.

5.2.3 Practical application case

The results of the application to a practical case of the developed model show good agreement with the reference experiemental data. The water level numerically computed and experimentally measured at several cross sections is presented in Fig. 5.14. Not only the flow surface tilt trends are consistently followed, but also good agreement is found between both sets of data, although the section expected to be less sensitive to errors, the curve inlet, presents the largest mismatch.

However, in the rest of sections, the agreement is practically total. Outward surface tilt is caused by the flow passing through the curve, although both models demonstrated that the proposed bank height is enough to contain it. As expected, this tilt inverts its direction downstream of the curve, in the stabilization region. Nevertheless, the deformation in this stretch is sensitively lower.

A gradual decrease of height is observed, which can be explained by the influence of the WES weir section, where critical flow is reached. Indeed, at the latter section, this variable reaches its minimum value. Also at the weir crest, it can be

observed how the stabilization stretch accomplishes its purpose, as flow surface is barely skewed. The only observable deformation of surface at this point is a height decrease in the vicinity of the channel banks. This is caused by the section expansion occurred throughout the weir.

Figure 5.14: Water surface tilt comparison between numerical model (CFD) and physical model (Ph.M.) at several cross sections.

As regards the stilling basin, good agreement is also found in the comparison of numerical results and experimental digitally-processed images. Fig. 5.15 shows the mean water profiles in this stretch according to the turbulence model used compared to the experimental results. On the upper part of the figure, it can be observed how the hydraulic jump occurs right downstream of the weir.

The sensitivity analysis to turbulence model leads to the conclusion that sensitively different results are obtained according to the model used. Nevertheless, as Fig. D.5 shows, all of them managed to perfectly reproduce the phenomenon and to capture all trends, consistently with the discussion in Sec. 5.2.2. The coefficient of determination (R^2) of the Standard $k - \varepsilon$, the RNG $k - \varepsilon$ and the SST $k - \omega$ with respect to the physical model results are 0.944, 0.927 and 0.941, respectively. The Standard $k - \varepsilon$ model reproducing best experimental hydraulic jumps is a phenomenon already observed by the Author [Bayon and Lopez-Jimenez, 2015].

However, in previous experiences, SST $k - \omega$ generally did not manage to capture hydraulic jump water profiles as accurately as in this case. The turbulence model used also implies non-negligible differences in computation time, which is a matter of paramount importance in practical application cases. The authors have found through experience that the Standard $k - \varepsilon$ model tends to be faster in this kind of applications, followed by the RNG $k - \varepsilon$ model and, in the last place, the SST $k - \omega$ model.
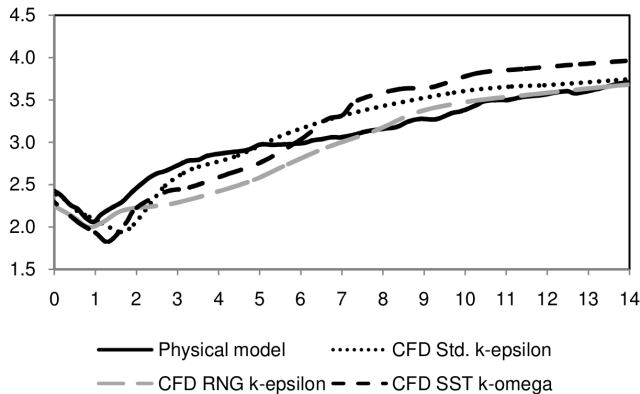
Figure 5.15: Hydraulic jump surface profile comparison among different turbulence models at stilling basin.

Another phenomenon experimentally observed is consistently reproduced by the numerical model: a small flow detachment on the channel banks at the WES weir section. On the left-hand side of Fig. 5.16, this process, caused by a sudden flow expansion, is depicted. Areas of negative longitudinal velocity values, where recirculation occurs can be observed due to two reasons, namely: the occurrence of the aforementioned lateral flow detachment and the presence of the hydraulic jump roller.

Flow detachment is an undesirable phenomenon in cases like this and could be avoided by using a smoother transition approach. Nevertheless, in the case under study, this recirculation region remains small and does not seem to be prone to cause problems such as instabilities, fluctuations, etc.

Numerical and experimental results demonstrate that the downstream water level $(5.01m)$ is not reached at the end of the stilling basin so, technically, the hydraulic jump would not be completely confined within this stretch. However, as Fig. 5.17 shows, the hydraulic jump feature most prone to cause damage to the SCS structure, i.e. shear stress, is perfectly controlled and only affects to the tips of the first three macro-roughness elements. An important decrease and stabilization of this variable is observed before the flow reaches the transition section. It is
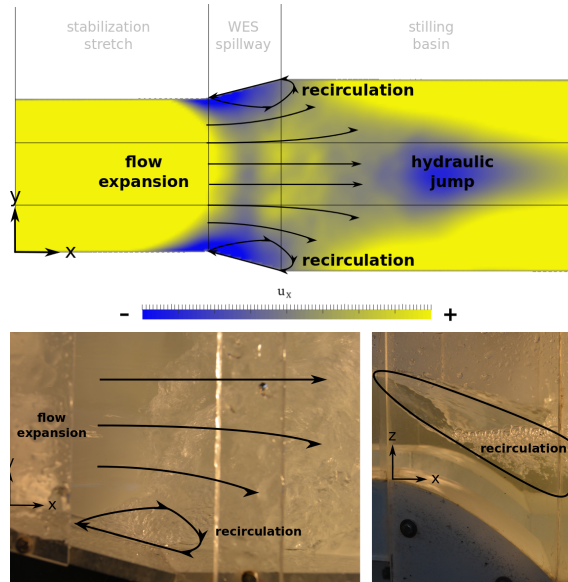
Figure 5.16: Recirculation region comparison between numerical model (top) and physical model (bottom) at spillway.

important to remark that, as a wall function is employed, the exact quantification of shear stresses is uncertain. For this reason, a maximum-minimum qualitative scale is used instead of the actual values yielded by the numerical model.
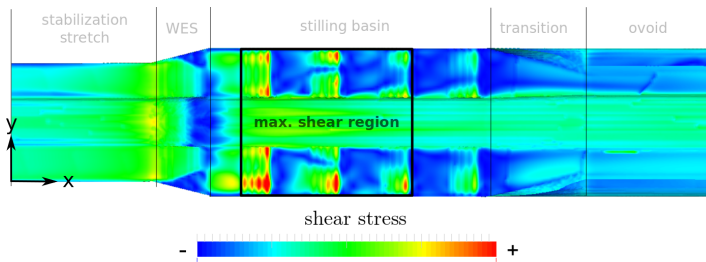
Figure 5.17: Shear stresses on streambed at spillway, stilling basin and transition to old channel section.

Chapter 6

Conclusions

An analysis of behavior of CFD models applied to the flow in hydraulic structures is presented herein. To this end, a fully three-dimensional CFD-based method to model the behavior of different types of air-water flows in dams and flumes using CFD techniques is developed and tested. Structured rectangular meshes are employed to model the analyzed domain. The presence of two fluids is modeled using the VOF approach and simulations are run using the PIMPLE algorithm. The analysis is conducted separately on stepped spillways (see Appx. C) and stilling basins, where a hydraulic jump is forced to disipate energy (see Appx. A and B). Finally, a case of practical application, where the model is applied to an entire structure, is also presented (see Appx. D), proving the applicability of the model to real design cases. To the best of the Author's knowledge, such a thorough analysis has not been conducted so far, which constitutes the main novelty of this PhD thesis.

Mesh independence is assessed and validation using experimental data is conducted on all the study cases. The sensitivity of the model to certain parameters is extensively discussed. Among them, special attention is paid to turbulence model, discretization scheme, surface tracking approach, CFD code or boundary conditions. Pros and contras of the different possibilities are discussed.

In the case of stepped spillways, the analyzed turbulence models are the Standard $k - \varepsilon$, the Realizable $k - \varepsilon$, the RNG $k - \varepsilon$, and the SST $k - \omega$. The effect of three different discretization schemes is also analyzed, namely: a first-order upwind method, the second-order limited Van Leer [1977] method, and a second-order limited central difference method. Additionally, the performance of two different VOF approaches is studied: the Partial VOF, as implemented in OpenFOAM, and the TruVOF, as implemented in FLOW-3D.

Second-order discretization schemes yield more accurate results than their first-order counterparts. The limited central-difference scheme seems to systematically achieve accuracies between 5% and 10% higher employing approximately 30% smaller computational times than the Van Leer [1977] scheme. The $k - \varepsilon$ models yield virtually the same results (differences are on average below 1%), although a slightly better performance can be attributed to the RNG $k - \varepsilon$ model in the prediction of certain variables, such as water depths or the profiles within the boundary layer, although this difference is not significant. The SST $k - \omega$ model tends to be slightly less accurate in the prediction of most of indicator variables.

Both codes, OpenFOAM and FLOW-3D, with their respective VOF approaches, reproduce well the flow behavior. Both tend to slightly overestimate free surface heights, although results with FLOW-3D are marginally closer to the experimental data. The RMSE remains in all cases between 4% and 6%. As regards velocity profiles, OpenFOAM achieves better results than FLOW-3D. This may be due, among other causes, to the fact that the TruVOF does not account for free-surface tangential stresses.

The largest errors occurr in the estimation of the distance to the inception point. Both Partial VOF and TruVOF overestimate this variable by 14% and 30%, respectively, compared to the reference experimental data. Compared to Chanson [2002] these errors decrease to 2% and 7%, respectively. It is worth remarking that determining the precise location of the inception point, either numerically or experimentally, entails high degrees of uncertainty. All details concerning the stepped spillway model are discussed in depth in Appx. C and published in Bayon et al. [2017].

As regards the analysis of hydraulic jumps occuring in stilling basins, the analyzed turbulence models are the Standard $k - \varepsilon$, the RNG $k - \varepsilon$ model, and the SST $k - \omega$ model. The performance of both codes, OpenFOAM and FLOW-3D, is compared as well. The roller length appears to be the most sensitive variable to model parameters (the SST $k - \omega$ is not even able to capture this magnitude).

The water free surface is accurately reproduced by all turbulence models in average terms, being the Standard $k - \varepsilon$ the most accurate approach. An instant observation of the results shows that the SST $k - \omega$ model surface looks more turbulent than that of its $k - \varepsilon$ counterparts. Anyway, the accuracy of all of the variables analyzed is above 98%.

As discussed above, the most accurate turbulence model in this kind of applications is the RNG $k - \varepsilon$, although this model proved to be slightly slower than the Standard $k - \varepsilon$. The latter turbulence model could be a better choice in cases where low computational requirements are preferred without compromising accuracy excessively.

The comparison of the influence of the employed CFD code shows that certain variables are best modeled by one code and others, by the other one. Thus, FLOW-3D reproduces better the interaction between supercritical and subcritical flow and all derived variables, such as sequent depth ratio. However, OpenFOAM reproduces better the internal structure of the hydraulic jump, which can be observed in the more accurate estimation of the roller length. Regarding velocity fields, backward velocities and velocity profiles are slightly better reproduced by OpenFOAM, whereas the maximum velocity decay is better estimated by FLOW-3D.

The flow in hydraulic jumps shows a more chaotic behavior and patterns of longer periods than than the flow in stepped spillways. This quasi-periodic behavior is observed in some variables, such as the hydraulic jump toe location, the roller end location and the subcritical flow depth. This phenomenon is analized using the so-called Autocorrelation Function and the Fast Fourier Transform, leading to the conclusion that all these variables show dominant frequencies in the same order of magnitude.

Additionally, a different type of subcritical flow outlet boundary condition is presented. This novel approach avoids the need to add an additional stretch of channel with an obstacle to force the subcritical flow to occur, with the subsequent saving of computational resources (up to 30% in some cases) with no effects on the model accuracy and stability. All details concerning the hydraulic jump model are discussed in depth in Appx. A and B and published in Bayon and Lopez-Jimenez [2015] and Bayon et al. [2016].

A practical case of application is also presented to check the model applicability to real design cases. The case consists of a stretch of the South Valencia Sewage Collection System (SCS) modification proposed to avoid conflict with the new high-speed railway access to the city. A case corresponding to the design flow rate $(100 m^3/s)$ is run, which passes over a WES-type spillway, rapidly reentering the original channel section. In order to ensure appropriate flow restitution conditions to the old SCS layout downstream of the modification analyzed, a hydraulic jump has to be forced at a stilling basin placed after the critical flow section.

The water level profile is numerically computed and compared to experimental results and good agreement is found among both sets of data. Although the whole hydraulic jump is not contained within the stilling basin stricto senso, its position is perfectly stabilized right downstream of the weir. Besides, it is observed that no flow pressurization occurs when reaching the old channel layout and shear stresses, one of the most hazardous effects of hydraulic jumps in hydraulic structures, are proved to be confined within the stilling basin.

Besides the model validation, a sensitivity analysis to three turbulence models is conducted, namely: Standard $k - \varepsilon$, RNG $k - \varepsilon$, and SST $k - \omega$. Again, the Standard $k - \varepsilon$ proved to be the most reliable in capturing the hydraulic jump free

surface profile, achieving an accuracy of $R^2 = 0.944$. The other two turbulence tested models also managed to reproduce the physics of the phenomenon under study and yielded R^2 values just slightly below that of the Standard $k - \varepsilon$.

All details concerning the stepped spillway model are discussed in depth in Appx. D and published in Bayon et al. [2015b]. Further work on this particular numerical model has been conducted by Teuber et al. [2017].

As discussed below, given the result accuracy achieved in all cases, the proposed model is fully applicable to more complex design cases, where stilling basins, stepped spillways and hydraulic structures in general are to be investigated. The model could also be part of an integral method to design real-life hydraulic structures, provided that reliable validation elements support its results. Another asset of this model is that it is entirely based on open source software, which allows the application of the model to a wider range of hydraulic engineering cases without having to pay for costly software licenses.

As future work, the most immediate improvement to the CFD modeling of hydraulic structures would be the implementation of an aeration sub-model, capable of going beyond the current state of the art of VOF approaches by providing reliable information on air concentration profiles, bubble count rate, bubble chord time and bubble pseudo-chord length. This model should be capable of estimating these variables both in the aerated region of the flow in stepped spillways and in hydraulic jumps or any other phenomenon characterized by free surface breakage and large air entrainment processes.

Appendices

Appendix A

Numerical analysis of hydraulic jumps using OpenFOAM

Reference

Arnau Bayon and Petra Amparo Lopez-Jimenez. Numerical analysis of hydraulic jumps using OpenFOAM. *Journal of Hydroinformatics*, 17(4):662–678, 2015. DOI: https://doi.org/10.2166/hydro.2015.041.

Abstract

The present paper deals with the hydraulic jump study, characterization and numerical modeling. Hydraulic jumps constitute a common phenomenon in hydraulics of open channels that increases the shear stress on streambeds, so promoting their erosion. A three-dimensional computational fluid dynamics (CFD) model is proposed to analyze hydraulic jumps in horizontal smooth rectangular prismatic open air channels (i.e. the so-called classical hydraulic jump). Turbulence is modeled using three widely used RANS models, namely: Standard $k - \varepsilon$, RNG $k - \varepsilon$ and SST $k - \omega$. The coexistence of two-fluids and the definition of an interface between them are treated using a volume method in Cartesian grids of several element sizes. An innovative way to deal with the outlet boundary condition that allows reducing the size of the simulated domain is presented. A case study is conducted for validation purposes ($Fr_1 \approx 6.10$, $Re_1 \approx 3.5 \cdot 10^5$): several variables of interest are computed (sequent depths, efficiency, roller length, free surface profile, etc.) and compared to previous studies, achieving accuracies above 98% in all cases. In the light of the results, the model can be applied to real-life cases of design of hydraulic structures.

Keywords: Hydraulic jump; Open channel; OpenFOAM; RANS; k-ϵ; k-ω.

A.1 Introduction

Hydraulic jumps are the most used method to dissipate energy in hydraulic structures and occur in water flows suddenly changing of regime from supercritical to subcritical. This virulent phenomenon is characterized by large pressure and velocity fluctuations, air entrainment and turbulent dissipation processes. It can therefore trigger erosion processes or scour on hydraulic structures of calamitous consequences. By definition, hydraulic jumps occur in gravity-driven flows when the Froude number (ratio of inertia to gravitational forces) drops below unity. The Froude number is a dimensionless number of Fluid Mechanics that, in horizontal channels at a given section i, can be computed as Eq. A.1 indicates:

$$Fr_i = \frac{u_i}{\sqrt{gh_i}} \tag{A.1}$$

Where u_i is flow freestream velocity, g, acceleration of gravity, and h_i, water depth. Despite the fact that the nature of hydraulic jumps is essentially chaotic, within a certain range of approaching Froude numbers (Fr_1), this phenomenon can become stable to a certain extent. According to Hager [1992] stabilized hydraulic jumps occur when $Fr_1 \in [4.5, 9.0]$. Lower values produce transition jumps, characterized by low efficiencies and the formation of long waves of irregular period, whereas higher Froude numbers produce choppy jumps, which are unstable and prone to

flow detachment and wave and spray formation. For this reason, most of stilling basin design guidelines, such as that of the U.S. Bureau of Reclamation [Peterka, 1984], recommend aiming at Froude number values that produce stabilized hydraulic jumps.

Characterizing and analyzing this phenomenon is of paramount importance from both the technical and the environmental point of view. Hager [1992] and Chanson [2013] performed extensive reviews on the attempts to study this phenomenon throughout history. Some of these works focused in a theoretical comprehension of the characteristic features of the classical hydraulic jump. The so-called classical hydraulic jump is defined by Hager [1992] as the hydraulic jump that occurs in smooth horizontal prismatic rectangular channels. Resch and Leutheusser [1972] performed a thorough study on air entrapment and energy dissipation processes depending on the inlet flow characteristics. Gualtieri and Chanson [2007] extended this analysis to a wider range of inlet flow conditions.

Most of the studies performed up until today focused on the analysis of easily-measurable external macroscopic variables using an experimental approach. This can partially be explained by the difficulty of measuring certain variables using non-intrusive acoustic and optical methods in highly aerated flows [Ma et al., 2011]. However, since the 1970s, coinciding with the emergence of computational fluid dynamics (CFD), more and more studies on the hydraulic jump are conducted by means of numerical methods. In this regard, computational techniques brought a brand new approach to water engineering modeling. E.g., some hard-to-model phenomena, such as heat transfer [Thomas et al., 1990] or coupled biological processes [Muttil and Chau, 2006], could be for the first time implemented thanks to numerical methods. This implied a whole paradigm shift and so the literature on this topic is vast: e.g. Ma et al. [2011], among others, modeled hydraulic jumps using different CFD techniques. Caisley et al. [1999] managed to reproduce accurately a hydraulic jump in a canoe chute using FLOW-3D. Also Bombardelli et al. [2011] used this commercial software to successfully model a stepped spillway following a similar approach of that proposed here. Other approaches different from CFD have also been used in all kind of water engineering applications. E.g. De Padova et al. [2013] successfully reproduced a hydraulic jump using techniques of Smoothed Particle Hydrodynamics (SPH).

However, as Murzyn and Chanson [2009b] state, mathematical models still have problems to reproduce the physics of certain hydraulic phenomena, although they can contribute to their better comprehension. As Romagnoli et al. [2009] remark, an entire comprehension of the hydraulic jump internal flow features and turbulence structures has not been achieved so far. For Murzyn and Chanson [2009b], the main features of hydraulic jumps that have not been fully understood are the following: fluid mixing, bubble break-up and coalescence, free surface turbulent interactions and wave formation and breaking processes.

Other authors used a CFD approach to analyze hydraulic jumps in terms of shear stresses, potential erosion on stream boundaries and other more practical applications [Chanson, 2000]. Liu and Garcia [2008] published a model combining the CFD code OpenFOAM and the Exner Equation to model erosion and sedimentation processes in hydraulic structures using mesh deformation.

Nevertheless, despite the increasing number of publications in this area, in the numerical modeling of hydraulic structures and water engineering applications, deterministic models (e.g. CFD) are overwhelmed in number by their statistical counterparts, also known as "black box" models [Chau et al., 2005]. Thus, several authors used artificial neural networks (AAN) to successfully predict the scour occurred at hydraulic structures, such as bridge piers [Toth and Brandimarte, 2011] or culvert outlets [Liriano and Day, 2001]. Taormina et al. [2012] and Cheng et al. [2005] used AAN to successfully predict aquifer discharge processes. Farhoudi et al. [2010] used fuzzy logic methods to analyze the scour downstream of stilling basins. Other authors used one-dimensional and two-dimensional approaches to reproduce the flow in similar geometries [Dewals et al., 2004]. However, in hydraulic engineering, flows are generally strongly three-dimensional [Ahmed and Rajaratnam, 1997]. Therefore, the use of a fully three-dimensional deterministic model, such as here proposed, allows its application to a wider range of cases. Comparisons among different numerical methods to model hydrological and hydraulic phenomena can be found in the literature [Chen and Chau, 2006, Wu et al., 2009].

The main goal of this work is to propose a fully three-dimensional CFD-based method to model classical hydraulic jumps using the open-source platform Open-FOAM. The use of freely-available open source codes allows a continuous community-based improvement of the model and avoids having to pay for costly software licenses. In this sense, other models can be found, also reproducing hydraulic jumps using OpenFOAM [Romagnoli et al., 2009, Witt et al., 2013]. However, different outlet boundary conditions are herein presented. This change constitutes an asset as it allows bringing the model boundaries closer to the hydraulic jump, which involves a significant saving of computational resources.

A case study is also conducted, where several variables of interest, such as hydraulic jump efficiency or roller length, are computed and compared to previous analytical and experimental studies. The sensitivity of the model to certain parameters, such as mesh element size, turbulence model used or boundary conditions, is assessed.

As discussed in further sections, given the result accuracy achieved, this model is fully applicable to more complex geometries where hydraulic jumps have to be investigated, such as dam spillways, stilling basins, river rapids, etc.

A.2 Methods

A.2.1 Geometry and mesh

In this model of the hydraulic jump, the geometry to discretize is rather simple: the domain consists of a prismatic rectangular channel. For this discretization, two big categories of approaches are normally used, namely: unstructured and structured meshing.

Unstructured meshes are generally better suited for a selective refinement, so preventing the over-refinement of regions where no large gradients of property are expected [Kim and Boysan, 1999]. Besides, this kind of meshes fit better into complex geometries, show less closure issues and their arbitrary topology makes automatizing the meshing process easier [Biswas and Strawn, 1998]. Neverthe-les, none of these advantages applies to the case under study, as the geometry is extremely simple and no mesh refinement is required.

Some authors state that mesh non-orthogonality does not affect results as long as the skewness of its elements is kept low enough [Huang and Prosperetti, 1994]. Nevertheless, structured meshes tend to be more accurate than their unstructured counterparts caeteris paribus [Biswas and Strawn, 1998]. Besides, structured meshing algorithms are generally more straight forward to implement and faster to execute. According to Keyes et al. [2000], structured meshing algorithms present a more regular access to memory, which significantly reduces its latency. Also, as discussed below, in multiphase flows, topologically orthogonal meshes with their axis aligned with the fluid interface tend to show less numerical problems. For all these reasons, a static structured rectangular hexahedral mesh is considered the best choice.

In some cases, meshes can be slightly refined in the vicinity of solid boundaries for accurately resolving the flow features in boundary layers, where larger property gradients occur. This may result in the formation of highly skewed elements, although this is not a real issue as long as orthogonality between the mesh axes and solid boundaries is ensured [Hirsch, 2007]. However, in this case, experience demonstrates that the mesh element size necessary to capture the freestream flow features is not smaller than that necessary to resolve the boundary layer features. As a consequence, cubic mesh elements of uniform size Δx are used throughout the entire domain (see Fig. A.1). The optimum mesh element size is highly case specific so, it is determined by means of a mesh sensitivity analysis.
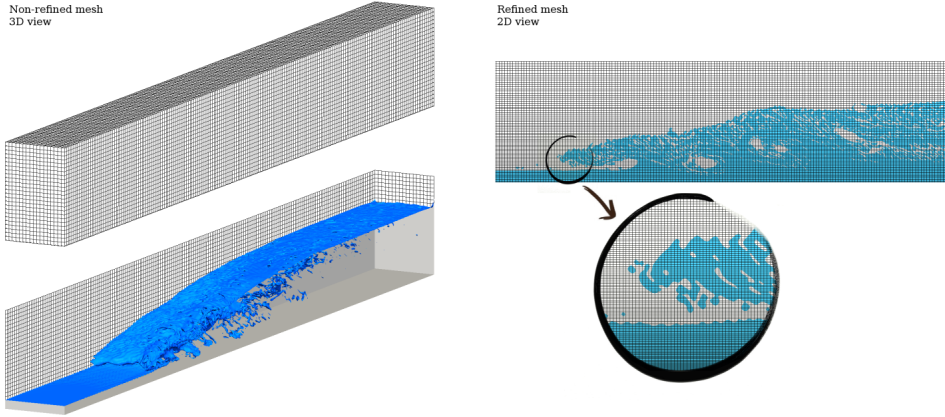
Figure A.1: Example of a mesh used in the model with zoom on the jump toe region.

A.2.2 Numerical model

Water level of open channel flows can be obtained by shallow wave approaches. However, they are not sufficient when modeling complex geometries as only a water depth value is assigned to each point on the streambed. In cases where a full description of the flow characteristics is necessary, resolving the Navier-Stokes Equations becomes a must. Eq. A.2 and A.3 are the Navier-Stokes Equations for mass and momentum conservation in their incompressible form. Unfortunately, their complete analytical resolution has not been achieved so far, so numerical models are necessary to approximate a solution to every problem involving fluid motion.

$$\nabla \vec{u} = 0 \tag{A.2}$$

$$\frac{\partial \vec{u}}{\partial t} + \vec{u} \cdot \nabla \vec{u} = \frac{-1}{\rho} \nabla p + \upsilon \nabla^2 \vec{u} + \vec{f_b} \tag{A.3}$$

Where u is velocity, p, pressure, t, time, ρ, density, υ, kinematic viscosity, and f_b, body forces (gravity and surface tension). The flow is assumed to be incompressible in order to save computational resources and so density varying terms have been cancelled out. This assumption can be done as Mach numbers (ratio of the flow velocity to the sound velocity) are below the commonly accepted threshold of $Ma < 0.3$ [Young et al., 2010]).

A wealth of algorithms has been developed to approximate numerically the Navier-Stokes Equations during the last decades. Nevertheless, none of them constitutes

a perfect solution as their performance is highly case specific. Indeed, this is a topic extensively discussed in the literature [Barton, 1998, Jang et al., 1986]. It is important to remark that the algorithm performances are generally assessed in terms of computation requirements and stability as, eventually, all algorithms should converge to a similar solution. The most widely used algorithm to execute stationary simulations and normally the default option in all CFD codes is the SIMPLE algorithm [Patankar and Spalding, 1972]. Several improvements to its original implementation, such as SIMPLER or SIMPLEC, have been made since the model was developed. One of the most used variations is the PISO algorithm [Issa, 1985]. However, problems may arise when dealing with multiphase flows where phase changes are abrupt or the density difference is large [Brennan, 2001]. In order to overcome this issue, an algorithm was developed combining the best features of SIMPLE and PISO; the so-called PIMPLE [OpenFOAM User Guide, 2011]. This algorithm merges the outer-correction tools of SIMPLE with the inner-corrector loop of PISO in order to achieve a more robust and generalizable pressure-velocity coupling [Rodrigues et al., 2011].

Hence, the PIMPLE algorithm is here used as a good compromise between computation requirements and stability. This algorithm is implemented in OpenFOAM, a freely available open source platform constituted by all sort of C++ applications and libraries to solve all kinds of continuum mechanics problems [Weller et al., 1998]. This code uses a tensorial approach and object-oriented programming techniques following the widely known Finite Volume Method (FVM), first used by McDonald [1971]. An in-depth explanation of the algortihm implementation can be found in the PhD Thesis of Jasak [1996], Ubbink [1997] and Rusche [2002].

A.2.3   Water surface tracking

The coexistence and interaction of several fluids and the way that the interface among them is defined is of paramount importance in numerical modeling of multiphase flows. Complex algorithms must be developed to model this phenomenon, whose stability and accuracy have a strong influence on the model final results [Hyman, 1984]. Surface tracking methods fall into two families of approaches, namely: the surface methods and the volume methods. On the one hand, surface methods explicitly define the free interface either using a Lagrangian approach, i.e. tracking a set of surface marker particles [Daly, 1969], or using an Eulerian approach, i.e. defining functions that determine the free surface position [Osher and Sethian, 1988]. These methods present topology issues when dealing with highly deformed flows and breaking surfaces. For this reason, they are not considered appropriate to model hydraulic jumps.

On the other hand, volume methods adapt better to this kind of phenomena, but do not define a neat flow interface explicitly. Instead, a surface tracking method has to be implemented in the model. Some models use an Eulerian-Lagrangian approach

(particles on fluid methods) combining an Eulerian flow resolution with particle tracking [Harlow and Welch, 1965]. However, in three-dimensional models, the large number of necessary particles makes the computational cost of this approach unaffordable. For this reason, an entirely Eulerian approach is used in the present model. This kind of approaches proved to be more computationally efficient as they only have to deal with a single variable value per mesh element [Ubbink, 1997]. This variable is an indicator property (α) expressing the proportion of one fluid or another that every mesh element contains. Its distribution throughout the domain is modeled by approximating an additional convection transport equation (Eq. A.4). This implies considering both fluids, A and B, as a single multiphase fluid, whose properties are treated as weighted averages according to the fraction occupied by one fluid or another in each mesh element (see Eq. A.5). This results in a set of α values between 0 and 1 throughout the entire modeled domain but no clear water-air interface is defined a priori.

$$\frac{\partial \alpha}{\partial t} + \nabla \cdot (\vec{u}\alpha) = 0 \tag{A.4}$$

$$\xi = \xi_a \alpha + \xi_b (1 - \alpha) \tag{A.5}$$

Where α is fluid fraction, u, velocity, t, time, and ξ represents a flow generic property. As regards the method used to clean up the misty zones and so define a neat interface, a wealth of approaches has been developed during the last decades. The traditional line techniques, such as SLIC [Noh and Woodward, 1976], PLIC [Youngs, 1984] or FLAIR [Ashgriz and Poo, 1991], provided the first viable solutions to the surface definition issue in volume methods. However, they present problems of generalization to unstructured meshes. The donor-acceptor methods, such as the original implementation of the VOF [Hirt and Nichols, 1981], have been widely used in the past, but they are prone to show false interface deformation issues.

In the present model, an interface compression algorithm is implemented in order to overcome the aforementioned issues. This method adds an extra term in the left hand side of Eq. A.4: $\nabla \cdot (\vec{u}_c \alpha [1 - \alpha])$, where $\vec{u}_c$ is a compression velocity with normal direction to the fluid interface. Multiplying $\vec{u}_c$ by $\alpha[1 - \alpha]$ ensures that it will only affect those regions where the flow fraction is close to 0.5 [Rusche, 2002].

A.2.4 Flow aeration

The aeration of a water flow modifies its volume, depth, density and compressibility [Carvalho, 2002], thus affecting the momentum transfer. It also reduces the scour risk by cavitation [Bung and Schlenkhoff, 2010] and the shear stresses on the channel boundaries [Chanson, 1994]. Therefore, this is a phenomenon of paramount importance in highly aerated flows as hydraulic jumps, bores, breaking waves, etc. Unfortunately, surface tracking methods per se cannot reproduce phenomena smaller than the mesh element size, such as bubbles and droplets, or the entrapment of large amounts of air [Toge, 2012]. To overcome this issue, additional air-entrainment models are implemented. In low-aerated flows, an Eulerian-Lagrangian approach is possible, where the Navier-Stokes Equations are resolved and air is treated as a set of discrete particles. With larger air fractions, this approach is no longer possible and an entirely Eulerian method is necessary. Eulerian-Eulerian approaches yield better results than their Eulerian-Lagrangian counterparts in the latter case. Despite the fact that they require longer computation times, in entirely Eulerian approaches, buoyancy, drag and lift forces are taken into account. For this reason, in the case of the model proposed here, an Eulerian-Eulerian approach is implemented.

A.2.5 Turbulence

Turbulence features can either be resolved down to their lowest scales (Direct Numerical Simulation or DNS), if the mesh is accordingly fine, or modeled under a wealth of different approaches. Despite it has been reported the application of DNS models to multiphase flows [Borue et al., 1995], in most cases turbulence features are partial or completely modeled in common engineering applications.

Large Eddy Simulation (LES) approaches are also feasible to model multiphase flows. Nevertheless, the most used technique is the Reynolds Averaged Navier-Stokes (RANS). In these models, the so-called Reynolds stresses are averaged to find a closure to the Navier-Stokes equations. To do so, additional transport equations are implemented in order to model the behavior of flow turbulence. Among the available models, the performance of three of the most used is here studied. The assessed models are the Standard $k - \varepsilon$ [Launder and Sharma, 1974], the RNG $k - \varepsilon$ [Yakhot et al., 1992] and the SST $k - \omega$ [Menter, 1993]. The Standard $k - \varepsilon$ model has been widely used in this kind of applications [Lopez and Garcia, 2001]. Its formulation is depicted in Eq. A.6 and A.7:

$$\frac{\partial}{\partial t}\left(\rho k\right) + \frac{\partial}{\partial x_i}\left(\rho k u_i\right) = \frac{\partial}{\partial x_j}\left[\left(\mu + \frac{\mu_t}{\sigma_k}\right)\frac{\partial k}{\partial x_j}\right] + P_k + P_b - \rho\varepsilon - Y_M + S_k \quad \text{(A.6)}$$

$$\frac{\partial}{\partial t}\left(\rho\varepsilon\right) + \frac{\partial}{\partial x_i}\left(\rho\varepsilon u_i\right) = \frac{\partial}{\partial x_j}\left[\left(\mu + \frac{\mu_t}{\sigma_\varepsilon}\right)\frac{\partial\varepsilon}{\partial x_j}\right] + C_{1\varepsilon}\frac{\varepsilon}{k}\left(P_k + C_{3\varepsilon}P_b\right) - C_{2\varepsilon}\rho\frac{\varepsilon^2}{k} + S_\varepsilon$$

$$\text{(A.7)}$$

Where k is turbulence kinetic energy, ε, dissipation rate of k, t, time, ρ, density, x_i, coordinate in the i axis, μ, dynamic viscosity, μ_t, turbulent dynamic viscosity, P_k, production of turbulent kinetic energy, P_b, buoyancy effect, Y_M, dilatation effect, and S_k and S_ε, modulus of mean rate-of-strain tensor. The rest of terms, $(C_\mu, C_{1\varepsilon}, C_{2\varepsilon}, C_{3\varepsilon}, \sigma_k, \text{ and } \sigma_\varepsilon)$ are model parameters that, in the Standard $k - \varepsilon$ model, are 0.09, 1.44, 1.92, −0.33, 1.0, and 1.3, respectively.

The RNG $k - \varepsilon$ model formulation differs from that of the Standard $k - \varepsilon$, essentially, in the values of the aforementioned parameters. These changes seem to improve the model results to such an extent that, according to Bradshaw [1996], the RNG $k - \varepsilon$ is the most used model in hydraulic applications.

Several authors claim that $k - \varepsilon$ models are not suitable to model large adverse-pressure gradient flows [Menter, 1993, Wilcox et al., 1998]. In order to overcome this issue, $k - \omega$ models were first introduced by [Wilcox et al., 1998]. Their implementation is significantly different from that of $k - \varepsilon$, as the dissipation rate of turbulence kinetic energy (ε) is not modeled. Instead, a transport equation for its relative value ($\omega = \varepsilon/k$) is implemented. Among them, the SST $k - \omega$ [Menter, 1993] proved to perform better than the Standard and the BSL $k - \omega$.

The suitability of one model or another is highly case specific and differences from using one model or another are normally remarkable. Hence, in order to determine which model performs best at a reasonable computational cost, a sensitivity analysis is conducted. To do so, simulations are run using the three RANS models discussed above caeteris paribus.

A.2.6   Boundary conditions

The boundary conditions imposed to force the hydraulic jump to occur consist of a supercritical flow inlet, a subcritical flow outlet, smooth bottom and side walls and an upper open air patch (see Fig. A.2). At the inlet, in order to fulfill the desired Froude number, a water depth (h_1) and a potential velocity profile are imposed using a Dirichlet boundary condition. The pressure value is defined as a null von Neumann boundary condition, so forcing a hydrostatic profile. As regards the inlet variables of the RANS model, i.e. k, ε and ω, they cannot be directly estimated from measurements. Instead, they are set to an arbitrary low value and a short initial stretch of channel is added in order for the flow to develop while approaching the hydraulic jump.
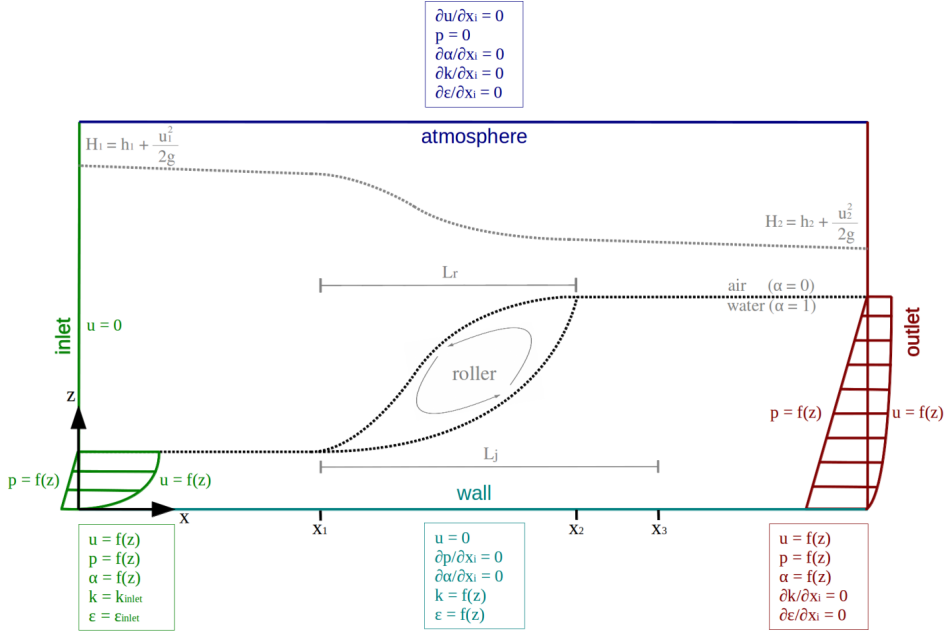
Figure A.2: General scheme of a hydraulic jump and boundary conditions used in the model.

As regards the outlet, the subcritical water height that forces the hydraulic jump to occur within the simulated domain (h_2) has to be imposed. This variable has to be obtained by iteratively testing values until the resulting hydraulic jump remains stable within the domain. Normally, a subcritical water height and a hydrostatic profile should be imposed at the outlet by means of a Dirichlet water level boundary condition. This, combined with a null Von Neumann boundary condition for velocity, would allow the flow to leave the domain freely. However, the imposition of a subcritical outlet by means of this approach in OpenFOAM appears to cause stability issues.

Indeed, to the knowledge of the authors, all cases of hydraulic jump simulations using OpenFOAM reported in the literature, such as Romagnoli et al. [2009] or Witt et al. [2013], have had to bypass this issue. To do so, they added an additional stretch of channel with an obstacle on the streambed, such as a step, a gate or a ramp, followed by a conventional free outlet.

In the present model, this problem is overcome by imposing a velocity profile at the outlet and so letting the hydrostatic profile to develop, as it is done at the inlet boundary condition. Assuming mass conservation, this approach univocally produces a given water height. This avoids having to model the aforementioned

extra stretch of channel. As this implies bringing the boundary conditions closer to the phenomenon under study, comparative simulations are run in order to assess the model sensitivity to the boundary condition type.

A no-slip condition is imposed at the walls and roughness is not considered [Hager, 1992]. An atmospheric boundary condition is imposed at the top of the channel to allow fluids to enter and leave the channel. This is achieved by imposing a null Von Neumann condition to all variables except for pressure, which is set to zero (atmospheric pressure). Fig. A.2 summarizes the model boundary conditions and some of its most relevant variables to analyze.

A.2.7   Wall treatment

The way the boundary layer is treated is of paramount importance in fluid modeling. Von Karman [1930] established a universal law of the wall which defines the flow velocity profiles in the boundary layer. Velocity (u) and distance to wall (y) are respectively adimensionalized using the shear velocity (u_τ) and the viscosity (v):

$$y^+ = y\frac{u_\tau}{v} \tag{A.8}$$

$$u^+ = \frac{u}{u_\tau} \tag{A.9}$$

The lowest y^+ regions, the so-called viscous sub-layer [Schlichting and Gersten, 2000], are characterized by large gradients of velocity and other properties and the predominance of viscous effects. In order to avoid having to resolve these regions, wall functions are often used in CFD models. These functions are imposed as boundary conditions on solid patches to avoid the use of excessively fine meshes, with the subsequent saving of computational resources. As a consequence, the model mesh has to be refined so that the y^+ coordinate of the center of all mesh elements in touch with solid walls be somewhere between the buffer and the logarithmic sub-layers ($y^+{\sim}30$). It is important not to over-refine meshes when using wall functions. If this happens, wall functions will be modeling the viscous sub-layer, whereas the model itself would be resolving the flow in this region. This controversy may cause that finer meshes yield less accurate results.

In terms of accuracy, the best choice would be using a low-Reynolds-number model with no wall function at all. However, this implies refining the mesh to such an extent that the computational cost may become unaffordable. There is vast literature on improvements to the original implementation of wall functions, such as Johnson and Launder [1982], but most of the solutions proposed have not been adopted by most of CFD codes. This is due to the fact that, despite these

approaches are valid from a theoretical point of view, many of them may cause stability issues [Blocken et al., 2007].

In this research, a high-Reynolds-number wall function for RANS models and smooth solid surfaces is implemented. The boundary layer in a case of these characteristics is likely to be slightly skewed [Taylor, 1959]. Nevertheless, as the flow mainstream direction is completely longitudinal, a bi-dimensional wall function is used for the sake of simplicity.

A.2.8 Discretization schemes

As regards the discretization schemes used to make the CFD model partial differential equations numerically approximable, a good choice always must be a good compromise between accuracy and stability. In spatial discretization, upwind models are generally preferred to downwind approaches as the latter tend to show severe stability issues. Compared to central differencing schemes, upwind approaches are slower, but also less diffusive and so more accurate. The problem is that, when abrupt property gradients occur, the latter schemes may require limiters in order to prevent spurious oscillations [Blazek, 2005]. Once limited, upwind schemes, such as Van Leer [1982], are very appealing to discretize abruptly-varied properties. The only drawback is that, when limited, these schemes become first order accurate.

In the present model, the fluid fraction divergence terms (α) are discretized using a limited Van Leer approach due to its abruptly variable nature. In the case of the RANS model variables, divergence terms are discretized using an unlimited upwind approach as they are less prone to cause stability issues. The velocity divergence terms are discretized using a central differencing scheme in order to avoid possible instabilities as well as to reduce computation times. Also all gradient and interpolation terms of the model are discretized using this approach. Gaussian standard FVM is used to interpolate the variable values from cell centers to their faces. In order to save computational resources, as this mesh is strictly Cartesian, no orthogonality corrector is applied.

As regards the discretization of time derivatives, explicit schemes tend to be computationally lighter than their implicit homologues. However, they are also more unstable, especially, in simulations with skewed meshes [Blazek, 2005] or when solving RANS equations [Lafon and Yee, 1992-01-06]. Therefore, implicit time discretization schemes are preferred in this model. This implies slightly longer computation times and eventual accuracy problems due to phenomena such as wave damping [Casulli and Cattani, 1994], but also higher stability. Hence, a first order accurate bounded implicit Euler scheme is used to discretize time derivative terms.

The time step length is variable throughout the simulation resolution process. Its value is automatically updated after every time step in order to ensure that the maximum Courant number never overcomes a threshold of $Cr < 0.75$, ensuring convergence and stability of simulations.

A.2.9 Postprocessing

The variables analyzed and compared to previous studies are discussed in the next lines. The reference values to which model results are compared are denoted by a super-index asterisk $(*)$.

The sequent depth (Y), i.e. the ratio of subcritical to supercritical flow depth $(h_1$ and h_2, respectively), is a characteristic parameter of hydraulic jumps. According to Belanger [1841], it can be estimated as a function of the approaching Froude number using a series of simplifications of the Momentum Equation. Nevertheless, in channels of low aspect ratio (h_1/w), side walls can play an important role and this equation is no longer valid. In this regard, [Murzyn and Chanson, 2008] claim that scale effects can play an important role in channels of aspect ratio above 0.1. In order to overcome this issue, Hager and Bremen [1989] proposed the following approach introducing Blasius Equation to account for side wall friction effects, resulting:

$$Y^* = \frac{h_2}{h_1} = \frac{1}{2} \cdot \left[\sqrt{1 + 8 \cdot Fr_1^2} - 1 \right] \cdot \left[1 - 0.7 \left[\log Re_1 \right]^{-2.5} e^{\frac{Fr_1}{8}} \right] \cdot$$
$$\left[1 - 3.25 \frac{h_1}{w} e^{\frac{Fr_1}{7}} \left(\log Re_1 \right)^{-3} \right] \tag{A.10}$$

Where h_1 is supercritical water depth, w, channel width, Fr_1, approaching Froude number, Re_1, supercritical height-based Reynolds number. Another relevant variable of hydraulic jumps is the roller length (L_r), i.e. the stretch right downstream of the jump toe where water recirculation occurs and most of the air entrainment occurs. Some authors, such as Murzyn and Chanson [2009a], define the roller length as the hydraulic jump region over which the water height increases monotonically. However, in this study the stagnation point is used as a criterion to delimit the roller end. Hager [1992] proposes the following expression to estimate the roller length:

$$L_r^* = -12h_1 + 100 \cdot h_1 \cdot \tanh \frac{Fr_1}{12.5} \tag{A.11}$$

The efficiency of hydraulic jumps is defined as the ratio of the energy drop to the upstream hydraulic head. These variables are obtained from Eq. A.12 as a function of water height (h_i), flow velocity (u_i) and acceleration of gravity (g).

Eq. A.13 represents how hydraulic jump efficiency is computed. According to Hager and Sinniger [1985], in classical hydraulic jumps, the latter variable can be estimated as a function of the approaching Froude number using Eq. A.14:

$$H_i = h_i + \frac{u_i^2}{2g} \tag{A.12}$$

$$\eta = \frac{\Delta H}{H_1} = \frac{H_1 - H_2}{H_1} \tag{A.13}$$

$$\eta^* = \left(1 - \frac{\sqrt{2}}{Fr_1}\right)^2 \tag{A.14}$$

Water surface levels are a variable of paramount importance in the design of hydraulic structures. Its accurate estimation is crucial for a proper stilling basin design that avoids bank bursts. In the present work, the average water surface levels are numerically computed and compared to the expression by Bakhmeteff and Matzke [1936]:

$$\Gamma^*(x) = \tanh(1.5 \cdot X) \tag{A.15}$$

Where $\Gamma(x)$ is water level at x (h_i), non-dimensionalized following Eq. A.16, where h_1 and h_2 are supercritical and subcritical water level, respectively. The variable X is the non-dimensional longitudinal coordinate (x), computed as a function of x_0 (hydraulic jump toe position) and x_r (roller end position) as Eq. A.17 indicates:

$$\Gamma(x) = \frac{h_i - h_2}{h_1 - h_2} \tag{A.16}$$

$$X = \frac{x - x_0}{x_r - x_0} \tag{A.17}$$

The nature of hydraulic jumps is highly chaotic and unstable and so most of its characteristic variables show a quasi-periodic behavior (i.e. patterns can eventually be observed, but their characteristic period is not constant). For this reason, it is crucial to extend sufficiently the simulation time to avoid bias in the results. The authors observe that stability of the solution can be assumed when the residuals of all the variables drop below the 10^{-3} threshold and the water content of the whole modeled channel stays stable during at least $10s$.

A.2.10   Case study

A case particular study is conducted for validation purposes. The simulated case consists of a prismatic rectangular channel of dimensions $6.00m \times 0.50m \times 0.75m$ (length, width and height). The inlet flow is $Q = 0.177m^3/s$ and the supercritical depth is $h_1 = 0.070m$. Hence, the inlet velocity is $u_1 = 5.057m/s$. The subcritical depth is obtained following the procedure discussed above in this section. The density and the kinematic viscosity are $\rho = 1000kg/m^3$ and $\upsilon = 10^{-6}m/s^2$.

The approaching Froude and Reynolds numbers are $Fr_1 = 6.125$ and $Re_1 = 3.54 \cdot 10^5$, respectively. A case of Fr_1 between 6 and 7 is considered optimum for model validation as it corresponds to the middle of the range of Fr_1 values recommended by the U.S. Bureau of Reclamation [Peterka, 1984]. This approaching Froude number is assumed to be representative of the behavior of all stabilized hydraulic jumps, as described by Hager [1992].

As discussed above in this section, a mesh, turbulence and boundary condition model sensitivity analysis is conducted. Each of the turbulence models mentioned above (Standard $k - \varepsilon$, RNG $k - \varepsilon$ and SST $k - \omega$) are tested in four different sized meshes. The mesh element sizes assessed are $7.00mm$, $7.50mm$, $7.78mm$ and $8.75mm$, which means meshes of 6.511, 6.360, 4.737 and 3.467 million cells, respectively. In order to fulfill the wall treatment function hypothesis, it is checked in all cases that the y^+ coordinate mostly remains in the range of values between 20 and 70.

A.3   Results and discussion

A.3.1   Graphic analysis

A de visu analysis of the model results leads to the conclusion that a stabilized hydraulic jump is reached (see Fig. A.3). All the characteristic features of this kind of jumps described by Hager [1992] can be observed, namely: compact and stable appearance, low wave generation, gradual bubble deaeration, vortex formation within the roller, no flow separation in the entering jet, etc. Fig. A.3 shows how, downstream of the hydraulic jump, where bubble deaeration occurs, hydrostatic pressure and velocity profiles quickly reappear. Also the deaeration of large bubbles can be observed throughout the region where streamlines cut the water free surface. Downstream of that, despite waves and small bubbles do not disappear completely, the characteristics of developed flows can be observed again.

Fig. A.3 shows the wide span of bubble sizes occurred in the turbulent shear and the recirculation region of hydraulic jumps. Chanson [1994] found experimentally that the range of bubble sizes in hydraulic jumps can extend over several orders of
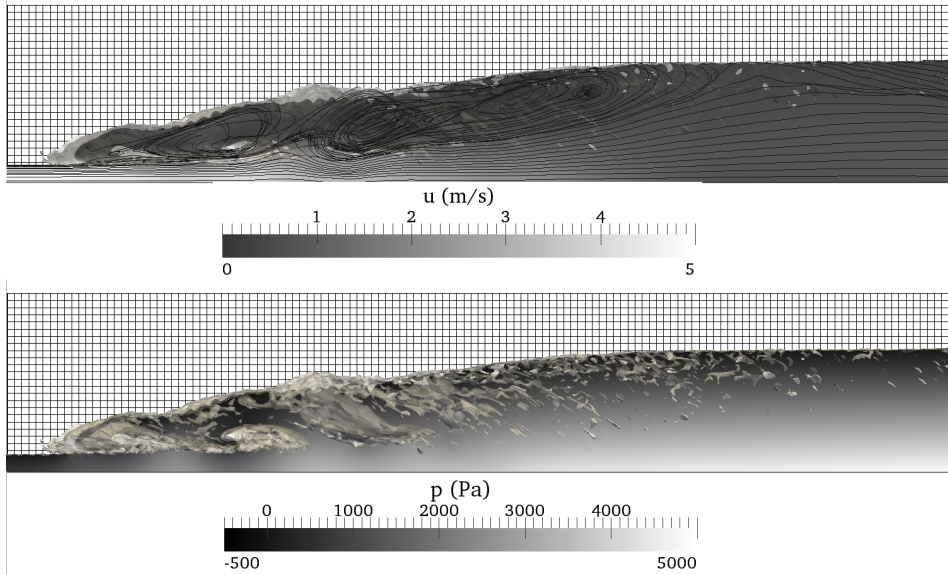
Figure A.3: Instant representation of bubble formation and velocity and pressure fields.

magnitude. The average bubble size rapidly decreases longitudinally. This is due to the fact that large bubbles cannot stay long in the recirculation region as shear stresses break them up and buoyancy forces tend to expel them [Babb and Aus, 1981]. Small bubbles are not deaerated so quickly. Indeed, they can be dragged by advection forces throughout long distances until buoyancy finally expels them.

A.3.2 Sensitivity analysis

As discussed above, a mesh, turbulence and boundary condition model sensitivity analysis is conducted in order to determine the best combination of them to achieve accurate results at an affordable computational cost.

As regards the outlet boundary condition used, Fig. A.4 shows examples of hydraulic jumps simulated using both approaches. A closer comparison between them shows no significant effect on the model outcome accuracy. Although an instant comparison, such as that in Fig. A.4, shows differences in water level profile and flow aeration, these differences completely disappear when results are averaged. No undesirable effects, such as wave formation, occur despite the new approach implies bringing the boundary conditions significantly closer to the phenomenon under study. The domain reduction achieves computation times up to 30% shorter in some cases.

Figure A.4: Instant comparison of hydraulic jumps simulated using two different outlet boundary conditions: the traditional approach (top) and a new approach (bottom).

The three tested turbulence models show small influence on the sequent depth (Y) estimations. The most accurate model is the RNG $k - \varepsilon$, followed by the SST $k - \omega$ and the Standard $k - \varepsilon$, although all errors are below 4%. The inflexion point in the accuracy of the all models can be clearly observed at a mesh size of $7.50mm$, thus being the RNG $k - \varepsilon$ model with $7.50mm$ size mesh the most accurate approach.

As regards the estimation of roller lengths, the SST $k - \omega$ model appears not to be able to capture accurately this variable. The Standard $k - \varepsilon$ model shows a reasonable accuracy (all errors are below 6%) and low sensitivity to mesh size, which is an asseet. However, RNG $k - \varepsilon$ is even more accurate and shows a perfect monotonically decreasing trend in errors, although the model is also highly sensitive to mesh size variations. The RNG $k - \varepsilon$ model with $7.00mm$ size mesh appears to be the most accurate approach in the roller length prediction.

The prediction of the hydraulic jump efficiency achieves the highest accuracy values, being the error of all models below 2%. The Standard $k - \varepsilon$ with $7.00mm$ size mesh is the most accurate (0.1%) but, as it is observed in Fig. A.5, the sensitivity of this variable to the model parameters is extremely low.

All further discussion on the results and model validation is exclusively conducted using the results of RNG $k - \varepsilon$ model with $7.00mm$ size mesh. The reason is because this approach achieved the most accurate results in the most sensitive variable (i.e. roller length) while being reasonably accurate in the prediction of the less sensitive variables.
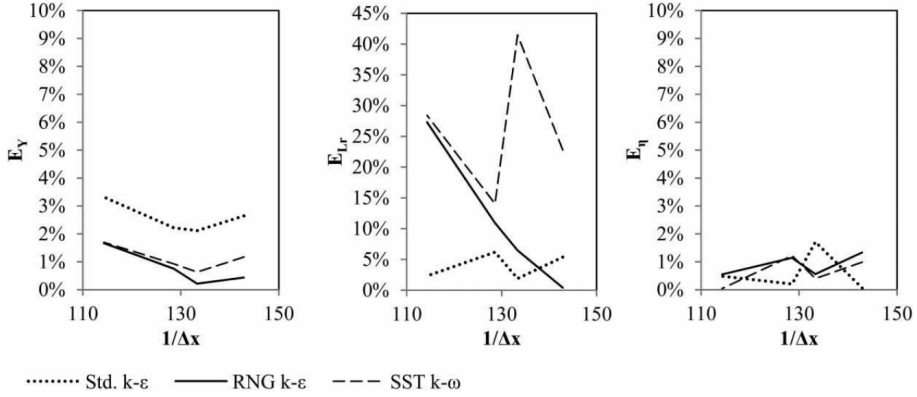
Figure A.5: Mesh and turbulence model sensitivity analysis. Relative errors in the computation of sequent depths (Y), roller lengths (L_r) and hydraulic jump efficiency (η) with respect to bilbiography.

A.3.3   Quantitative analysis

The mean subcritical water depth obtained from the CFD model is $h_2 = 0.553m$, which leads to a mean ratio of sequent depths of $Y = 7.916$. Following Eq. A.10, the reference value for this variable in classical hydraulic jumps is $Y^* = 7.951$. This means that the model yields a value approximately 0.4% lower than that obtained using the expression proposed by Hager and Bremen [1989].

Regarding the mean roller length, the model yields an mean value of $L_r = 2.320m$, being $L_r^* = 2.330m$ the value computed using Eq. A.11. This implies an underestimation of only 0.4%. The accuracy in the prediction of this variable is crucial, as the largest shear stresses on the streambed generally occur within this stretch. In stilling basin design cases, this can be very helpful in order to determine the region of the structure that must be protected against scour.

Following Eq. A.13, the mean efficiency of the hydraulic jump is $\eta = 58.2\%$. This agrees with the result obtained from Eq. A.14 [Hager and Sinniger, 1985], which estimates an efficiency of 59.0%, with only a 1.3% error. The good agreement in the computation of these three variables compared to other works is depicted in Fig. A.6.

The comparison of water surfaces to previous studies [Bakhmeteff and Matzke, 1936] proves the consistency of the model presented herein. Fig. A.7 shows the mean water levels computed using the three different turbulence models. The most accurate RANS model is the Standard $k - \varepsilon$ ($R^2 = 99.6\%$), followed by the RNG $k - \varepsilon$ ($R^2 = 99.2\%$) and the SST $k - \omega$ ($R^2 = 98.5\%$). It can be deduced from
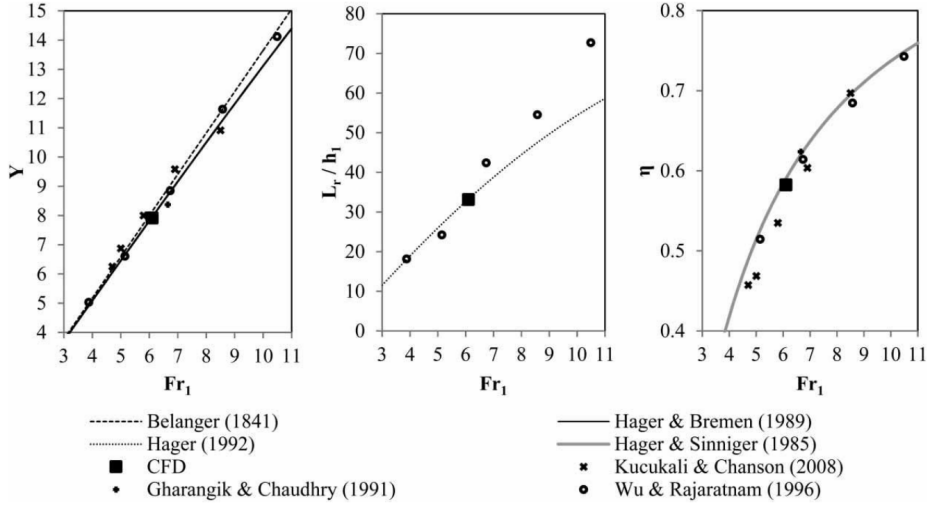
Figure A.6: CFD model result comparison with analytical and experimental previous works. The analyzed variables are: sequent depth (Y), roller length (L_r) and hydraulic jump efficiency (η).

the above that turbulence models exert very little effect on the water free surface definition in average terms.

Nevertheless, an instant observation of the evolution of this variable shows that SST $k - \omega$ models produce a more unstable and bursting water surface with high bubble and spray production. Both $k - \varepsilon$ models produce smoother surfaces, being the Standard $k - \varepsilon$ also the model that yields a more uniform and less turbulent free surface.

Tab. A.1 shows the accuracy of the model according to the variable predicted using the most accurate approach (RNG $k - \varepsilon$ turbulence model with $7.0mm$ size mesh). It can be deduced from such accurate results that the model proposed herein is validated and so can be applied to real-life design cases.

Variable	Model output	Reference result	Accuracy
Sequent depth (Y)	7.916	7.951	99.6%
Roller length (L_r)	$2.320m$	$2.330m$	99.6%
Hydraulic jump efficiency (η)	58.2%	59.0%	98.7%
Surface (Γ)	–	–	99.2%

Table A.1: RNG k$-\varepsilon$ with $7.0mm$ mesh model outcome and analytical/experimental data comparison.
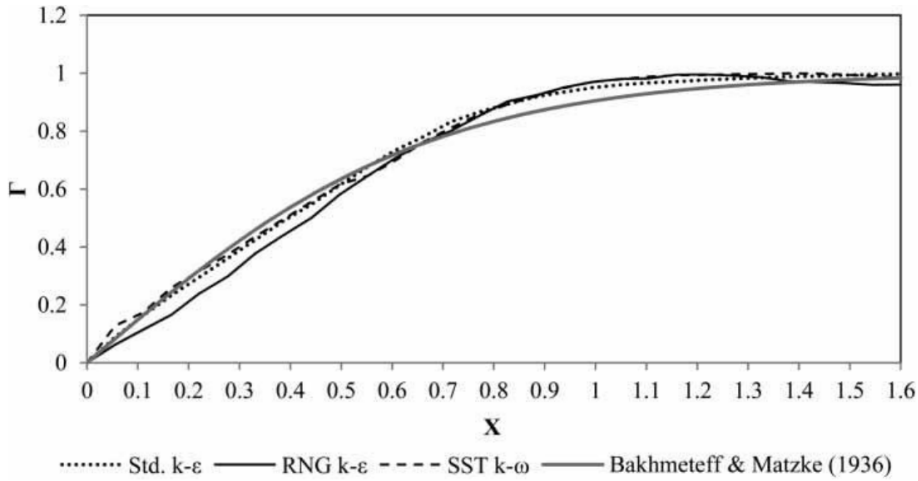
Figure A.7: Water free surface level according to turbulence model used compared to previous studies.

A.4   Conclusions

A three-dimensional CFD model for transient multiphase incompressible flow is developed in order to predict the behavior of classical hydraulic jumps. After analyzing the effects on the results of several model parameters, such as the mesh refinement degree, the turbulence model or the boundary conditions, a stable hydraulic jump and accurate results are obtained. The model is built using exclusively free open source code, which implies avoiding expensive software licenses. Also a problem found in other cases where OpenFOAM is used to model hydraulic jumps is addressed and solved. This problem involves the outlet boundary condition, where an additional stretch of channel with an obstacle attached to its bottom has to be added in order to force the subcritical flow to occur. Using the approach proposed in this paper, this additional stretch of channel can be removed by modifying the outlet boundary condition, with the subsequent saving of computational resources (up to 30% in some cases) with no effects on the model accuracy whatsoever.

A case study of approaching Froude number $Fr_1 = 6.125$ is simulated and the results are compared to previous studies of similar characteristics, such as that of Hager [1992] and Wu and Rajaratnam [1996]. The roller length appears to be the most sensitive variable to model parameters (the SST $k - \omega$ is not even able to capture this magnitude). Some hydraulic jump variables are better reproduced in comparison with other authors' results, such as the sequent depth (error of only 0.4%), whereas others show lower accuracies, e.g. the hydraulic efficiency (error of

1.3%). The water free surface is accurately reproduced by all turbulence models in average terms, being the Standard $k - \varepsilon$ the most accurate approach. An instant observation of the results shows that the SST $k - \omega$ model surface looks more turbulent than its $k - \varepsilon$ counterparts. Anyway, the accuracy of all of the variables analyzed is above 98% in all cases so the model can be considered validated.

In the light of the results, the model is ready to be applied to real-life design cases, such as dam stilling basins, stepped spillways, river rapids, meandering channels, etc. As discussed above, the most accurate turbulence model in this kind of applications is the RNG $k - \varepsilon$, although very fine meshes are necessary to ensure good performance and this model proved to be slightly slower than the Standard $k - \varepsilon$. The latter turbulence model could be a better choice in cases where low computational requirements are preferred without compromising accuracy excessively. The Standard $k - \varepsilon$ also proved to reproduce slightly better the average water free surface.

As future work, the model is currently being used in similar applications, both theoretical, such as triangular, circular and radial hydraulic jumps, and real-life cases. Also the air entrainment and concentration distribution in hydraulic jumps is being studied using this model and compared to experimental data.

Acknowledgements

Appendix B

Performance assessment of OpenFOAM and FLOW-3D in the numerical modeling of a low Reynolds number hydraulic jump

Reference

Arnau Bayon, Daniel Valero, Rafael Garcia-Bartual, Francisco Jose Valles-Moran, and Petra Amparo Lopez-Jimenez. Performance assessment of OpenFOAM and FLOW-3D in the numerical modeling of a low reynolds number hydraulic jump. *Environmental Modelling & Software*, 80:322–335, 2016. DOI: `https://doi.org/10.1016/j.envsoft.2016.02.018`.

Abstract

A comparative performance analysis of the CFD platforms OpenFOAM and FLOW-3D is presented, focusing on a 3D swirling turbulent flow: a steady hydraulic jump at low Reynolds number. Turbulence is treated using RANS approach RNG k-ε. A Volume Of Fluid (VOF) method is used to track the air-water interface, consequently aeration is modeled using an Eulerian-Eulerian approach. Structured meshes of cubic elements are used to discretize the channel geometry. The numerical model accuracy is assessed comparing representative hydraulic jump variables (sequent depth ratio, roller length, mean velocity profiles, velocity decay or free surface profile) to experimental data. The model results are also compared to previous studies to broaden the result validation. Both codes reproduced the phenomenon under study concurring with experimental data, although special care must be taken when swirling flows occur. Both models can be used to reproduce the hydraulic performance of energy dissipation structures at low Reynolds numbers.

Keywords: CFD; RANS; OpenFOAM; FLOW-3D; hydraulic jump; air-water flow; low Reynolds Number.

B.1   Introduction

A hydraulic jump is the abrupt transition from supercritical to subcritical flow (Fig. B.1). It constitutes a highly chaotic phenomenon characterized by large turbulent fluctuations of velocity and pressure, air entrainment and energy dissipation. Hydraulic jumps are usually described in terms of the well-known Froude number (Fr_i) which, in rectangular channels at a given section i, is computed as follows:

$$Fr_i = \frac{u_i}{\sqrt{gy_i}} \tag{B.1}$$

Where y_i, is water depth, u_i is depth-averaged velocity, and g is gravity acceleration. One of the most interesting aspects of hydraulic jumps is that, despite their chaotic nature, some of their properties remain steady within a certain range of approaching Froude numbers (Fr_1). This allows studying some representative features, such as the jump toe position (flow impingement location) or the roller length (stretch downstream of the jump toe where flow recirculates). Some of these phenomena behave in a quasi-periodic fashion and so can be analyzed statistically [Wang and Chanson, 2015a, Wang et al., 2014b, Mossa, 1999].

Since first known hydraulic jump experiences [Belanger, 1841, Bidone, 1819], a wealth of studies on this topic has been conducted. One of the main reasons is

that hydraulic jumps are the most used method to dissipate energy in hydraulic structures [Chow, 1959]. Classic literature on the area states that approaching Froude numbers between 4.5 and 9.0 yield stabilized hydraulic jumps, least dependent on tailwater variations [Hager, 1992, Peterka, 1984]. Lower values of Fr_1 lead to undular or transition jumps, characterized by lower efficiencies and formation of waves of irregular period [Chanson and Montes, 1995, Chow, 1959, Fawer, 1937]. Higher values of Fr_1 produce choppy jumps, where flow detachment, as well as bubble and spray formation are frequent. For these reasons, the U.S. Bureau of Reclamation [Peterka, 1984] recommends designing energy dissipation structures so that only steady hydraulic jumps occur.
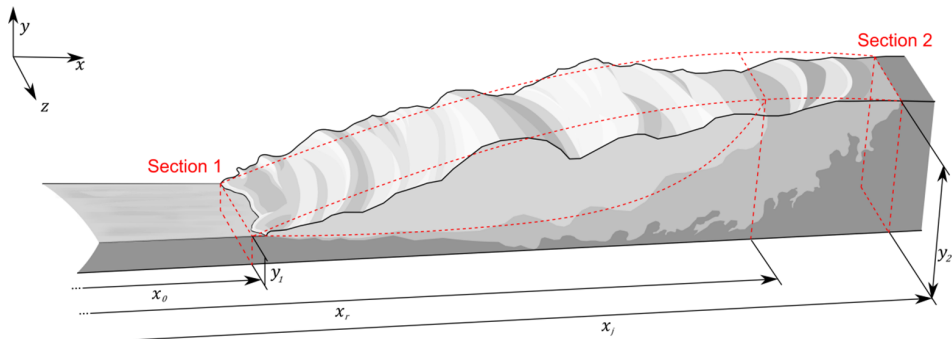
Figure B.1: Hydraulic jump flow structure.

The first known study reporting turbulence quantities in hydraulic jumps was conducted by Rouse et al. [1959] and was later completed by Rajaratnam [1965] and Long et al. [1991]. On the flow structure description, Resch and Leutheusser [1972] also reported turbulence quantities and pointed out dependence on the inlet flow conditions. Gualtieri and Chanson [2007, 2010] further analyzed the inlet sensitivity conditions and Liu et al. [2004] provided a complete turbulence description for low Froude numbers. Additionally, Chanson and Brattberg [2000], Murzyn et al. [2005], Chanson and Gualtieri [2008], and Zhang et al. [2014] focused on the flow aeration properties. Recently, Chanson [2007], Wang et al. [2014a], Zhang et al. [2013], Chachereau and Chanson [2011], Murzyn et al. [2007], and Chanson [2007] reported turbulent integral length and time scales, which might contribute to a better validation and understanding of numerical models.

Given the nature of experimental techniques [Bung, 2013, Borges et al., 2010, Matos et al., 2002], Computational Fluid Dynamics (CFD) can supplement and assist in the design of energy dissipation structures [Bombardelli, 2012, Meireles et al., 2014, Chanson and Carvalho, 2015]. Nevertheless, mathematical models still present accuracy issues when modeling some hydraulic phenomena [Blocken and Gualtieri, 2012, Murzyn and Chanson, 2009b], to which the lack of validation is usually pointed out [Chanson, 2013, Chanson and Lubin, 2010]. Carvalho et al.

[2008] and Ma et al. [2011], among others, managed to reproduce the hydraulic jump structure using different CFD approaches. Caisley et al. [1999] accurately modeled a hydraulic jump using FLOW-3D. Bayon and Lopez-Jimenez [2015], Romagnoli et al. [2009], and Witt et al. [2015] used OpenFOAM to successfully model hydraulic jumps as well.

Numerical approaches different from CFD have also been used to model hydraulic jumps, such as Smoothed Particle Hydrodynamics [De Padova et al., 2013] or Artificial Neural Networks [Omid et al., 2005]. Other authors preferred one-dimensional and two-dimensional models to study the hydraulic behavior of rivers or stilling basins and erosion-sedimentation phenomena [Hartanto et al., 2011, Dewals et al., 2004, Juez et al., 2013]. Nevertheless, flows occurring in hydraulic structures tend to be highly three-dimensional [Ahmed and Rajaratnam, 1997, Chanson and Montes, 1995]. For this reason, the use of three-dimensional models, such as that proposed in this paper, becomes a must in most cases.

In real life applications, choosing the most suitable numerical model when facing fluid mechanics problems can be a tedious and confusing task given the large amount of possible choices. As stated above, two of the most widely used CFD codes in hydraulic engineering applications are the open source platform Open-FOAM and the commercial software FLOW-3D. The main goal of this paper is to conduct a systematic comparison between them in terms of accuracy. To do so, a RANS model for classical hydraulic jumps is set similarly in OpenFOAM and FLOW-3D using the RNG $k - \varepsilon$ turbulence model [Yakhot et al., 1992] and a two-phase VOF approach [Hirt and Nichols, 1981]. A case study based on a steady hydraulic jump ($Fr_1 \approx 6$) of low Reynolds number ($Re_1 = 30,000$) is simulated. For validation purposes, the results are compared to data obtained using an open channel physical model and previous authors' experimental studies. Additionally, sensitivity to certain parameters, such as mesh refinement and time-averaging window size, is also assessed. Low Reynolds number might prevent from extrapolating present results to prototype scale structures where air-water flows prevail and Reynolds numbers are 2 to 4 orders of magnitude larger.

B.2   Numerical model

The present model is implemented using two widespread numerical codes, namely: OpenFOAM and FLOW-3D. OpenFOAM User Guide [2011] is a freely available open source platform containing several C++ libraries and applications which can numerically solve continuum mechanics problems [Weller et al., 1998]. Its implementation is based on a tensorial approach using object-oriented programming techniques and the Finite Volume Method or FVM [McDonald, 1971]. FLOW-3D is a commercial software package based as well on the FVM, developed by Flow-Science, Inc. FLOW-3D includes the Volume of Fluid (VOF) method as originally

described by Hirt and Nichols [1981]. FLOW-3D allows using one-fluid approach for free surface flows [Prosperetti and Tryggvason, 2009, Bombardelli et al., 2011, Oertel and Bung, 2012], although this approach is not used in this study. This code has been widely used in hydraulic applications since it was released in 1986. In this section, an in-depth discussion on the proposed model implementation using both CFD platforms used is presented. Special attention is paid to those aspects where the OpenFOAM and FLOW-3D approaches differ (see Tab. B.1).

	OpenFOAM
Mesh	3D structured (cubic cells)
Turbulence model	RANS RNG $k - \varepsilon$
Solid contours	No slip, smooth surface, high Re wall function
Advection scheme	Explicit 2nd order limited [Van Leer, 1977][*]
Diffusion scheme	Explicit 2nd order
Courant number limit	0.75
Multiphase treatment	VOF with two fluids
Free surface tracking	Interface compression velocity [Ubbink, 1997]
Aeration	Eulerian-Eulerian approach

	FLOW-3D
Mesh	3D structured (cubic cells)
Turbulence model	RANS RNG $k - \varepsilon$
Solid contours	No slip, smooth surface, high Re wall function
Advection scheme	Explicit 2nd order limited [Van Leer, 1977]
Diffusion scheme	Explicit 2nd order
Courant number limit	0.75
Multiphase treatment	VOF with two fluids
Free surface tracking	Donor-acceptor method [Hirt and Nichols, 1981]
Aeration	Eulerian-Eulerian approach

Table B.1: Summary of numerical model setup according to the code used. [*] In OpenFOAM, scalar variables with no abrupt gradients, such as k or ε, are discretized using an explicit 1st order scheme

B.2.1 Geometry and mesh

According to the definition of classical hydraulic jump, the discretized spatial domain is rather simple: it consists of a horizontal rectangular channel. Unstructured meshes would allow a selective refinement of regions where large gradients of flow variables are expected [Kim and Boysan, 1999]. Furthermore, their arbitrary topology makes them fit better into complex geometries as well as show fewer closure issues [Biswas and Strawn, 1998]. However, none of these facts implies an

advantage in the case of this study, as the modeled geometry constitutes one of the simplest possible cases.

However, according to Biswas and Strawn [1998] and Hirsch [2007], structured meshes are generally more accurate than unstructured meshes. In addition, their algorithms tend to be more straight forward and faster. Also structured meshes produce a more regular access to memory and so lower the latency of simulations [Keyes et al., 2000]. Besides, topologically orthogonal meshes tend to cause less numerical issues in multiphase flows. As a consequence, a structured rectangular hexahedral mesh is considered more suitable to the problem in this study.

Thus, uniform cubic mesh elements of size Δx are used to discretize the channel (see Fig. B.2) which may yield higher order of accuracy as higher order errors are neglected in some numerical schemes [Hirsch, 2007]. The optimum mesh element size is case specific. Hence, it must be determined by means of a mesh sensitivity analysis, described below.

Inlet	Floor & Walls	Atmosphere	Outlet
$\alpha = 1$ (if $y \leq y_1$); $= 0$ (if $y > y_1$)	$\frac{\partial \alpha}{\partial x_i} = 0$	$\frac{\partial \alpha}{\partial x_i} = 0$	$\alpha = 1$ (if $y \leq y_2$); $= 0$ (if $y > y_2$)
$u = u_1$	$u = 0$	$\frac{\partial u}{\partial x_i} = 0$	$\frac{\partial u}{\partial x_i} = 0$
$\frac{\partial p}{\partial x_i} = 0$	$\frac{\partial p}{\partial x_i} = 0$	$p = 0$	$p = f(x_i)$
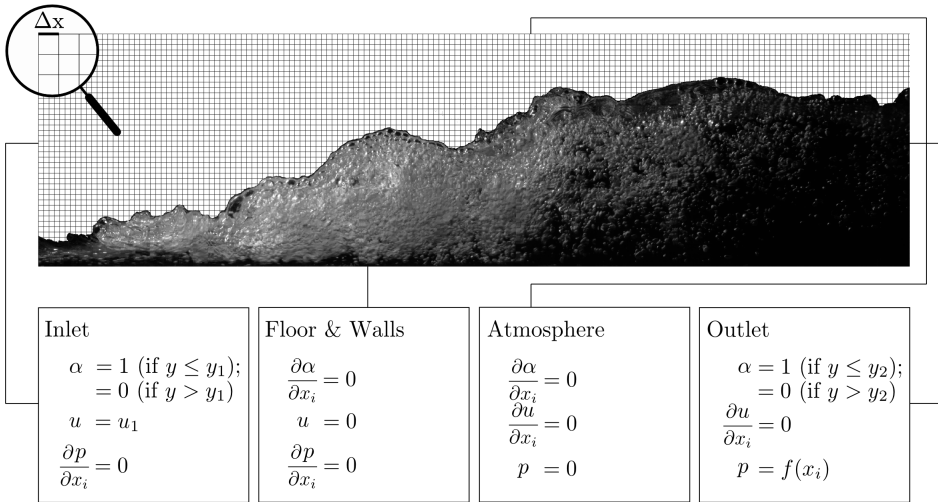
Figure B.2: Mesh overlapping a hydraulic jump snapshot and description of the boundary conditions.

B.2.2 Flow equations

A complete description of flows with breaking free surfaces, air entrapment and three-dimensional flow patterns cannot be achieved using shallow water approaches, such as Saint-Venant [1871] or Boussinesq [1871]. In these cases, a full description of the flow characteristics requires the use of the Navier-Stokes Equations (Eq. B.2 and B.3). In their general form, these equations govern fluid motion. Despite

the VOF method can be applied to variable-density flows [Chen and Li, 1998], in this particular case Navier-Stokes equations are used in their incompressible form (this assumption can generally be done in flows where the Mach number is $Ma < 0.3$). For the numerical solution of the flow equations, the Finite Volume Method (FVM) has been employed.

$$\nabla \cdot \vec{u} = 0 \tag{B.2}$$

$$\frac{\partial \vec{u}}{\partial t} + \vec{u} \cdot \nabla \vec{u} = -\frac{1}{\rho}\nabla p + \upsilon \nabla^2 \vec{u} + \vec{f_b} \tag{B.3}$$

Where u is velocity, p is pressure, ρ is density, υ is kinematic viscosity, f_b is body forces (gravity and surface tension); and t is time. Concerning time discretization, the time step length is automatically adjusted in order to ensure that Courant numbers remain below a threshold of $Cr < 0.75$.

B.2.3 Free surface modeling

The way that the coexistence of several fluids is treated is of paramount importance in multiphase flow numerical modeling. The stability and accuracy of the algorithm used to define the interface between fluid phases proved to exert a significant effect on the final model outcome [Hyman, 1984]. A large number of surface tracking approaches has been reported since the first Lagrangian model proposed by Daly [1969]. Among all these, Eulerian-Eulerian methods are generally preferred in models like that presented herein, as discussed in Bayon and Lopez-Jimenez [2015]. These kind of methods are comparatively computationally more efficient since, unlike Lagrangian approaches, they only use a single variable value in every mesh element [Ubbink, 1997]. This scalar variable (α) expresses the fraction of one fluid contained at each mesh element. When only two fluids are modeled, both fluid fractions are complementary. An additional transport equation must be approximated to determine the value of the fluid fraction throughout the computational domain [Hirt and Nichols, 1981]:

$$\frac{\partial \alpha}{\partial t} + \nabla \cdot (\vec{u}\alpha) = 0 \tag{B.4}$$

Where α is fluid fraction, u is velocity, and t is time. It is important to remark that this approach considers both fluids, say A and B, to be a single multiphase fluid. The transport of other properties (ξ) is treated by means of weighted averages, according to the fluid fraction in each mesh element:

$$\xi = \xi_A \alpha + \xi_B (1 - \alpha) \tag{B.5}$$

As a result, a set of values between 0 and 1 is obtained but no neat fluid interface is explicitly defined. Different methods for this purpose have been reported during the last decades. Line techniques, e.g. SLIC [Noh and Woodward, 1976], PLIC [Youngs, 1984] or FLAIR [Ashgriz and Poo, 1991], were the first viable approaches in this regard. Nevertheless, problems of generalization to unstructured meshes made them fall into disuse. The so-called donor-acceptor methods, such as the VOF [Hirt and Nichols, 1981], implemented in FLOW-3D, have been widely used, although they used to depict false interface deformation issues. Higher order differencing schemes were aimed to overcome these problems, although they still can suffer from surface smearing and numerical diffusion issues, leading to spurious currents in the vicinity of fluid interfaces [Ubbink, 1997]. As regards OpenFOAM, an interface compression algorithm is implemented to avoid the aforementioned problems. This is achieved by adding an extra term to the left hand side of Eq. B.4: $\nabla \cdot (\vec{u_c} \alpha [1 - \alpha])$, where $\vec{u_c}$ is an arbitrarily defined compression velocity term to which the direction is perpendicular to the fluid interface. This term is multiplied by $\alpha [1 - \alpha]$ to ensure that it will only be relevant in zones where the fluid fraction variable is close to 0.5 (where the fluid interfaces are defined). A more in-depth discussion on this topic can be found in Rusche [2002] and Berberovic et al. [2009].

B.2.4   Flow aeration

In air-water flows, aeration induces volume bulking, increases flow depth, adds compressibility to the flow and modifies its macroscopic density [Chanson, 2013, Falvey, 1980], thus affecting momentum distribution of the carrier phase. Flow aeration also bounds scour phenomena caused by cavitation [Bung and Schlenkhoff, 2010, Wood, 1991, Pfister, 2011] and shear stresses on the channel boundaries [Chanson, 1994]. A stable and accurate method to treat this phenomenon is of paramount importance when dealing with bores, breaking waves or hydraulic jumps. Unfortunately, no method per se can accurately reproduce phenomena with a characteristic length scale smaller than mesh elements, e.g. bubbles or droplets [Valero and Bung, 2015, Lobosco et al., 2011, Toge, 2012].

Subscale air-entrainment models can be implemented in order to overcome this issue [Valero and Garcia-Bartual, 2016, Ma et al., 2011]. In low-aerated flows, Eulerian-Lagrangian approaches are a good choice. These methods consist of the approximation of the Navier-Stokes Equations, while air bubbles are treated as flow-driven discrete particles. However, this approach becomes computationally expensive in highly aerated flows. In these cases, Eulerian-Eulerian methods arise as an efficient approach. An entirely Eulerian method with two fluids has been used in the present study, allowing both fluids to mix in the same cell but locating the free surface where $\alpha = 0.5$. However no additional equation is employed for bubble and droplet dynamics. A detailed discussion on more advanced methods can be found in Balachandar and Eaton [2010].

B.2.5 Turbulence modeling

One of the key aspects of CFD models is the way turbulence is treated. Velocity and pressure fluctuations can be numerically resolved down to their lowest scales (Direct Numerical Simulation or DNS) as long as the mesh is accordingly fine [Pope, 2000, Hirsch, 2007]. However, this approach is still unaffordable in terms of computational cost for any engineering application. The use of DNS in multiphase flows has been reported in the literature [Borue et al., 1995, Nagosa, 1999, Prosperetti and Tryggvason, 2009], although in engineering applications turbulence is partially modeled.

Large Eddy Simulation (LES) methods offer accurate multiphase flow simulations at lower computational costs, being however still unaffordable for most engineering applications [Spalart, 2000]. Thus, the most widely used approach in engineering applications is the Reynolds Averaged Navier-Stokes (RANS). The models of this kind are based on averaging the flow equations yielding the Reynolds Averaged Navier-Stokes (RANS) equations. Further hypothesis are needed for closure. This is commonly achieved by adding transport equations to reproduce the behavior of flow turbulence and then relate the turbulence scales to a turbulent viscosity (μ_t), which is introduced in the flow equations aiming to account for the Reynolds stresses. The first complete models are the two equation models; they are able to provide a full description in turbulence in terms of length and time scales, thus they could reproduce a wide variety of flows [Pope, 2000]. An extended description of RANS equations and turbulence closures can be found in Pope [2000] and Wilcox et al. [1998].

The turbulence model used in this study is the RNG $k - \varepsilon$ [Yakhot et al., 1992], which usually provides better performance for swirling flows than the standard $k - \varepsilon$ model [Bombardelli et al., 2011, Bradshaw, 1996, Kim and Baik, 2004, Pope, 2000, Speziale and Thangam, 1992]. Its formulation is depicted in Eq. B.6 and B.7:

$$\frac{\partial}{\partial t} (\rho k) + \frac{\partial}{\partial x_i} (\rho k u_i) = \frac{\partial}{\partial x_j} \left[\left(\mu + \frac{\mu_t}{\sigma_k} \right) \frac{\partial k}{\partial x_j} \right] + P_k - \rho \varepsilon \qquad (B.6)$$

$$\frac{\partial}{\partial t} (\rho \varepsilon) + \frac{\partial}{\partial x_i} (\rho \varepsilon u_i) = \frac{\partial}{\partial x_j} \left[\left(\mu + \frac{\mu_t}{\sigma_\varepsilon} \right) \frac{\partial \varepsilon}{\partial x_j} \right] + C_{1\varepsilon} \frac{\varepsilon}{k} P_k - C_{2\varepsilon} \rho \frac{\varepsilon^2}{k} \qquad (B.7)$$

Where k is turbulence kinetic energy (henceforth, TKE), ε is dissipation rate, ρ is density, t is time, x_i is coordinate in the i axis, μ is dynamic viscosity, μ_t is turbulent dynamic viscosity, and P_k is production of TKE. The remaining terms, ($C_{1\varepsilon}$, $C_{2\varepsilon}$, σ_k, and σ_ε) are model parameters whose values can be found in Yakhot et al. [1992]. Finally, the turbulence viscosity can be computed using the parameter $C_\mu = 0.085$:

$$\mu_t = \rho C_\mu \frac{k^2}{\epsilon} \qquad (B.8)$$

B.2.6 Boundary conditions

In order to force the hydraulic jump to occur within the modeled channel stretch, a supercritical flow inlet and a subcritical flow outlet are imposed. The desired approaching Froude number is ensured by imposing a constant flow depth at the inlet (h_1) with corresponding velocity value using a Dirichlet boundary condition. Pressure is defined by a null von Neumann boundary condition allowing a hydrostatic profile to develop, which is easily specified in FLOW-3D. In OpenFOAM, this is achieved thanks to the swak4Foam library. The inlet variables of the RANS model, i.e. k and ε, cannot be defined a priori as this is a theoretical case study. Their values at the channel inlet and outlet are set to arbitrary low values so that they can develop while approaching the hydraulic jump. An outlet subcritical flow depth (h_2) has to be imposed so that the hydraulic jump occurs within the simulation domain. This variable cannot be accurately set a priori due to the numerous sources of uncertainty and the high sensitivity shown by the jump location. Hence, the subcritical flow depth has to be obtained by iteratively testing values by means of a Dirichlet boundary condition until a compact steady hydraulic jump is formed far enough from both upstream and downstream boundary conditions.

Wall roughness has been neglected given the small roughness of the material of the experimental facility which was used for validation. An atmospheric boundary condition is set to the upper boundary of the channel. This allows the flow to enter and leave the domain as null von Neumann conditions are imposed to all variables except for pressure, which is set to zero (i.e. atmospheric pressure). In Fig.B.2 are the summarized boundary conditions which were used.

Boundary layers, the viscous flow region attached to solid boundaries, require special treatment. The so-called universal law of the wall [Von Karman, 1930] describes the flow profiles in such regions. This is achieved through defining a dimensionless velocity (u) and the distance to wall (d) as a function of shear velocity (u_τ) and viscosity (v):

$$y^+ = y \frac{u_\tau}{v} \qquad (B.9)$$

Schlichting and Gersten [2000] subdivide boundary layers into three zones according to the shape of their velocity profile: the viscous sub-layer $(y^+ < 5)$ is characterized by a linear correlation between $u^+ = u/u_\tau$ and y^+; the buffer sub-layer $(5 < y^+ < 70)$, where no analytical profiles are observable as turbulent and laminar features coexist [Olivari and Benocci, 2010]; and the logarithmic sub-layer

($y^+ > 70$), characterized by a full development of turbulence and where TKE production and dissipation terms tend to balance.

It is known that large gradients of property occur in the lowest y^+ regions. For this reason, wall functions can be implemented in CFD codes in order to model these regions instead of directly solving them. This allows the use of coarser meshes, thus saving significant amounts of computational resources. These functions assume that the behavior of viscous sub-layers is universal. Therefore, their main requirement is that mesh elements in contact with solid boundaries must have y^+ values between the buffer and the logarithmic sub-layers ($y^+ \sim 35$).

B.3 Experimental setup

In order to validate the numerical model outcome, altogether with previous studies, a small scale open channel installed at the Hydraulics Laboratory of the Universitat Politècnica de València (UPV) is used. The device consists of methacrylate walls and a PVC streambed, a recirculation tank and a water pump is employed to provide the desired flow rate. The water pump can reach flow rates up to $4 \cdot 10^{-3} m^3/s$ (2% uncertainty) and can be maneuvered with a frequency regulator. Given the channel dimensions ($3.00m$ long, $0.10m$ wide and $0.15m$ high), Froude numbers spanning from 4.5 to 13 can be obtained. The inlet boundary condition is imposed by an adjustable vertical sluice gate and a jetbox. Both ensure a smooth transition from pressurized to supercritical flow at a desired flow depth. The outlet boundary condition is imposed by a drop-down door, to which the slope can be adjusted to obtain the desired flow depth downstream. Once boundary conditions are set, flow rate and fluid temperature are monitored. Thus, it is ensured that neither flow nor fluid conditions change throughout the test.

In this experimental facility, flow depth measurements are conducted by means of digital image processing. To do so, $10s$ videos of the hydraulic jump profile are recorded at $50Hz$ and $1280 \times 720px$ ($4.1 \cdot 10^{-4} m/px$ in average, before perspective effect correction). After decomposing videos in frames, flow depth is automatically determined using edge detection tools to track the sudden changes of light intensity that an air-water interfaces cause. Filtering algorithms are applied to raw results to remove the bias caused by reflections, droplets, etc. The water surface tracking provides information on the hydraulic jump profile (Γ) and the supercritical and subcritical flow depths (h_1 and h_2) for comparison with the CFD model outcome. In order to validate the data obtained by digital image treatment, point gauge measurements are simultaneously conducted upstream and downstream of the hydraulic jump.

B.4   Case study

As stated above, a case study is conducted to assess OpenFOAM and FLOW-3D model accuracy using experimental data and results from previous studies. The case consists of a classical hydraulic jump in a channel of dimensions $1.00m \times 0.10m \times 0.15m$ (length, width and height). Inlet flow is set to $Q = 0.003m^3/s$ and supercritical flow depth is set to $h_1 = 0.013m$, so inlet mean velocity is $u_1 = 2.308m/s$. The resulting approaching Froude number remains $Fr_1 \approx 6$. Reynolds numbers are $Re_1 \approx 30,000$ and Weber numbers are $We \approx 40$. According to Hager [1992], these conditions lead to a stabilized jump. A case study of approaching Froude number (Fr_1) between 6 and 7 is suitable for model validation as it is exactly in the middle of the Fr_1 value span recommended by the U.S. Bureau of Reclamation for stilling basin design [Peterka, 1953]. Therefore, this Fr_1 value is considered representative of the behavior of all steady hydraulic jumps within this range. Density and kinematic viscosity are $\rho_w = 1000kg/m^3$ and $v_w = 10^{-6}m/s^2$, respectively, for water. For air, $\rho_a = 1.20kg/m^3$ and $v_a = 10^{-3}m/s^2$ have been assumed. Despite the air and water temperatures were monitored during the experiments, differences in their properties can occur and so be an additional source of result bias.

	$q[m^2/s]$	$u_1[m/s]$	Re_1 [-]	Fr_1 [-]
Present study	0.030	2.308	30000	6.5

Table B.2: Description of simulated cases. Specific flow rate (q), inlet mean velocity (u_1), Reynolds number (Re_1) and inlet Froude number (Fr_1).

B.4.1   Mesh sensitivity analysis

As discussed above, a mesh sensitivity analysis is conducted. To do so, each of the codes (OpenFOAM and FLOW-3D) are tested in five meshes with different cell sizes using sequent depths and roller length as indicators and following the ASME's criteria [Celik et al., 2008]. The mesh cell sizes employed are $7.50mm$, $5.00mm$, $4.00mm$, $3.00mm$ and $1.5mm$, being the global refinement ratio 5, way above the recommended minimum value of 1.3 [Celik et al., 2008].

As Fig. B.3 (a and b) show, sequent depths seem to be less sensitive to mesh size than roller lengths. Except for the sequent depth in FLOW-3D, the data analysis demonstrates that oscillatory convergence is reached in mesh sizes below $3mm$ according to Celik et al. [2008]. Fig. B.3 (c) corroborates that mesh size has converged and is in the asymptotic range, as the model apparent order approaches the model formal order in all cases. For this reason, all subsequent considerations regarding the quantitative analysis of results are exclusively referred to the $3mm$ mesh case. The numerical uncertainty of the model is assessed according to [Celik
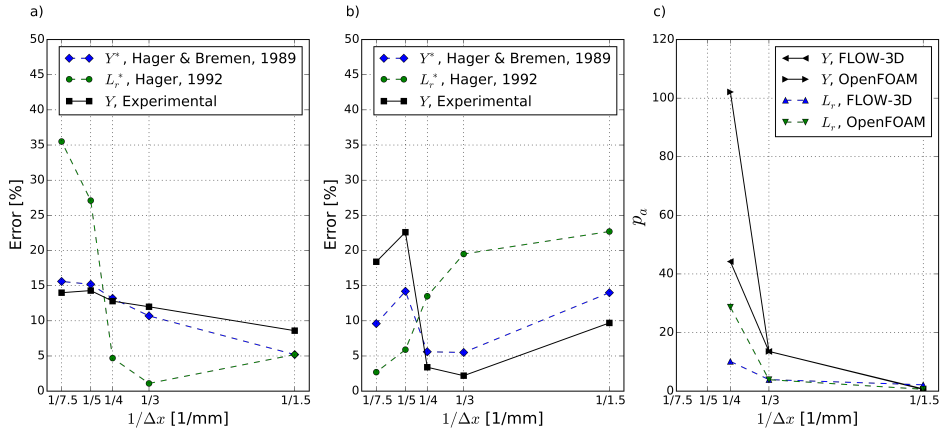
Figure B.3: Mesh sensitivity analysis. Model error in estimation of roller lengths (L_r^*) and sequent depths ratio, both according to experimental results (Y_e) and to Hager and Bremen [1989] (Y^*): a) OpenFOAM; b) FLOW-3D; c) Model apparent order (p'), according to [Celik et al., 2008].

et al., 2008] and spans from 6.0 to 6.7. It is worth mentioning that, according to the results, FLOW-3D appears to be less dependent on mesh size variations than OpenFOAM.

B.4.2 Time-averaging window size sensitivity analysis

Most of the flows are essentially chaotic and so most of its characteristic variables show, in best case scenario, a statistically-stationary behavior. Hence, it is of paramount importance to extend the simulation time sufficiently and then average the variables in order to avoid bias in the model outcome. The authors observe that stability of the solution can be assumed when the residuals of all the variables drop below the 10^{-3} threshold and the water content of the whole modeled channel stays stable during at least $10s$.

However, this is a rather empirical criterion. In order to ensure that the time-averaging window size does not affect results significantly, a sensitivity analysis is also conducted. Some oscillating variables are carefully observed, namely: jump toe position (x_0), roller end position (x_r) and subcritical flow depth (h_2). As a conclusion, it can be stated that the sampling period chosen of $10s$ captures several characteristic oscillation periods of these variables, so avoiding bias in the averaging process.

During this analysis, certain quasi-periodicity in the variables is observed (i.e. patterns can eventually be detected, although their characteristic period seems

not to be constant). The autocorrelation function is computed to investigate whether the monitored variables show periodic behavior or not, and if so, what is the characteristic time scale of their oscillations. Fig. B.4 shows how all variables are quasi-periodic. Indeed, the autocorrelation function of all variables tested shows an attenuation trend comparable to that of a sine wave with a characteristic time scale way smaller than the averaging window size. Further discussion on the fluctuating behavior of hydraulic jumps is conducted during the analysis of results.
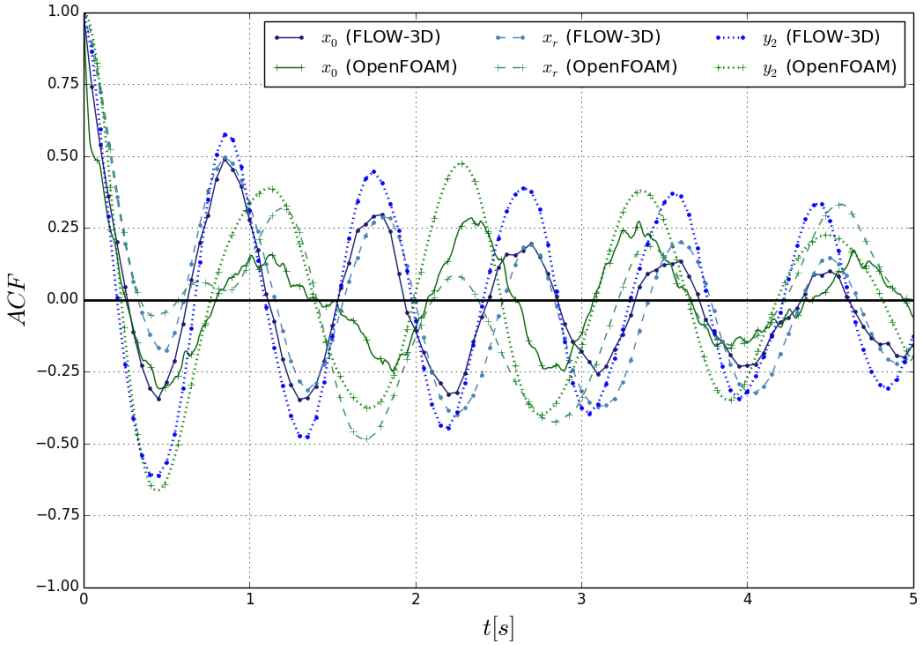
Figure B.4: Comparison of autocorrelation function (ACF) of hydraulic jump toe location (x_0), roller end position (x_r) and subcritical flow depth (h_2) in OpenFOAM and FLOW-3D.

B.5 Results and discussion

B.5.1 Graphical analysis

Both models managed to produce physically-consistent hydraulic jumps. A close observation of the results shows that all features expectable in hydraulic jumps of these characteristics can be identified: stable and compact appearance, gradual air detrainment, low wave generation, high vorticity within the roller, no flow

detachment around the hydraulic jump toe, etc. [Hager, 1992]. At the end of hydraulic jumps, hydrostatic flow profiles are restituted.
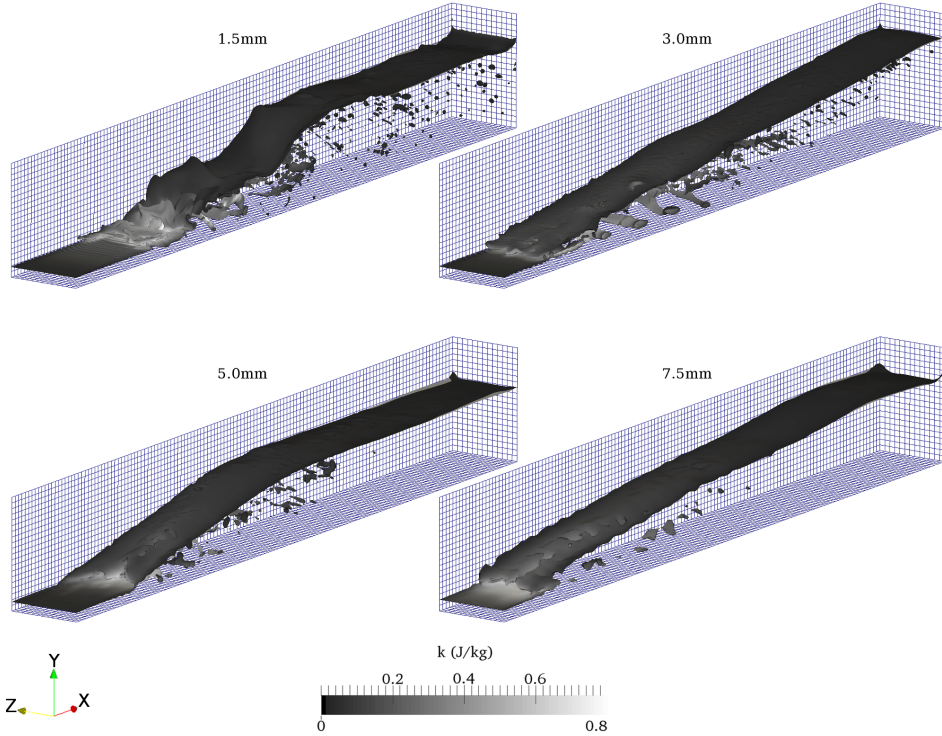
Figure B.5: Example of instant representation of numerically simulated hydraulic jumps, showing that different mesh sizes lead to different free surface profiles, TKE distributions and air entrapment patterns.

B.5.2 Average variable analysis

The quantitative analysis of the hydraulic jump variables is conducted using the results of the case study described in Tab. B.2. The sequent depth values are compared to the expression proposed by Hager and Bremen [1989] and yield accuracies of 89.3% and 94.5% for OpenFOAM and FLOW-3D, respectively. These variables, when compared to experimental results, yield accuracies of 88.0% and 97.8%, respectively.

The hydraulic jump efficiency is also better predicted by FLOW-3D (97.1%) than by OpenFOAM (94.6%). The fact that the same model estimates better sequent depths and efficiencies is normal to a certain extent, as both variables are strongly correlated and their estimation depends on how models treat momentum transfer.

Another important variable in the analysis of hydraulic jumps is the roller length (L_r). This variable is easier to determine as a flow stagnation region, where streamwise velocity tends to zero, can always be identified. Murzyn and Chanson [2009a] define the roller as the stretch of hydraulic jumps where the flow depth increases monotonically. Nevertheless, the stagnation point is used as criterion in the present work for it is easier to identify in CFD modeling.

FLOW-3D appears to be less accurate when estimating the roller length: this model achieved an accuracy of 80.5%, whereas OpenFOAM reached 98.9%, both compared to Hager [1992]. Compared to Wang and Chanson [2015a], the accuracy decreased to 77.4% and 91.5% respectively. This variable shows the largest sensitivity to model parameters, such as mesh element size, as Fig. B.3 shows. This makes model calibration and validation crucial as models must accurately predict where the roller is going to occur. It must be beared in mind that the largest energy release, shear stress and free surface fluctuation occur in this region, so its delimitation is of utmost importance in hydraulic engineering. Correct roller behavior estimations can avoid bank overflow issues and structure failure due to excessive dynamic loads.

As regards to the free surface profile throughout the hydraulic jump, it is also accurately defined by the models presented herein. Compared to the expression proposed by Bakhmeteff and Matzke [1936], OpenFOAM achieves a coefficient of determination of $R^2 = 0.999$ and FLOW-3D, $R^2 = 0.988$. Compared to more recent studies [Chanson, 2015], the coefficients of determination are $R^2 = 0.962$ and $R^2 = 0.952$, respectively. Compared to experimental results, the models yield accuracies of $R^2 = 0.982$ and $R^2 = 0.966$, respectively. The coefficient of determination (R^2) is commonly used to measure the efficiency of a model. This metric varies between 0 and 1.0, with perfect agreement for 1.0 [Bennett et al., 2013].

Fig. B.6 shows the dimensionless free surface profile obtained by both codes compared to Bakhmeteff and Matzke [1936], Chanson [2015], and experimental results. It can be observed that numerically determined flow depths mostly fall between the profiles proposed by Bakhmeteff and Matzke [1936] and Chanson [2015]. The slight overestimation of flow depths compared to Bakhmeteff and Matzke [1936], observable over $X > 1$, is in agreement with experiments reported by Hager [1992]. The experimental results follow the trend of all previously exposed free surface profiles. However, they show a sudden increase of flow depth around $X \approx 0.7$, which is not observed in other profiles. A close observation of the images from which this profile is obtained points out that the most likely source of this mismatch is that large bubbles are expelled from the flow at this stretch, which cannot be filtered out by the surface detection algorithm. The bias caused by bubbles in the digital image treatment is currently being dealt with.
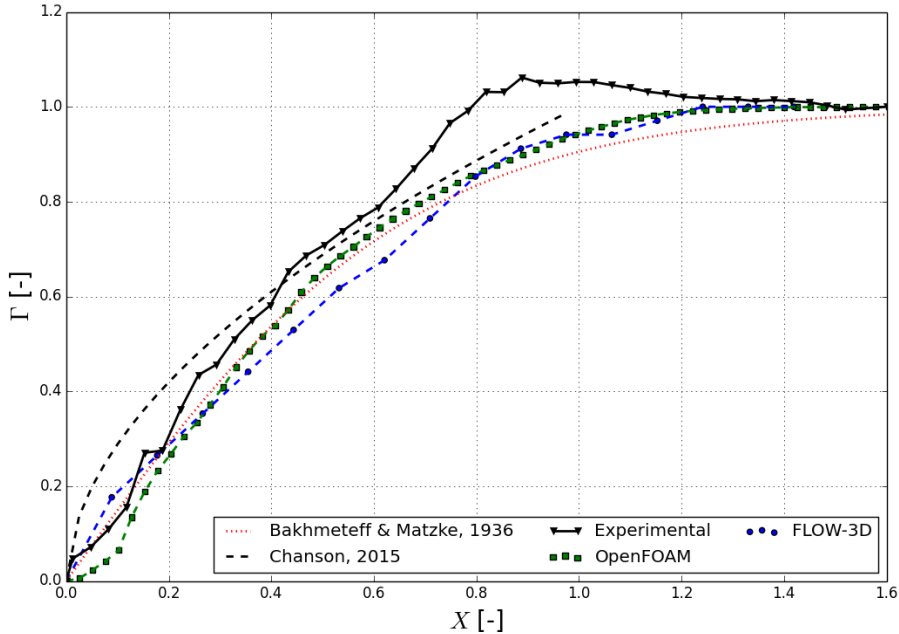
Figure B.6: Dimensionless free surface profile computed with OpenFOAM and FLOW-3D compared to Bakhmeteff and Matzke [1936], Chanson [2015], and experimental results.

Concerning flow velocity distributions, Fig. B.7 shows that the maximum differences with values reported by Hager [1992] occur for backward velocities (U_s). The flow processes in this region of hydraulic jumps are particularly complex. It is therefore expectable that the maximum errors take place in the swirling region, where turbulence models are most prone to fail in reproducing the flow behavior [Wilcox et al., 1998]. Better accuracy can be expected for the rest of the analyzed flow variables. For the maximum velocity decay, FLOW-3D achieves higher degree of accuracy (99.7%) than OpenFOAM (99.5%) measured with the coefficient of determination (R^2). However, OpenFOAM yields better results than FLOW-3D in the estimation of backward velocities (88.2% and 83.7%) and vertical velocity profiles (97.6% and 90.3%), respectively. Anyway, these differences are rather small as both numerical codes reproduce the shape and main features fairly well as reported in the literature, as shown in Fig. B.7 and B.8. Tab. B.3 summarizes the accuracy of all the results according to the variable analyzed and the model used. For this purpose, mean square relative error (MSRE) has been used where R^2 could not be applied [Bennett et al., 2013].

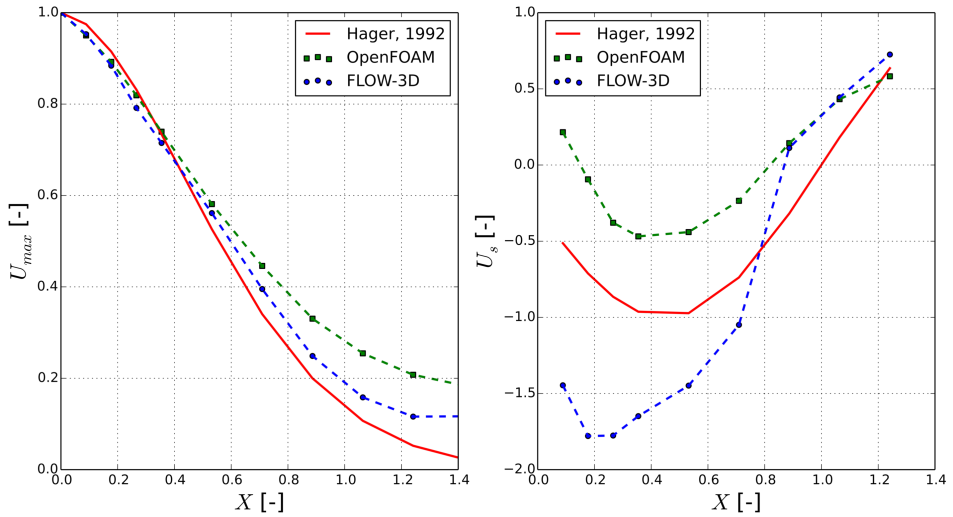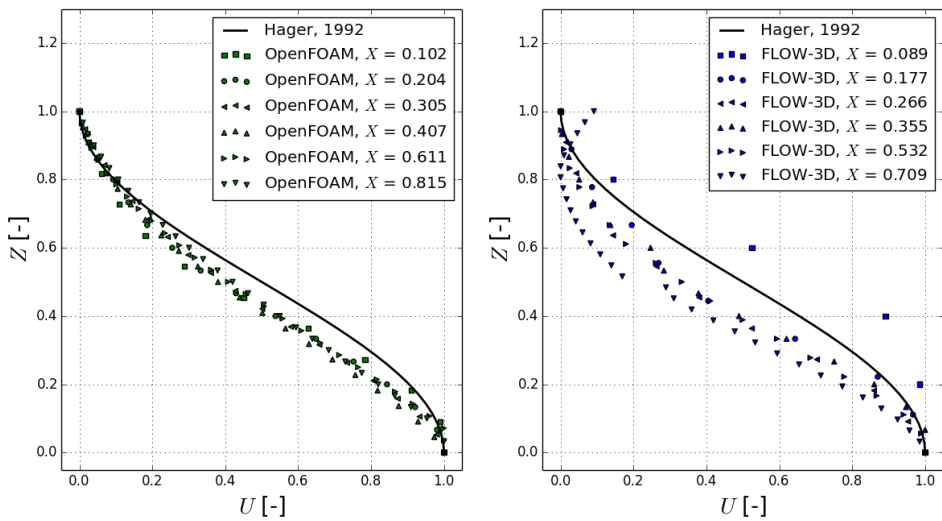**Figure B.7:** Velocity analysis: a) Maximum velocity decay; b) Maximum backward velocity.

Figure B.8: Vertical velocity profiles along the longitudinal axis: a) OpenFOAM; b) FLOW-3D.

Variable	Referred to	Accuracy		Compared to
		OpenFOAM	FLOW-3D	
Y^*		89.3%	94.5%	Hager and Bremen [1989]
Y_{exp}		88.0%	97.8%	Experimental
L_r^*	$1 - RMSE$	98.9%	80.5%	Hager [1992]
L_r^*		91.5%	77.4%	Wang and Chanson [2015b]
η^*		94.6%	97.1%	Hager and Sinniger [1985]
Γ^*		0.999	0.988	Bakhmeteff and Matzke [1936]
Γ^*		0.962	0.952	Chanson [2015]
Γ_{exp}	R^2	0.982	0.966	Experimental
U^*		0.976	0.903	Hager [1992]
U_{max}^*		0.995	0.997	Hager [1992]
U_s^*		0.882	0.837	Hager [1992]

Table B.3: Model accuracy summary. $MSRE$ is mean square relative error and R^2 is coefficient of determination. Flow conditions are summarized in Tab. B.2

B.5.3   Time analysis

As mentioned above, the time domain analysis of certain hydraulic jump variables demonstrates that certain patterns tend to repeat in a periodic fashion, which is corroborated by the ACF analysis. In order to further infer this phenomenon, three variables are analyzed in the frequency domain using the Fast Fourier Transform (FFT), namely: jump toe position (x_0,), roller end position (x_r), and subcritical flow depth (h_2). FFT converts data from temporal domain to frequency domain. This allows direct comparison of different temporal series in the frequency domain. This is of special interest in turbulence since repeating two temporal series representing the same phenomenon is impossible. Besides, transforming data can give insights into model performance that might not be obvious in untransformed data [Bennett et al., 2013]. Fig. B.9 (a, b and c) show the normalized power spectrum density (PSD) of these three variables according to the code used and the experimental data, respectively.

The analysis shows that the observed quasi-periodic oscillations have well defined periods. In fact, for the variables considered in the analysis of numerical results, a peak in each spectrum can be observed at a frequency around $1.0Hz$. The three variables analyzed oscillate at the same frequency according to the numerical code used. In the case of OpenFOAM, the dominant frequency is $0.90Hz$ (period of $1.11s$), whereas in FLOW-3D, the dominant frequency is $1.10Hz$ (period of $0.91s$), with an uncertainty of $0.1Hz$. The experimental data PSD (Fig. B.9 c) depicts slightly higher dominant frequencies for x_0 ($1.6Hz$) and h_2 ($2.9Hz$).
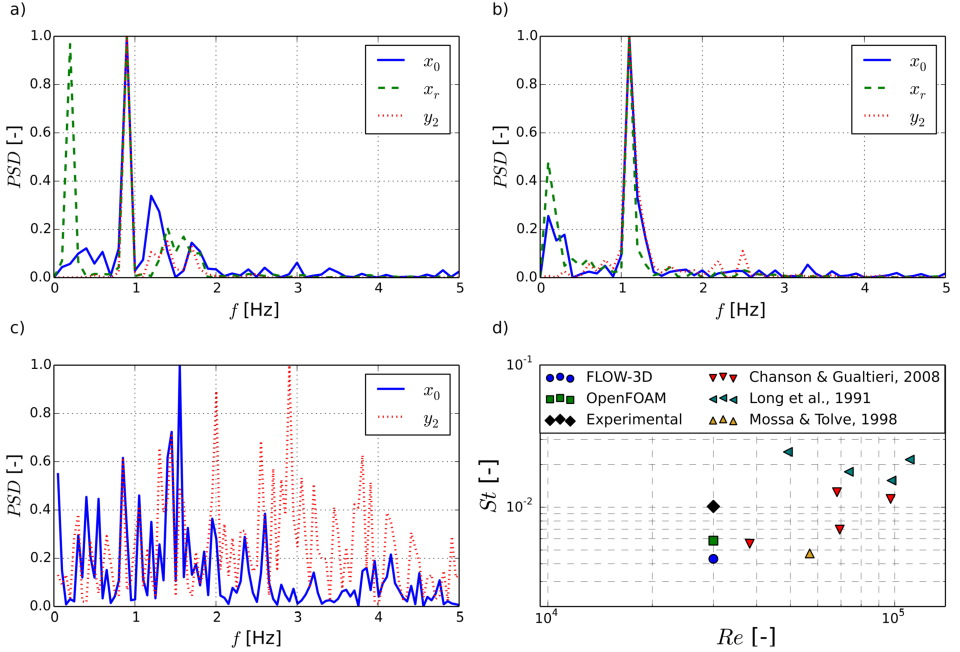
Figure B.9: Power spectrum density (PSD) of hydraulic jump toe location (x_0), roller end location (x_r) and subcritical depth (h_2): a) OpenFOAM; b) FLOW-3D; c) Experimental results; d) Comparison of resulting Strouhal numbers (St) to previous studies.

Despite of that, all these results compare well to previous works in terms of Strouhal number (St), showing certain correlation to Reynolds number (see Fig. B.9 d). It should be remarked that the similar dominant frequency found using both modeling approaches, not far from those experimentally determined, suggests that the regularity of the oscillating phenomena can be well described as a non-random and orderly process, which is superimposed on a background of turbulent random motion [Mossa, 1999]. This fact obviously results from the complex relationship among vortex structures, internal features of the hydraulic jump and observable external variables.

B.5.4   Hydraulic jump length

In the present paper, a measureable variable is proposed to determine the hydraulic jump end position: the TKE decay. To obtain this variable, the values of TKE provided by the CFD models are estimated along the channel longitudinal axis, starting at the jump toe, where maximum values of TKE occur. An exponential decay for the TKE throughout the hydraulic jump is assumed:

$$k = k_{min} + (k_{max} - k_{min}) \cdot \exp(-\gamma[x - x_0]) \tag{B.10}$$

Where k_{min} is TKE asymptotic value that occurs downstream of the hydraulic jump, k_{max}, is TKE at the jump toe,γ quantifies the characteristic TKE decay along the hydraulic jump, and x_0 is the location of the jump toe. Using Eq. B.10, the fraction of dissipated TKE throughout the hydraulic jump at a given x coordinate can be approximated as follows:

$$\sigma = 1 - e^{-\gamma[x - x_0]} \tag{B.11}$$

For both model results; FLOW-3D and OpenFOAM, it is computed at which TKE decay value (σ) the hydraulic jump end must be placed to fulfill Bradley [1945] hydraulic jump length criterion. Using least squares method, the characteristic decays obtained with OpenFOAM and FLOW-3D are $\gamma_{OF} = 6.293 J/(kg \cdot m)$ and $\gamma_{F3D} = 4.915 J/(kg \cdot m)$, respectively. It can be observed that the TKE minimum value (at the end of the hydraulic jump) is almost equal for both models ($k_{min} = 0.01 J/kg$), althoughk_{max} differs significantly from one to another (Fig. B.10). In particular, OpenFOAM yields $k_{max,OF} = 0.302 J/kg$, whereas FLOW-3D yields $k_{max,F3D} = 0.559 J/kg$.

The TKE decay threshold that makes hydraulic jump length (L_j) match with the expression by Bradley [1945] is $\sigma_{OF} = 98.3\%$ and $\sigma_{F3D} = 96.6\%$ for OpenFOAM and FLOW-3D, respectively. Thus, a 95 % decay of the maximum TKE could be established as an approximate threshold to define the jump end location in a numerical model.

Hydraulic jump length is a hard to determine variable and so involves a significant degree of uncertainty, no matter where the measurements are conducted: field, laboratory, or even numerical simulations, as it is the case analyzed herein [Chaudhry, 2007]. This is basically due to the sudden changes in water surface level, linked to the formation of internal rollers and eddies. Several observable variables, such as velocity profile in the section or subcritical flow depths, can be used in practice to develop systematic criteria for determination of hydraulic jump end-section. Also, in the light of the results herein reported, TKE can also be used to this end.
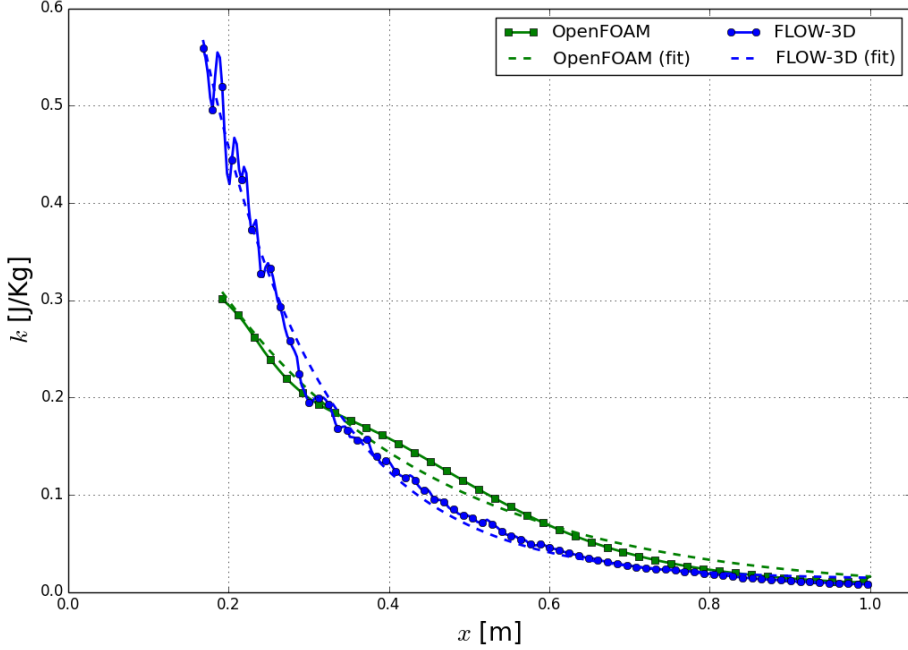
Figure B.10: TKE decay within the hydraulic jump along the longitudinal axis.

B.6   Conclusions

Choosing the most suitable CFD code among the large amount of available options is crucial, but it can also be a tedious task as criteria are strongly case dependent. When modeling hydraulic structures, one of the most widely used codes has traditionally been FLOW-3D, although the open source platform OpenFOAM is also gaining use in this kind of applications. A similar CFD model is implemented using both codes and a classical hydraulic jump case at low Reynolds number is studied. In order to assess and compare both model accuracies, both experimental data and bibliography sources are used for validation purposes.

A mesh sensitivity analysis is conducted to determine the mesh cell size that provides a good compromise between accuracy and computational cost. Besides, as all the variables analyzed are highly variable in time, an analysis of the model sensitivity to the time-averaging window is conducted. Thus, results are not affected by the size of the averaging window. As a consequence of the latter analysis, certain quasi-periodic behavior is observed in some variables, such as the hydraulic jump toe location, the roller end location and the subcritical flow depth. Autocorrelation function has been employed to analyze the characteristic temporal length

of the variable oscillation. Using FFT analysis, it is found that all these variables show similar dominant frequencies.

The comparison of the numerical model outcome to experimental and bibliography data shows that certain variables are best modeled by one code and others, by the other one. For instance, FLOW-3D appears to reproduce better the interaction between supercritical and subcritical flow and all derived variables, such as sequent depth ratio. However, OpenFOAM reproduces better the structure of the hydraulic jump. This can be observed in the more accurate estimation of the roller length. Regarding velocity fields, backward velocities and velocity profiles are slightly better reproduced by OpenFOAM, whereas the maximum velocity decay is better foreseen by FLOW-3D. However, major difficulties for both models arise in the roller region, where the swirling flow takes place. Fig. B.11 summarizes clearly the accuracy of both codes according to the variable analyzed.
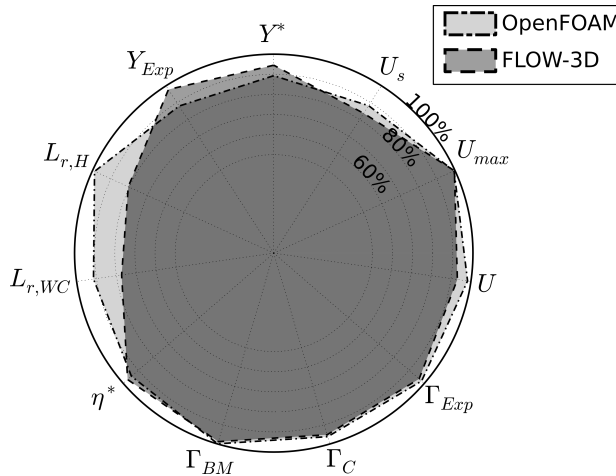
Figure B.11: Summary of code accuracies (%) of OpenFOAM and FLOW-3D.

B.6.1 Future work

Major differences between the model estimates and previous works have been observed in the roller region, where strong recirculation takes place. The behavior of this region might be difficult to capture for the most commonly used turbulence models. However, this fact does not seem to exert a relevant effect on the overall description of the phenomenon (see Fig. B.11 and Tab. B.3). Anyway, modeling higher-Reynolds-number hydraulic jumps may improve current knowledge on turbulence model performance applied to the design of energy dissipation structures.

As it can be observed in Fig. B.5, CFD model parameters can exert significant effects on flow aeration. In this case, air entrapment and bubble size is obviously conditioned by mesh element size as noticed by other authors [Witt et al., 2015]. Other model parameters, such as turbulence model used, can also play an important role in flow aeration that so far, to the knowledge of the authors, has not been analyzed in depth and constitutes an interesting field of study. As mentioned above, the effects of flow aeration on hydraulic structure behavior are not negligible at all.

The fluctuation of certain hydraulic jump characteristic variables following visible patterns outlines possible further studies in this direction. CFD models can provide results at sufficient sampling rate to capture a wealth of phenomena related to the water surface turbulence and results can be compared to experimental data.

Acknowledgements

Appendix C

Influence of VOF technique, turbulence model and discretization scheme on the numerical modeling of the non-aerated skimming flow in stepped spillways

Reference

Arnau Bayon, Juan Pablo Toro, Fabian A. Bombardelli, and Jorge Matos. Influence of VOF technique, turbulence model and discretization scheme on the numerical modeling of the non-aerated skimming flow in stepped spillways. *Journal of Hydro-environment Research* (in revision), 2017.

Abstract

An accurate description of the hydrodynamics in the non-aerated region of the skimming flow on stepped spillways is of outmost importance, particularly in small structures at large discharges. In addition, the flow features upstream of the inception point of air entrainment determine the flow behavior in the downstream self-aerated region. In this work, numerical models of the flow in the non-aerated region of stepped spillways have been developed using diverse turbulence closures and discretization schemes implemented in two CFD codes: OpenFOAM and FLOW-3D. Partial VOF (Volume of Fluid) and "True" VOF (TruVOF) approaches are employed to capture the position of the free surface. The Standard, RNG and Realizable $k - \varepsilon$, in addition to the SST $k - \omega$ model, are used for turbulence closure. Numerical results are compared against reference experimental results obtained from a physical model of constant slope of 0.75H:1V. Models with turbulence closures of the $k - \varepsilon$ family provide nearly the same predictions for the mean flow velocity with maximum differences on average smaller than 1%. Regarding discretization schemes, the first-order upwind method provides predictions for the mean flow velocity which are not significantly different (within 6%) than those obtained with second-order counterparts. However, these differences can be large when maximum values of turbulent kinetic energy (TKE) and dissipation rate of TKE at the step edges are compared. In spite of the fact that the TruVOF (FLOW-3D) method does not account for the tangential stresses at the air-water interface, differences in the tracking of the free surface position among this method and the Partial VOF method (OpenFOAM) were found to be smaller than 3% along the stepped spillway.

Keywords: Stepped spillway; Computational Fluid Dynamics (CFD); Open-FOAM; FLOW-3D; RANS; VOF.

C.1   Introduction

Stepped spillways have been used for centuries as multi-purpose hydraulic structures: flow energy dissipation, aesthetics, flood evacuation, etc. [Chanson, 2002]. It was not until last century, in concomitance with the spreading of new construction methodologies such as roller compacted concrete (RCC), that stepped spillways became an appealing way to dissipate energy [Matos and Meireles, 2014].

The presence of macro-roughness elements increases the rate of boundary layer development in stepped spillway, thus displacing upstream the inception point of air entrainment, ; i.e. the section where the boundary layer encounters the water free surface and eddies possess enough energy to distort it [Meireles et al., 2014].

In terms of momentum transfer, flow aeration exerts a series of effects on flow properties. The presence of air in the flow reduces its friction with the pseudo-bottom surface [Chanson, 1996, 2002, Matos, 1999, Matos and Meireles, 2014, Wood, 1985, 1991], thus increasing the flow velocity and reducing the energy losses. On the other hand, there is an additional drag force caused by the air carried along the flow [Valles-Moran et al., 2015b]. Finally, flow aeration reduces cavitation damage by buffering its erosive effect [Chanson, 2002, 2014, Frizell et al., 2012, 2015, Pfister, 2011].

The number of studies regarding the flow on the non-aerated area of stepped spillways has multiplied during the last decades. Given the complexity of the flow processes, analytical approaches with simplifying assumptions are not in general viable to achieve a thorough description of the flow.

So far, most of the studies in the literature are based on experimental modeling [Amador, 2005, Andre, 2004, Andre and Schleiss, 2004, Boes and Hager, 2003, Chamani and Rajaratnam, 1999, Chanson, 2001, 2002, 2015, Felder and Chanson, 2009, Gomes, 2006, Gonzalez, 2005, Matos, 1999, Matos and Meireles, 2014, Meireles, 2004, 2011a, Ohtsu et al., 2004, Renna, 2004, Sanchez-Juny, 2001, Takahashi and Ohtsu, 2012]. These works focus primarily on skimming flows and provide clear insight into relevant processes, such as boundary layer development, air transfer through the air-water interface, air concentration distribution, pressure distribution, velocity profiles and distance to the inception point of air entrainment [Bayon et al., 2015a].

Especially during the last ten years, the amount of studies on stepped spillways has increased significantly, using both experimental [Bung, 2013, Hunt and Kadavy, 2010, 2014, Meireles, 2011a, Munta and Otun, 2014, Pfister and Hager, 2011, Sanchez-Juny et al., 2008, Wu et al., 2013] and numerical [Attarian et al., 2014, Bayon et al., 2015a, Bombardelli et al., 2011, Lopes et al., 2017, Toro et al., 2016, 2017]. Although most of these numerical works are devoted to structures containing flat steps, there are a few studies that have focused on other solutions such as pooled stepped spillways [Felder and Chanson, 2013] or gabion stepped spillways [Zhang and Chanson, 2016c].

Even though studies using numerical models to describe the flow in stepped spillways are overwhelmingly outnumbered by experimental works, the number of mathematical and numerical models in the field is also growing. Most of these contributions approach the problem using Eulerian-Eulerian Computational Fluid Dynamics (CFD) to achieve a full description of the flow behavior [Arantes, 2007, Bayon et al., 2015a, Bombardelli et al., 2011, Carvalho and Amador, 2009, Chen et al., 2002, Cheng et al., 2004a,b, Tabbara et al., 2005, Toro et al., 2016, 2017]. However, different Lagrangian techniques are also used, such as Smoothed Particle Hydrodynamics – SPH [Husain et al., 2014] or even non-deterministic models

based on Artificial Neural Networks – ANN [Roushangar et al., 2014, Azadeh et al., 2011].

The number of works dealing with the non-aerated part of the flow is limited [Amador, 2005, Amador et al., 2006, Bayon et al., 2015a, Bombardelli et al., 2011, Carvalho and Amador, 2009, Hunt and Kadavy, 2010, Meireles and Matos, 2009, Toro et al., 2016, Zhang and Chanson, 2016a,b]. This fact is, to a certain extent, justified as on most prototype applications self-aeration would occur in a considerable portion of the chute for the design discharge. Nevertheless, in some real-life cases, especially in small structures at large discharges, the non-aerated flow can dominate most of the flow [Bombardelli et al., 2011, Meireles, 2011a, Meireles et al., 2014]. Characterizing the non-aerated region of the flow is also important with regard to cavitation. It is well known that if maximum velocities in the non-aerated region are large enough, cavitation will occur [Wood, 1991]. In addition, an accurate description of maximum velocities and turbulence statistics close to the inception point of air entrainment is crucial for the understanding of the flow features downstream of the inception point [Toro et al., 2016]. To the best of the Authors' knowledge, a full description of the flow features in the aerated zone has not been achieved so far.

Recent numerical works focusing on the non-aerated region have provided good predictions of time-averaged velocities, water depths, development of the boundary layer and turbulence statistics [Bayon et al., 2015a, Bombardelli et al., 2011, Meireles, 2011a, Toro et al., 2016]. However, relatively little emphasis has been put into the influence of the VOF technique, the turbulence closure and the discretization schemes on the numerical results. There is the natural question as to whether these variables exert significant differences in the prediction of the main flow properties in such region.

In this paper, a new two-dimensional CFD model of the skimming flow in the non-aerated region on stepped spillways is presented. Incompressible turbulent flow is assumed and the free surface is captured by means of Partial- and Complete-VOF methods [Bombardelli et al., 2001, Hirt and Nichols, 1981]. The theoretical model is implemented in the open source toolbox OpenFOAM and the numerical results are compared against a dataset collected at a facility assembled at the National Laboratory of Civil Engineering (LNEC), in Lisbon, Portugal, available in Matos [1999], Meireles [2004], Meireles [2011b], Meireles et al. [2012], Meireles et al. [2014] and Bombardelli et al. [2011]. Further, those numerical data are compared with counterparts obtained with the use of the code FLOW-3D [Bombardelli et al., 2011]. A model sensitivity analysis to different turbulence models and discretization schemes is performed and discussed. The flow self-similarity at various locations of the spillway is also assessed by analyzing the flow turbulence properties.

C.2 Experimental data

The experimental model used for validation of the numerical model presented herein was built at LNEC, in Lisbon, Portugal. The experimental results have been already published elsewhere [Bombardelli et al., 2011, Matos, 1999, Meireles, 2004, 2011b, Meireles et al., 2012, 2014, Renna, 2004] so only a brief summary is provided in this section.

The facilities consisted of a reservoir, and a smooth crest following the profile of the Waterways Experimental Station (WES). The first steps downstream of the crest had variable size for their edges to fit the WES profile, as depicted in Fig. C.1. A tangent point was defined downstream, where the WES profile met the constant slope steps. These steps were $3 - cm$ long and $4 - cm$ tall, defining a chute slope of 1V:0.75H. The total height of the device, from crest to toe, was $2.9m$ and had a constant width of $1.0m$.
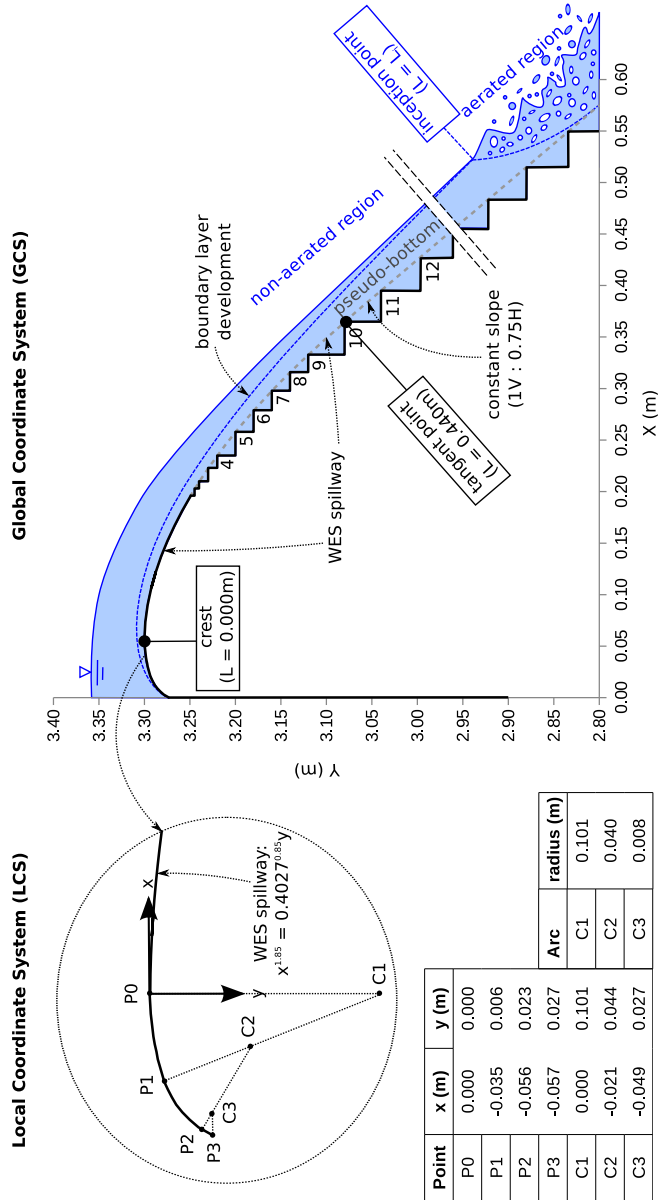
Figure C.1: Geometry of the case study and details of the spillway crest zone. Adapted from [Bayon et al., 2015a].

Measurements were taken using a conductivity probe and a back-flushing Pitot tube held in such a way that measurements could be taken perpendicularly to the spillway pseudo-bottom (see Fig. C.2). Even though this work focuses on the non-aerated region of the flow, air concentration measurements helped both to determine the equivalent clear water depth and to correct differential pressure data in the wavy region. A more thorough discussion on the experimental setup is available in Bombardelli et al. [2011], Matos [1999], Meireles [2004], Meireles [2011b], Meireles et al. [2012], Meireles et al. [2014], Renna [2004] and Bombardelli et al. [2011]. For the current paper, data presented in Bombardelli et al. [2011], and collected in the framework of Meireles [2004], was considered for the comparative analysis.

Figure C.2: Experimental stepped spillway facility at the LNEC, used for experimental validation [Matos, 1999, Meireles, 2004, Renna, 2004].

C.3 Theoretical and numerical models

C.3.1 Flow model

Turbulence features can in principle be resolved down to the smallest scale in the so-called Direct Numerical Simulation (DNS); however, this is computationally un-affordable in most applications, and corresponds to small Reynolds 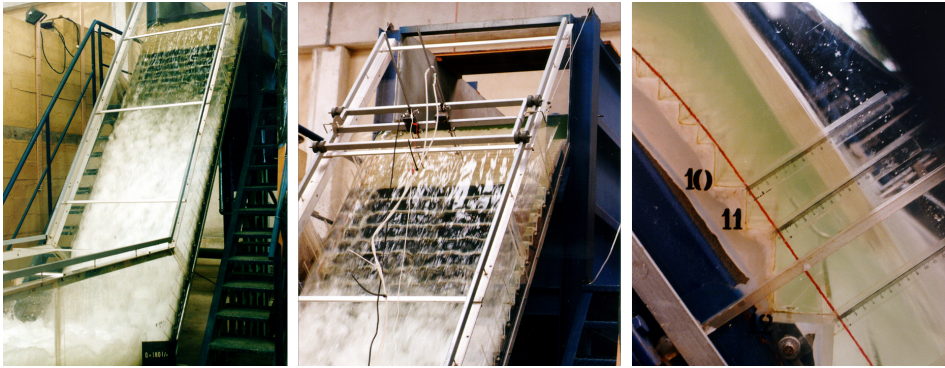numbers when it can be performed [Pope, 2000]. Modeling only the smallest scales of turbulence and solving the larger counterparts – the so-called Large Eddy Simulation (LES) – offers an appealing alternative, but computational costs are still considerable in engineering applications [Spalart, 2000].

In cases where large domains have to be modeled and no special attention is paid to what occurs at very small time and space scales, which generally takes place in most engineering applications, the turbulence averaging of the flow variables in the Navier-Stokes Equations, the Reynolds-Averaged Navier-Stokes (RANS), constitutes the best choice. This family of models can be applied to a wide range of flows [Pope, 2000], although some of the turbulence closures show limitations in certain types of flow, as discussed in Sec. C.3.3 The RANS Equations (Eqs. C.1 and C.2) are thus solved in this paper. The mass and momentum equations are expressed in vector/tensor notation in the following form, respectively:

$$\nabla \cdot \vec{u} = 0 \tag{C.1}$$

$$\frac{\partial \vec{u}}{\partial t} + \vec{u} \cdot \nabla \vec{u} = -\frac{1}{\rho}\nabla p + \frac{1}{\rho}\nabla \cdot \left(\overline{\tau} + \overline{\tau}^R\right) + \vec{f_b} \tag{C.2}$$

where u is the time-averaged velocity vector, p is pressure, ρ is density, t is time, $\overline{\tau}$ is the molecular deviatoric stress tensor, $\overline{\tau}^R$ is the Reynolds stress tensor and f_b includes the body forces. Surface tension was not included because Weber numbers were always above 110 (see Boes and Hager [2003]).

C.3.2 Free surface modeling

One of the most widely-used methods to capture the position of the free surface is the so-called VOF (Volume of Fluid) method, developed by [Hirt and Nichols, 1981]. This technique is based on three elements: a) the definition of the volume of fluid function (α), which is equal to one when the fluid is water, zero when it is air and between zero and one when the volume is occupied by both air and water; b) the imposition of boundary conditions (i.e., pressure) at the unknown free surface; and c) the use of an accurate numerical scheme to avoid numerical diffusion of the free surface solution [Bombardelli et al., 2011].

Small variants of this method are implemented in FLOW-3D, known as TruVOF [FLOW-3D User Manual, 2016] and those variants have demonstrated their validity in a wide range of hydraulic engineering applications [Bombardelli et al., 2001, 2011, Rodriguez et al., 2004]. In other codes in general, and in OpenFOAM in particular, a Partial VOF is employed, where both the water and air flows are solved [Bombardelli et al., 2001]. The transport of α in the simulated domain is modeled using the following advection equation:

$$\frac{\partial \alpha}{\partial t} + \nabla \cdot (\vec{u}\alpha) = 0 \tag{C.3}$$

where t is time and $\vec{u}$ is the shared velocity of the two-phase flow. In the Partial VOF method implemented in OpenFOAM, all variables in each mesh element, e.g., ξ, are weighted according to the fluid fraction:

$$\xi = \xi_A \alpha + \xi_B (1 - \alpha) \tag{C.4}$$

In the case of OpenFOAM, an extra velocity term is added perpendicularly to the water free surface to help to compress it: $\nabla \cdot (\vec{u}_c \alpha [1 - \alpha])$. The term $\alpha [1 - \alpha]$ ensures that the compression velocity only will affect those regions where flow fractions are close to 0.5 [Rusche, 2002]. The compression velocity term is computed according to a method based on the theory of two-phase flow [Berberovic et al., 2009]:

$$\vec{u}_c = |\vec{u}| \frac{\nabla \alpha}{|\nabla \alpha|} \tag{C.5}$$

although in Berberovic et al. [2009], the term u_c represents the relative velocity between both phases, $u_w - u_a$. The free surface position is at the point where $\alpha = 0.5$. More information on free surface modeling methods discussed herein can be found in Berberovic [2010], Bombardelli et al. [2001], [Rusche, 2002] and Ubbink [1997].

C.3.3 Turbulence modeling

Four different turbulence closures are employed, keeping all the other parameters constant, and their results are analyzed and compared. The four assessed models are the Standard $k - \varepsilon$ [Launder and Sharma, 1974], the Realizable $k - \varepsilon$ [Shih et al., 1995], the RNG $k - \varepsilon$ [Yakhot et al., 1992], and the SST $k - \omega$ [Menter, 1993]. The models of the $k - \varepsilon$ family have proven to yield good results in the modeling of hydraulic structures [Bayon and Lopez-Jimenez, 2015, Bayon et al., 2016, Bombardelli, 2004, Bombardelli et al., 2011, Bradshaw, 1996, Romagnoli

et al., 2009, Witt et al., 2015], whereas the $k - \omega$ model has been successfully applied by the Authors in a study of a hydraulic jump [Bayon and Lopez-Jimenez, 2015].

All comparative analysis is conducted exclusively using the RNG $k-\varepsilon$ simulations, so that the numerical data obtained with OpenFOAM are equivalent to the results obtained by Bombardelli et al. [2011] using FLOW-3D. The RNG $k-\varepsilon$ model is a two-equation turbulence model based on the concept of eddy viscosity ($\upsilon_t = \mu_t/\rho$), where the two additional variables to compute are k (turbulent kinetic energy, TKE) and ε (dissipation rate of TKE). The transport of these two variables is modeled according to the following advection-diffusion-reaction (ADR) equations:

$$\frac{\partial}{\partial t}(\rho k) + \nabla \cdot (\rho k \vec{u}) = \nabla \cdot [(\mu + \frac{\mu_t}{\sigma_k})\nabla k] + P_k + \rho \varepsilon \tag{C.6}$$

$$\frac{\partial}{\partial t}(\rho \varepsilon) + \nabla \cdot (\rho \varepsilon \vec{u}) = \nabla \cdot [(\mu + \frac{\mu_t}{\sigma_\varepsilon})\nabla \varepsilon] + (C_{1\varepsilon} - M)\ \frac{\varepsilon}{k}\ P_k - C_{2\varepsilon}\rho\frac{\varepsilon^2}{k} \tag{C.7}$$

$$M = \eta(-\frac{\eta}{\eta_0} + 1)\ /\ (\beta\eta^3 + 1); \quad \eta = S\frac{k}{\varepsilon}; \quad S = (2\overline{S}_{ij}\overline{S}_{ij})^{\frac{1}{2}} \tag{C.8}$$

where P_k is the production of TKE and $\overline{S}_{ij}$ is the strain-rate tensor. The formulation constants are $\sigma_k = 0.7194$, $\sigma_\varepsilon = 0.7194$, $c_{1\varepsilon} = 1.42$, $c_{2\varepsilon} = 1.68$, $C_\mu = 0.0845$, $\eta_0 = 4.38$, and $\beta = 0.012$. The eddy viscosity is computed as:

$$\upsilon_t = \frac{\mu_t}{\rho} = C_\mu\frac{k^2}{\varepsilon} \tag{C.9}$$

C.3.4   Boundary conditions

The boundary conditions imposed to the model are as follows. An inlet of constant-depth subcritical flow is followed by a stretch of reservoir of $1.2m$ in length (measured from the boundary to the crest of the spillway). This buffer zone is long enough according to the Authors' experience [Bombardelli et al., 2011, Toro et al., 2016]. Downstream of the spillway, an outlet boundary condition is imposed, where the flow leaves the domain in supercritical state. With regards to the turbulence model variables, k and ε, no measurements are available at the reservoir entrance. Therefore, a Dirichlet boundary condition is set to a low value for the actual profiles to develop along the reservoir buffer stretch.

The upper boundary condition of the model is atmospheric and so the flow can freely enter and exit the domain through it; all variables are set to a null von

Neumann boundary condition, except for pressure, which is set to atmospheric. A smooth no-slip boundary condition is applied to the solid contours of the model (the roughness of the methacrylate of the experimental device is negligible). Additionally, a wall function is imposed to the solid boundaries in the $k - \varepsilon$ models. The values of y^+ throughout the entire chute were such that the first node was located outside of the viscous sub-layer, thus ensuring that the wall function was operating as intended. Therefore, all mesh elements in contact with solid boundaries have a y^+ at the logarithmic layer, i.e. i.e. $y^+ \in [15, 100]$ [Ferziger and Perić, 2002, Schlichting and Gersten, 2000] . The y^+ variable is defined as:

On the other hand, since the SST $k - \omega$ is a low-Reynolds model, is a low-Reynolds model, a mesh refinement is required for all mesh elements in contact with solid boundaries, so that the first volume is in the viscous sub-layer. The y^+ variable is defined as:

$$y^+ = y \; \frac{u_\tau}{\upsilon} \tag{C.10}$$

where y is the distance of the center of the first volume to the wall, u_τ is the shear velocity and υ is the kinematic viscosity. On the other hand, since the SST $k - \omega$ is a low-Reynolds model, a mesh refinement is required for all mesh elements in contact with solid boundaries, so that the first volume is in the viscous sub-layer.

Details regarding the model wall treatment are available in Bayon and Lopez-Jimenez [2015] and Bombardelli et al. [2011].

C.3.5   Numerical models and schemes

The numerical solution of the equations presented above was developed via the finite volume method (FVM), and implemented in the codes OpenFOAM [Open-FOAM User Guide, 2011] and FLOW-3D [FLOW-3D User Manual, 2016]. In OpenFOAM, the numerical integration is conducted using the PIMPLE algorithm, a combination of two widely used algorithms: PISO [Issa, 1985] and SIMPLE [Patankar and Spalding, 1972].

The choice of one discretization scheme has consequences for both the accuracy and the stability of results [Blazek, 2005]. In the present work, three different discretization schemes are used to approximate the advection terms: a) a first-order upwind method; b) the second-order limited Van Leer [1977] method; and c) a second-order limited central difference method. A sensitivity analysis to the numerical discretization scheme is conducted along with the rest of model parameters.

Time derivatives are discretized using a second-order backward discretization scheme. The diffusive terms of the equations are discretized using a second-order accurate

Gauss linear corrected scheme in all cases. Also, to ensure stability of simulations, time steps are automatically modified so that Courant numbers always remain below 0.30.

C.4   Model implementation

C.4.1   Geometry and mesh

Unstructured meshes might allow in some cases a more flexible mesh refinement [Kim and Boysan, 1999] and fit in a natural way to geometrically complex domains [Biswas and Strawn, 1998]. Structured meshes allow in principle for more accurate numerical results [Hirsch, 2007] and make access to memory faster, thus reducing latency times [Keyes et al., 2000]. Given the nature of the geometry of this case, we selected a structured mesh, as used in Bombardelli et al. [2011].

A structured mesh formed by rectangular elements of 4/3 aspect ratio was employed. The mesh employed in the SST $k - \omega$ simulations required additional refinement in the near-wall region to ensure that y^+ remains within the viscous sub-layer. To this end, 10 extra layers of total thickness equal to 1/3 of the normal element size and a growth ratio of 1.175 were added to the elements adjacent to the spillway steps.

In order to fit the mesh to the modeled geometry, the OpenFOAM model uses the tool snappyHexMesh; its use in similar applications has yielded good results [Sweeney, 2014, Toro et al., 2016]. The FLOW-3D code uses the porosity-based FAVOR method to define solid objects, which, if correctly used, yields accurate results [Carvalho et al., 2008, Bombardelli et al., 2011].

To obtain mesh-independent results, 5 different mesh sizes were used and the grid convergence index (GCI) methodology proposed by Roache [2009] and discussed in Celik et al. [2008]. The grid refinement degree between consecutive sizes is $\sqrt{2}$, thus being the global refinement degree 4.0, way above the 1.3 minimum value proposed by Celik et al. [2008]. The characteristics of the tested meshes are summarized in Tab. C.1 . Water depths (h) at 6 different locations are used as indicator variables. Fig. C.3 shows mesh number 5 in the crest zone as an example.

Simulations were compared against LNEC experimental data for a discharge of $0.18 m^3/s$ (specific discharge of $0.18 m^2/s$). These simulations were run varying only one parameter from one simulation to another in order to capture the effect of that specific parameter.

Mesh number	Horiz. size (Δx) (mm)	Vert. size (Δy) (mm)	Aspect ratio (V/H)	$h' = \sqrt{\Delta x \Delta y}$ (mm)
1	1.06	1.41	4/3	1.22
2	1.50	2.00	4/3	1.73
3	2.12	2.83	4/3	2.45
4	3.00	4.00	4/3	3.46
5	4.24	5.66	4/3	4.9

Table C.1: Characteristics of the meshes tested in the convergence analysis.
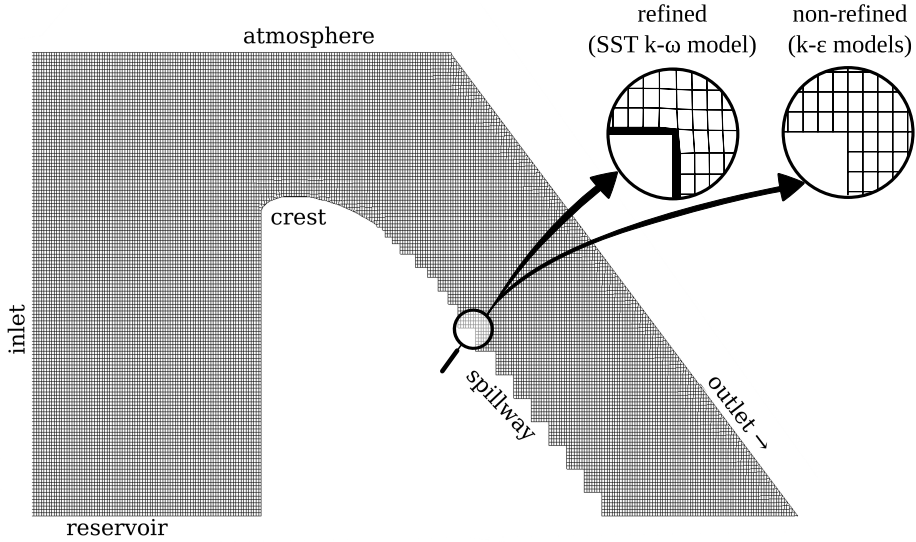

Figure C.3: Detail of mesh of the spillway crest zone.

C.5 Analysis of results

C.5.1 Mesh convergence

The mesh-convergence analysis was conducted using the results obtained with a first-order discretization scheme, as this was the setup used in Bombardelli et al. [2011]. In Fig. C.4 a comparison of water free surface profiles for $\alpha = 0.5$ and velocity profiles using different mesh sizes is shown. The apparent order (p'), the approximate relative error (e_a) and the grid convergence index (GCI) computed following the methodology proposed by Celik et al. [2008] are presented in Fig. C.5. The apparent order reaches a value of $p'_{k-\varepsilon} = 0.927$ and $p'_{k-\varepsilon} = 0.924$ for the RNG $k - \varepsilon$ and the SST $k - \omega$ model, respectively, both close to the model formal order in mesh number 2 ($h' = 1.73mm$), which indicates that the asymptotic range has been reached. The analysis of this mesh indicates that the average approximate relative error was $e_{a(k-\varepsilon)} = 3.7\%$ and $e_{a(k-\omega)} = 3.4\%$ and the grid convergence index was $GCI_{k-\varepsilon} = 4.9\%$ and $GCI_{k-\omega} = 4.4\%$, respectively, revealing that in both cases numerical uncertainty remains within an acceptable range. None of the indicator parameters of the mesh convergence analysis shows improvement at sizes below the size of mesh number 2 ($h' = 1.73mm$). All subsequent analyses are conducted on results employing the mesh of $h' = 1.73mm$.

Clearly, both codes, OpenFOAM and FLOW-3D, respond differently to mesh size reduction, which is a fact that has already been observed in diverse types of flows by Bombardelli et al. (2009).
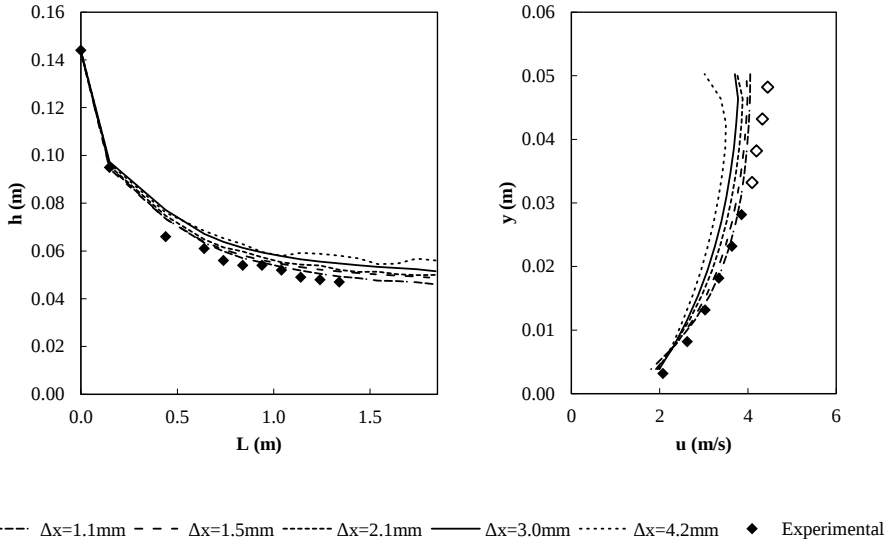
Figure C.4: Water free surface profiles (left) and velocity profiles (right) at $L = 1.04m$ (step 23) as a function of mesh element minimum size (Δx), with a first-order upwind scheme, Partial VOF and the RNG $k - \varepsilon$ model, compared against experimental data. Unfilled symbols indicate measurements affected by fluctuations either of the free surface or the inception point position.

Figure C.5: Mesh-convergence analysis results. Evolution of average apparent order (p'), average approximate relative error (e_a) and average grid convergence index (GCI) for mesh size $\Delta x = 1.5mm$ ($h' = 1.73mm$) and first order discretization scheme according to the employed turbulence model.

C.5.2   Sensitivity analysis

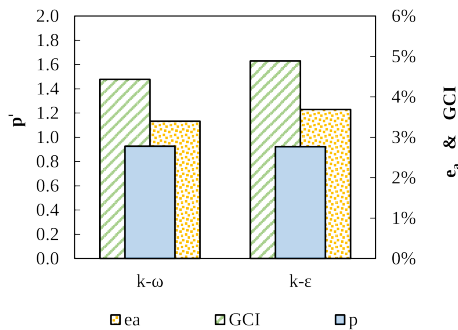This analysis was exclusively conducted using OpenFOAM results, as FLOW-3D results have already been analyzed in Bombardelli et al. [2011].

The differences in the model outcome are small among different second-order discretization schemes (Fig. C.6). Differences between first- and second-order methods are small when predicting the mean flow velocities (4%), but they reach larger values (not shown herein) when predicting maximum TKE on step edges. Both second-order limited central-difference and limited Van Leer discretization schemes yield very similar results, with differences in estimations below 4% for all the analyzed variables. Nevertheless, the limited central-difference scheme seems to systematically achieve accuracies between 5% and 10% higher employing approximately 30% smaller computational times than the Van Leer scheme.
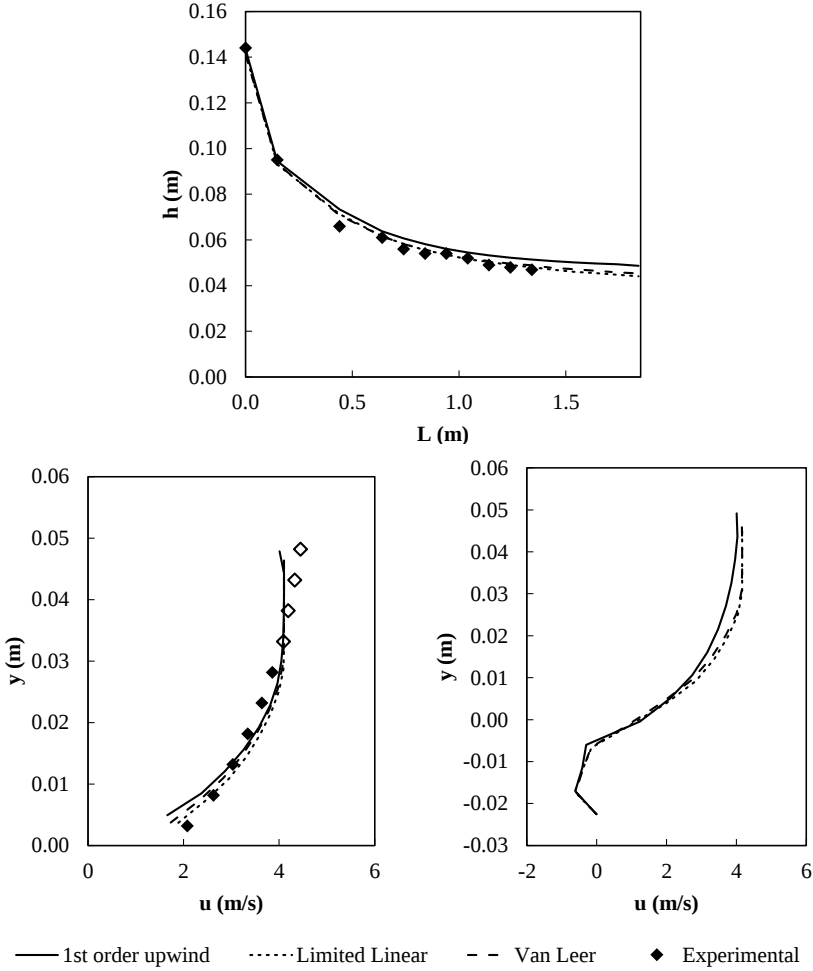
Figure C.6: Numerical results using RNG $k - \varepsilon$ model and diverse discretization schemes, with a converged mesh size of $\Delta x = 1.5mm$. a) Water free surface profiles; b) Velocity profile at step 23 ($L = 1.04m$); c) Velocity profile within the cavity at $L = 1.072m$. For the experimental data, unfilled symbols indicate measurements affected by either the fluctuations of the free surface or the location of the inception point.

With regard to turbulence models, it is shown in Fig. C.7 that the RNG $k - \varepsilon$, the Standard $k - \varepsilon$ and the Realizable $k - \varepsilon$ models yield virtually the same results (differences are on average below 1%). In average terms, a slightly better performance can be attributed to the RNG $k - \varepsilon$ model in the prediction of certain variables, such as water depths or the profiles within the boundary layer, but this difference is not significant. As depicted in Fig. C.7, the SST $k - \omega$ model tends to overestimate water depths (4%) with a consistent underestimation of velocities slightly above the RNG $k - \varepsilon$ (2% overestimation of water depths).
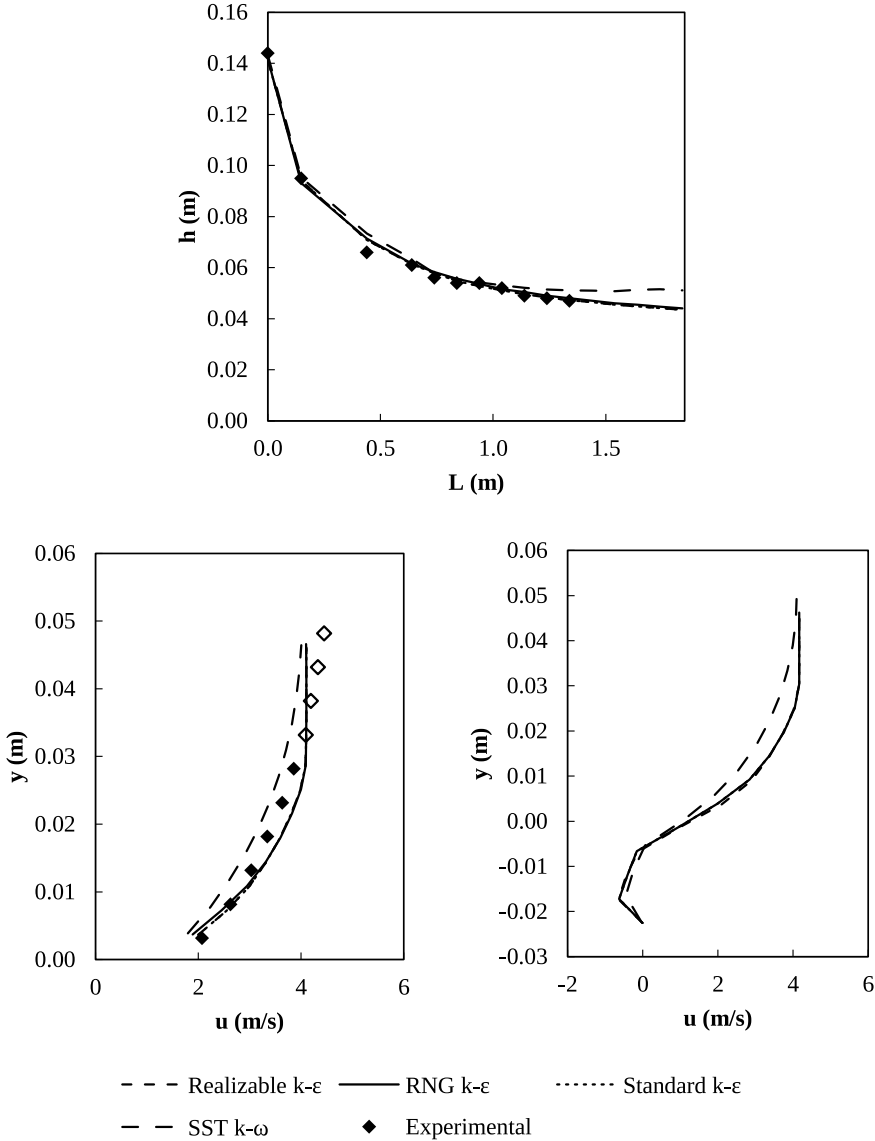
Figure C.7: Numerical results using a limited central-difference discretization scheme and diverse turbulence models, with a converged mesh size of $\Delta x = 1.5 mm$. a) Water free surface profiles; b) Velocity profile at step 23 ($L = 1.04 m$); c) Velocity profile within the cavity at $L = 1.072 m$. For the experimental data, unfilled symbols indicate measurements affected by either the fluctuations of the free surface or the location of the inception point.

C.5.3 Discussion of approaches

The flow depth throughout the stepped spillway is very well predicted by all approaches (see Fig. C.8). The first reach located over the smooth region near the spillway crest is reproduced with a root mean square error (RMSE) below 1%. In the last steps, all approaches seem to overestimate the experimental results, although results with TruVOF are slightly closer to the experimental data. The RMSE in the water profile estimation for the TruVOF method is 4.2%, slightly below the 6.2% attained by teh Partial VOF.

Figure C.8: Water free surface profile using RNG $k - \varepsilon$ model and first-order upwind discretization scheme and a converged mesh size of $\Delta x = 1.5mm$ according to type of VOF method: Partial VOF (OpenFOAM) and TruVOF (FLOW-3D).

With regards to velocity profiles, the formation of a boundary layer is accurately captured by both methodologies (see Fig. C.9). Despite both codes tend to underestimate the absolute velocity values, OpenFOAM achieves a smaller difference with the experimental data than FLOW-3D. Despite the fact that both approaches tend to slightly underestimate the velocity values, the Partial VOF achieves a smaller difference with the experimental data than the TruVOF method. This may be due, among other causes, to the fact that the TruVOF does not account for free-surface tangential stresses.
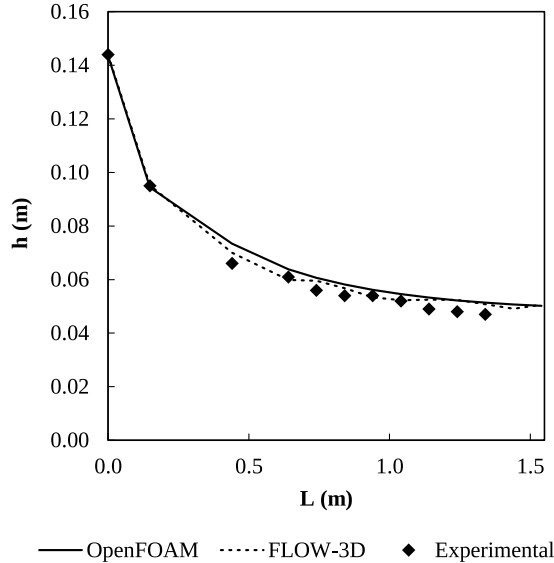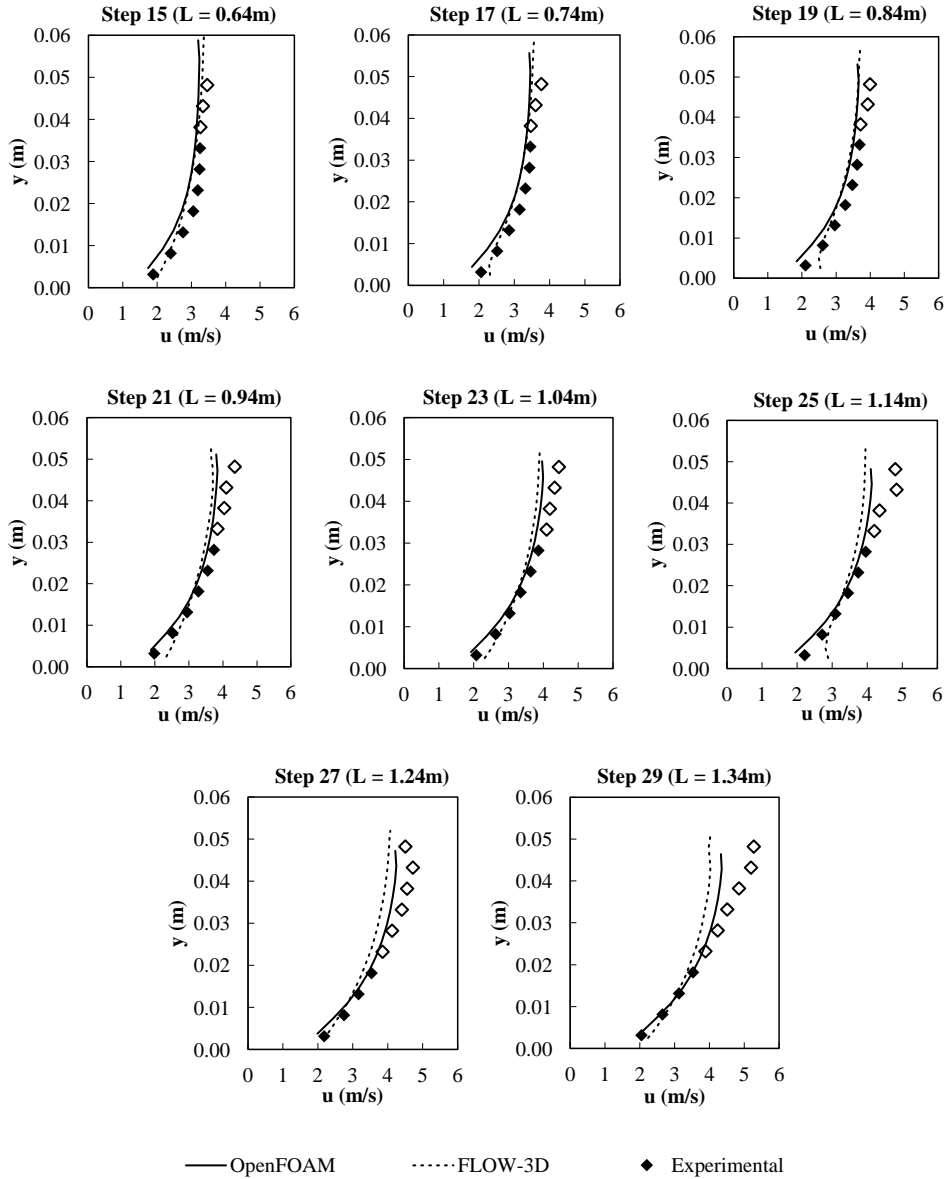
Figure C.9: Velocity profiles using RNG $k - \varepsilon$ model and a first-order upwind discretization scheme and a converged mesh size of $\Delta x = 1.5mm$ according to type of VOF method: Partial VOF (OpenFOAM) and TruVOF (FLOW-3D).

In Fig. C.10, the boundary layer of velocity profiles, normalized by using the 99%of the freestream velocity as upper limit for the boundary layer (U_{max}), is shown. The vertical coordinate is normalized by using the boundary layer thickness (δ), whereas the stream-wise velocity is normalized by using U_{max}. In this region of the flow, the pattern observed in the dimensional profiles is confirmed. However, in this case, OpenFOAM is significantly more accurate than FLOW-3D.

In Fig. C.10, the evolution of flow depths and boundary-layer development for both Partial VOF and TruVOF methods is presented. By extrapolating their trending curves, the approximate location of the inception point, i.e., where flow aeration should start, can be estimated. According to this extrapolation, Partial VOF predicted a distance to the inception point of 1.66 m, whereas the TruVOF estimated $1.87m$. Compared to the experimentally observed distance to the inception point, Partial VOF and TruVOF overestimated this variable by 14% and 30%, respectively. The experimental results and the inception point location computed according to Chanson [2002] are also included in Fig. C.10. Compared to this dataset, the results of Partial VOF and TruVOF differ with experiments in 2% and 7%, respectively. It bears emphasis that the experimental data have uncertainties on its own given the difficulty of determining the precise location due to unsteadiness.

A recent experimental work [Zhang and Chanson, 2016a] states that the inception point occurs where the boundary layer thickness reaches 80% of the water depth. Using this criterion, OpenFOAM and FLOW-3D estimate distances to the inception point of $1.33m$ and $1.28m$, respectively. Compared to the experimental data, the models underestimated this variable by 8% and 11.5%, respectively.

From the computations using OpenFOAM, a certain trend to yield more "developed" velocity profiles near the spillway crest, is observed resulting in a clear overestimation of the boundary-layer thickness within this region ($L < 0.75$).
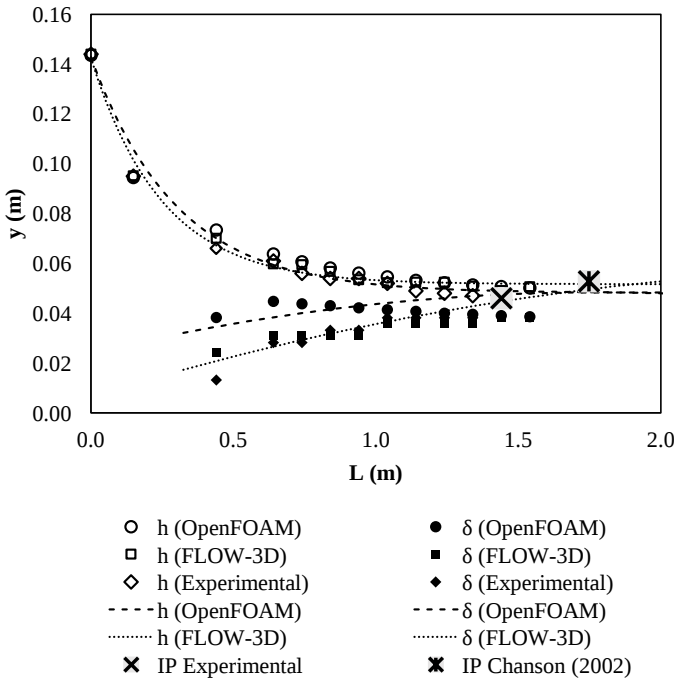
Figure C.10: Distribution of water depths, boundary-layer development and estimated inception point of air entrainment profile using RNG $k-\varepsilon$ model and a first-order upwind discretization scheme and a converged mesh size of $\Delta x = 1.5mm$ according to type of VOF method: Partial VOF (OpenFOAM) and TruVOF (FLOW-3D) with validation using experimental data and literature.

C.5.4 Self-similarity analysis

Meireles [2011a] and Toro et al. [2016] proposed and corroborated self-similarity of turbulence statistics in stepped spillways, an unprecedented result. Similarly, Felder and Chanson [2011] discussed self-similarity of the integral time scales in terms of similar trends in the flow distributions along the cavity. However, there was no clear description of the self-similarity in the flow velocity within the cavity, as no negative velocities were recorded in the recirculation region. Previously, in Gonzalez and Chanson [2004], similar trends of the flow velocity within the cavity were presented; in that study, non-dimensional velocities were obtained by using the velocity at which half of the freestream velocity is reached. For a description of a self-preserving boundary layer, the reader is referred to the experimental work by Gonzalez and Chanson [2004], one of the pioneer studies of the flow over rough walls.

In the case presented herein, the results show the occurrence of a certain pattern in the velocity and TKE distributions throughout the spillway (see Fig. C.11). Using a suitable normalization, most of flow variables present self-similar behavior throughout the spillway. This fact was investigated by using exclusively Open-FOAM data and the results indicate approximate flow self-similarity.

Fig. C.12 shows the normalized profiles of velocity, TKE, dissipation rate and pressure at different step edges compared with the results reported in previous works for the velocities. These profiles show an important degree of overlapping. Additionally, it was observed that the highest pressures always occur close to the pseudo-bottom at approximately $0.32cm$ upstream of the step edges (cf. also with Toro et al. [2016]).

A self-similar behavior can also be observed in the step cavities, as depicted in Fig. C.13. The velocity profiles predicted by the model in the recirculation zone attain an accuracy of 93.3%, compared to data by Amador et al. [2006]. The same authors state that the maximum recirculation velocity is 15% of u_{max}, which is confirmed by the results presented herein. With regards to pressure profiles, it can be observed how this variable drastically drops below the hydrostatic profile in the recirculation region, as reported in Toro et al. [2016].

Concerning the TKE and dissipation rate of TKE profiles, a peak can be neatly identified near the pseudo-bottom, so corroborating that the flow in the pseudo-bottom vicinity is responsible for the highest dissipation rates of TKE [Toro et al., 2016]. It was also observed that the dissipation rate profiles perfectly reproduce the shape of the integral turbulent length scale profiles reported in Amador et al. [2006].

Figure C.11: Velocity and TKE fields throughout the spillway obtained with Open-FOAM using a converged mesh ($\Delta x = 1.5mm$), an upwind first-order discretization scheme and the RNG $k - \varepsilon$ model.
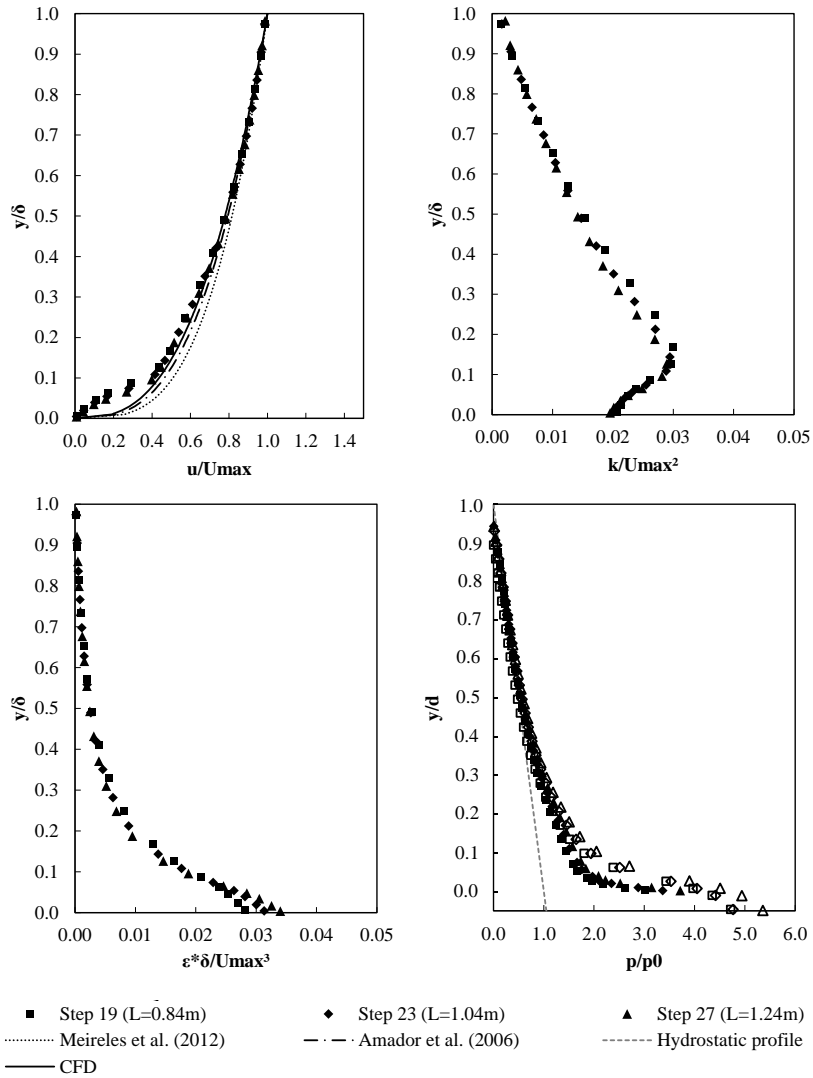
Figure C.12: Profiles of normalized velocity, turbulent kinetic energy (TKE), dissipation rate of TKE and pressure at different step edges using RNG $k - \varepsilon$ model and a first-order upwind discretization scheme and a converged mesh size of $\Delta x = 1.5mm$. In the pressure plot, unfilled symbols correspond to pressure profiles $0.32cm$ upstream of step edges, where maximum pressure occurs, and the dashed line represents the hydrostatic profile.
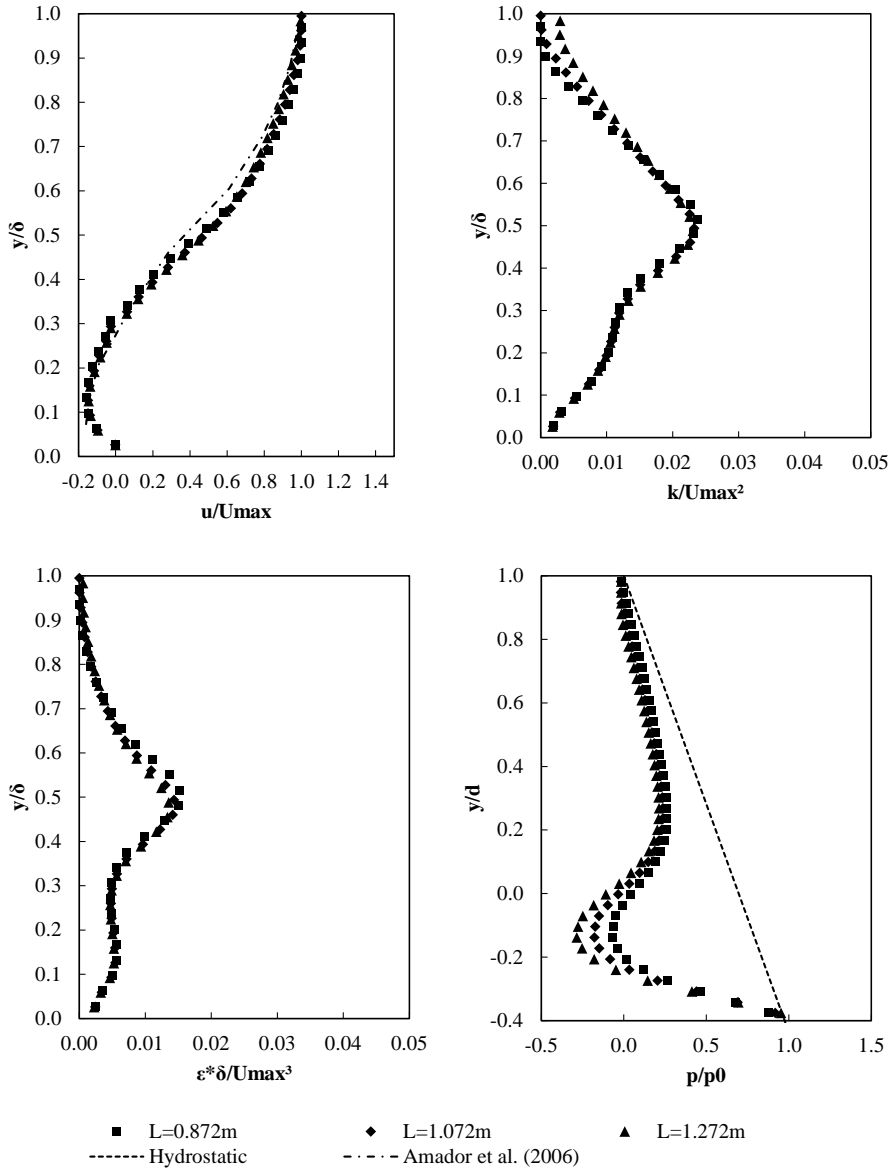
Figure C.13: Profiles of normalized velocity, turbulent kinetic energy (TKE), dissipation rate of TKE and pressure at different step gaps using RNG $k - \varepsilon$ model and a first-order upwind discretization scheme and a converged mesh size of $\Delta x = 1.5mm$.

C.6   Final remarks and conclusions

A numerical model, able to reproduce the behavior of the non-aerated region of the flow in stepped spillways, has been implemented using OpenFOAM. For its validation, experimental data previously collected at LNEC were used. After a satisfactory grid-independence and mesh-convergence analysis, the sensitivity to turbulence model, treatment of the free surface and numerical discretization scheme was assessed.

Numerical results indicate that the use of a Partial VOF instead of the TruVOF does not affect significantly the predictions of flow velocities and turbulence statistics. This result is especially important given the imposition of boundary conditions at the free surface in the TruVOF. The results obtained with several RANS $k - \varepsilon$ turbulence models indicate that their prediction errors are within 1%. The RNG $k - \varepsilon$ model performs marginally better, whereas the Standard $k - \varepsilon$ and the Realizable $k - \varepsilon$ yield virtually the same results. The SST $k - \omega$ model, in turn, overpredicts the water depths by 4%, with a consistent underprediction of velocities. Differences are more important than those obtained with the models of the $k - \varepsilon$ family while solving the flow within the viscous sub-layer.

The model sensitivity to different numerical discretization schemes shows that the limited central-difference scheme performs slightly better and at smaller computational costs than the limited Van Leer model, although both second-order schemes yield similar results for velocities and water depths.

Additionally, the approximate self-similar nature of turbulence quantities for these flows, proposed by our research group elsewhere, was further confirmed in this paper.

Acknowledgements

Appendix D

Numerical analysis and validation of south Valencia Sewage Collection System Diversion

Reference

Arnau Bayon, Francisco Jose Valles-Moran, and Petra Amparo Lopez-Jimenez. Numerical analysis and validation of South Valencia sewage collection system diversion. In *36th IAHR Conference*, The Hage (Holland), 2015.

Abstract

The old Sewage Collection System (SCS) of south Valencia, Spain, had to be recently diverted to avoid interference with the city high-speed railway works. Certain aspects of the proposed modification of this channel are complex from both the geometric and the hydraulic point of view. Besides, the structure is a unitary collector and must handle torrential flow rates up to $100m^3/s$. In the present work, the stretch most prone to suffer from hydraulic issues is numerically analyzed. This part of the SCS diversion project involves complex sections, critical and subcritical flow regimes, hydraulic jumps, flow expansions and contractions and other singularities not always easy to address. In order to analyze the hydraulic performance of the described design, a three-dimensional model based on the open-source CFD platform OpenFOAM is presented. In this model, turbulence is treated using three widely used RANS approaches, namely: Standard $k - \varepsilon$, RNG $k - \varepsilon$ and SST $k - \omega$, whose accuracies are compared by means of a sensitivity analysis. Structured meshes of different element size are tested, and the model sensitivity to this parameter is also studied. The air-water interface must be accurately defined, as the flow under study is gravity-driven and water depths have to be controlled to avoid flow pressurization. To do so, an Eulerian-Eulerian volume method is used. As a result, a full physically consistent description of the flow is achieved and so a wealth of interesting variables can be computed. In order to assess the accuracy of the numerical model, some variables regarding the water surface level are compared to experimental data. These experimental results are obtained from a 1/20 scale physical model, where Froude similarity is achieved and scale effects are proved not to be significant. Good agreement between numerical and experimental results is achieved despite the complexity of the system under study. In the light of the results, the model proposed can be applied to accurately model similar hydraulic structures.

Keywords: Open channel; OpenFOAM; CFD; $k - \varepsilon$; $k - \omega$.

D.1 Introduction

The Sewage Collection System (SCS) of South Valencia, Spain, is a unitary collector that delivers service to several hundred thousand people and drains the runoff of an area of about $14.75 \cdot 10^6 m^2$, most of it densely populated and where torrential rains are frequent. Indeed, this large hydraulic structure was built after the 1957 autumn rain episode, which flooded most of the city and caused about 100 casualties, and has been operating since then. Currently, the original SCS underground layout conflicts with that of the new high-speed railway access to the city and so has to be diverted. This is a challenging task as the SCS has to deal with flow rates up to $100m^3/s$ in a rather complex layout, which involves curves,

steep stretches and other singularities not always easy to address from both the hydraulic and the urbanistic point of view.

An original solution consisting of a uniform section of constant slope was first proposed. This design was analyzed using good practice criteria, empirical deduction and technical documentation, which quickly made some hydraulic issues surface. Among them, one of the most potentially hazardous was the occurrence of critical regimes in curved stretches, which could lead to an excessive water surface tilt and even a channel bank overflow. The original design could also lead to intolerably high velocities (up to almost $9m/s$) and the occurrence of hydraulic jumps of very unpredictable position and length. The latter effect was found to be prone to cause pressurized pulsatile flow in sections downstream of the modified stretch, which is completely unacceptable.

For the reasons exposed above, a series of solutions were proposed and preliminarily analyzed using, among others, the U.S. Bureau of Reclamation guidelines for stilling basin design [Peterka, 1984] and the one-dimensional model HEC-RAS. As a result, a new design was defined, which ensured stable Froude numbers throughout the entire channel with a single critical flow section. This control section was followed by a compact stabilized hydraulic jump completely confined within a stilling basin of more resistant concrete. Hence, according to HEC-RAS, this geometry, described in depth in the following section, should produce a perfectly predictable flow behavior and a peaceful delivery to the old SCS layout.

Nevertheless, a geometry of these characteristics indubitably leads to highly a three-dimensional flow. This implies that a one-dimensional model, such as HEC-RAS,is likely not enough to capture all relevant flow features. Hence, a fully three-dimensional numerical model based on a computational fluid dynamics (CFD) approach is developed to ensure the desired hydraulic behavior of the structure. The model description, based on the free open source platform OpenFOAM, and its results are presented herein. Despite this model has been previously validated using a classical hydraulic jump case study [Bayon and Lopez-Jimenez, 2015], experimental data, obtained using an ad hoc Froude-similar 1/20 scale physical model, are used to validate it.

The attempts to reproduce the behavior of all kinds of hydraulic structures are numerous [Caisley et al., 1999, Meireles et al., 2012]. The typology of these structures is extremely variable and so is the nature of the flow features to reproduce. Nevertheless, a close observation of the literature shows that one of the phenomena most difficult to address is the hydraulic jump [Romagnoli et al., 2009, Carvalho, 2002]. The literature treating this feature is vast and so is the number of approaches used: CFD [Witt et al., 2015], smooth particle hydrodynamics [De Padova et al., 2013], experimental [Chanson, 2013] or a combination of several of them [Bombardelli et al., 2011].

Nevertheless, most of the studies are rather theoretical and focus on the so-called classical hydraulic jump, i.e. the hydraulic jump occurring in a flat rectangular prismatic channel of smooth walls [Hager, 1992]. The number of real life cases of structures involving hydraulic jumps is small compared to the total amount of publications in this field. Besides, many of them use an experimental approach, as numerical models still fail to reproduce certain aspects of this phenomenon [Murzyn et al., 2005]. However, numerical approaches provide a clean non-intrusive way to measure some features of hydraulic jumps [Murzyn and Chanson, 2009a].

The present paper presents a real life application based on the CFD open source platform OpenFOAM, whose use is currently spreading surprisingly fast. The use of free open source software in this kind of applications is an asset as commercial licenses are generally expensive. The case presented, as it can be observed in the following sections, is complex both from the geometric and the hydraulic point of view: it combines quickly-varying section shapes, weirs, macro-roughness elements, fast and slow flow regimes and hydraulic jumps. Nevertheless, in the light of the results, these features are properly addressed and so the present model can be applied to other real case design cases in a reliable way.

D.2   Materials and methods

D.2.1   Geometry

The design solution proposed affects more than 180m of the original channel layout. However, in order to save resources, only a shorter stretch, the most prone to cause hydraulic issues, is analyzed. The channel modification starts with a $5.0m$ transition from the channel original section ($6.5m$ wide ovoid) to a $6.0m$ rectangular section with a central $2.5m$ wide circular channel to deal with urban black water in normal circumstances. The latter section extends for more than $50.0m$, including curves, but the one-dimensional analysis proved that flow will behave gently throughout this stretch. The modeled domain starts at the last $20.0m$ of this part of the channel. In the model, the initial $20.0m$ stretch of the section described above is used to allow the flow to develop and reduce the effect of the inlet boundary condition. Downstream of that, the flow reaches a constant radius curve that will likely tilt its surface outwards, followed by another straight stretch. In this part of the channel, water surface tilt in both directions will occur while flow stabilizes before it reaches a $1.44m$ high WES-type spillway. The main goal of this structure is to create a single control section in the channel, so ensuring that critical depths are not reached anywhere else. The aforementioned spillway also avoids the overlapping of the SCS layout with that of the high-speed railways. The slope of the whole stretch upstream of the spillway is 0.0021, whereas downstream

it is reduced to 0.0013. This allows a harmonic link between the SCS diversion stretch and the pre-existent layout upstream and downstream of it.

Throughout the channel spillway, which rests on the high-speed railway tunnel, the section width expands to $7.50m$ to match the subsequent stilling basin cross section. The stilling basin, placed right upstream of the transition back to the $7.50m$ ovoid section of the original channel, must slow the flow down before it is delivered to the original channel in subcritical regime. To do so, a hydraulic jump as stabilized and compact as possible is forced throughout a very short length. This is achieved by adding triangular macro-roughness elements to the stilling basin banks (the circular central channel is not altered). The channel modeling will help to prove that the hydraulic jump is confined within the stilling basin, built using more resistant concrete, so preventing high shear stresses to compromise the original channel downstream. The macro-roughness elements were designed to achieve the equivalent roughness value necessary to force the hydraulic jump to occur within the stilling basin. Should the hypotheses and simplifications made not be correct, the consequences may lead to the structure failure. This is one of the main reasons why fully three-dimensional and physical models are considered crucial for an appropriate SCS design. Tab. D.1 and Fig. D.1 describe the modeled stretch layout, plant, profile and sections.
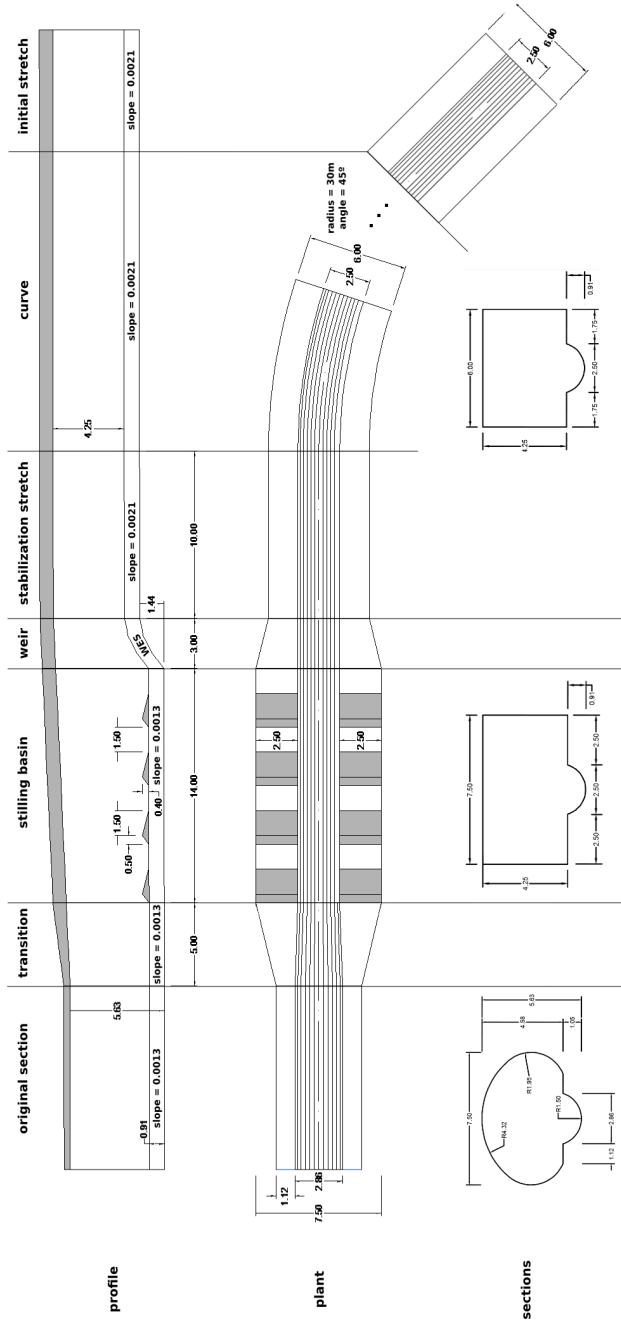
Figure D.1: Geometry description: SCS layoutand section according to stretch.

Table D.1: Geometry description according to stretch. W is width and L is length. All units in S.I.

Stretch name	$x_{initial}$	x_{final}	$z_{initial}$	z_{final}	W	L	Slope
Initial stretch	0.00	20.01	0.00	-0.04	6.00	20.01	0.0021
Curve	20.01	43.31	-0.04	-0.09	6.00	23.30	0.0021
Stabiliz. stretch	43.31	53.31	-0.09	-0.11	6.00	10.00	0.0021
WES spillway	53.31	56.31	-0.11	-1.55	trans.	3.000	WES
Stilling basin	56.31	70.31	-1.55	-1.57	7.50	14.00	0.0013
Transition	70.31	75.31	-1.57	-1.58	7.50	5.00	0.0013
Original section	75.31	95.32	-1.58	-1.60	7.50	20.01	0.0013

D.2.2   Numerical model

The numerical model most essential features are outlined in the following subsections. A more in-depth discussion on its implementation and its validation using a classical hydraulic jump case study have been conducted by Bayon and Lopez-Jimenez [2015].

D.2.3   Mesh

The discretization of the geometric domain to model is normally approached by means of structured or unstructured meshes. The latter kind of meshes adapt better to complex geometries, such as that of the SCS [Biswas and Strawn, 1998]. Also unstructured meshes allow a more selective refinement in regions where large property gradients are expected [Kim and Boysan, 1999]. However, structured meshes tend to reduce computation times [Keyes et al., 2000] and, as long as flow interfaces are relatively parallel to the mesh axes, cause less convergence problems in multiphase flow simulations. Therefore, a structured rectangular mesh of hexahedral elements is preferred in this model.

As regards mesh refinement of boundary layers and other regions where large gradients occur, preliminary simulations demonstrated that most of the domain modeled requires a similar mesh element size. For this reason, the model mesh is constituted by cubic elements of constant size, except for those cases where the mesh intersects solid boundaries and has to be snapped to adapt to the solid surface as smoothly as possible.

In order to determine the optimum mesh size and so avoid its excessive refinement, a mesh sensitivity analysis is conducted. To do so, simulations are run using five different mesh element sizes caeteris paribus, namely: $0.1236m$, $0.1115m$, $0.1030m$, $0.0932m$ and $0.0861m$. This will determine below which mesh element size no further improvement is obtained.

D.2.4 Implementation

Open channel flows can be analyzed using one-dimensional approaches, such as HEC-RAS. However, when a full description of flows with large three-dimensional components is required, this approach is no longer valid and so theNavier-Stokes equations have to be approximated:

$$\nabla \cdot \vec{u} = 0 \tag{D.1}$$

$$\frac{\partial \vec{u}}{\partial t} + \vec{u} \cdot \nabla \vec{u} = -\frac{1}{\rho}\nabla p + \upsilon \nabla^2 \vec{u} + \vec{f_b} \tag{D.2}$$

Where u is velocity, p, pressure, t, time, ρ, density, υ, kinematic viscosity, and f_b, body forces (gravity and surface tension). To do so, a wealth of numerical algorithms exists, such as SIMPLE [Patankar and Spalding, 1972] or PISO [Issa, 1985]. In the present model, a combination of both, PIMPLE, is used through its implementation in the open source platform OpenFOAM.

In multiphase flows, one of the most relevant aspects is how the coexistence of several fluids is treated and how interfaces among them are tracked. Complex algorithms are developed for this purpose given its high influence on the model accuracy [Hyman, 1984]. Two big categories of models can be defined, namely: the surface methods and the volume methods. Among the first kind, both Lagrangian and Eulerian approaches are possible, whether surface is defined by means of marker particles or by equations approximated on fix locations. However, both present problems in complex geometries with flow detachment and breaking fluid interfaces. Volume methods, adapt sensitively better to this situations. Lagrangian approaches are feasible (one of the fluids volume is defined by marker particles), but they are normally extremely slow when simulating large domains. Eulerian approaches, which use an indicator property to determine the volume occupied by one fluid or another) are preferred in that case and so are considered the best choice in the present model. The main drawback of volume methods is that they do not define a fluid interface explicitly, but need algorithms instead. This kind of models, such as the Volume of Fluid (VOF), developed by Hirt and Nichols [1981], are the most widely used in this kind of applications. The model implemented here differs from the original VOF implementation in many aspects, such as the use of an interface compression algorithm to clean a neat water-air interface [Rusche, 2002], but are based on a similar approach.

In highly aerated flows, such as that studied herein, air fraction becomes a variable of paramount importance. The air content of flows severely affects its depth, volume, density and compressibility [Carvalho, 2002], which strongly alters momentum transfer processes. In cases like this, most of the effects are desirable,

such as the reduction of both the cavitation risk [Bung and Schlenkhoff, 2010] and the shear stress on the streambed [Chanson, 1994].

In order to reproduce bubbles or droplets smaller than the mesh element size, additional models are necessary [Toge, 2012]. Lagrangian approaches are feasible in not very aerated flows and allow an important computation time saving. Nevertheless, when modeling hydraulic jumps and other phenomena involving breaking surfaces, Eulerian approaches are generally preferred. Besides, they can reproduce the effects of drag, lift and buoyancy, although generally imply longer computational times. In the present model, a fully Eulerian model is implemented.

D.2.5 Turbulence

Turbulence can be fully resolved by CFD models down to its smallest scales if meshes are accordingly fine, approach known as Direct Numerical Simulation (DNS). However, this implies computational costs that are completely unaffordable in most engineering applications. Velocity and pressure fluctuations can be partially modeled to make models computationally lighter using approaches such as the so-called Large Eddy Simulation (LES). This kind of models is more common in engineering applications and constitutes an appealing solution in many cases. Nevertheless, in the model presented herein a full modeling of turbulence is preferred as quickly varying properties do not play an important role in this kind of structures.

This approach, known as Reynolds Averaged Navier-Stokes (RANS), is therefore implemented. This family of models is based on modeling the so-called Reynolds stresses. To do so, one or more transport equations of additional variables are implemented in the numerical model. In the case of $k-\varepsilon$ models, these variables are k (turbulent kinetic energy) and ε (turbulent kinetic energy dissipation rate). In the case of $k-\omega$ models, the latter variable is replaced by ω (turbulent kinetic energy specific dissipation rate). Many RANS models have been developed and the choice of one or another can exert significant effect on the model accuracy. Unfortunately, none of them constitutes a perfect definitive solution and their suitability is highly case specific. In order to determine which RANS model yields best results in cases like that analyzed herein, a turbulence model sensitivity analysis is conducted. To do so, simulations are run using three of the most used models caeteris paribus, namely: Standard $k-\varepsilon$ [Launder and Sharma, 1974], RNG $k-\varepsilon$ [Yakhot et al., 1992] and SST $k-\omega$ [Menter, 1993].

D.2.6   Boundary conditions

In order to ensure a proper behavior of the model, appropriate boundary conditions have to be defined. The inlet flow rate is imposed to $100m^3/s$, which derives from administrative prescriptions and hydrological plans. Using this value and given the section and the slope of both the inlet and the outlet, the water depth is set to the corresponding natural heights, $4.09m$ and $5.01m$. At the inlet, velocity is imposed by a constant Dirichlet boundary condition as the channel initial stretch allows the flow to develop and so reach a hydrostatic profile. A null Neumann boundary condition is imposed to pressure at the inlet. This stretch also helps k and ε to adjust, so these variables are set to an arbitrary value close to zero at the inlet. At the outlet, all variables are defined by null Neumann conditions except for velocity, which is set to a constant value that univocally forces the desired water height at this section. Fig. D.2 provides a schematic description of the model boundary conditions.
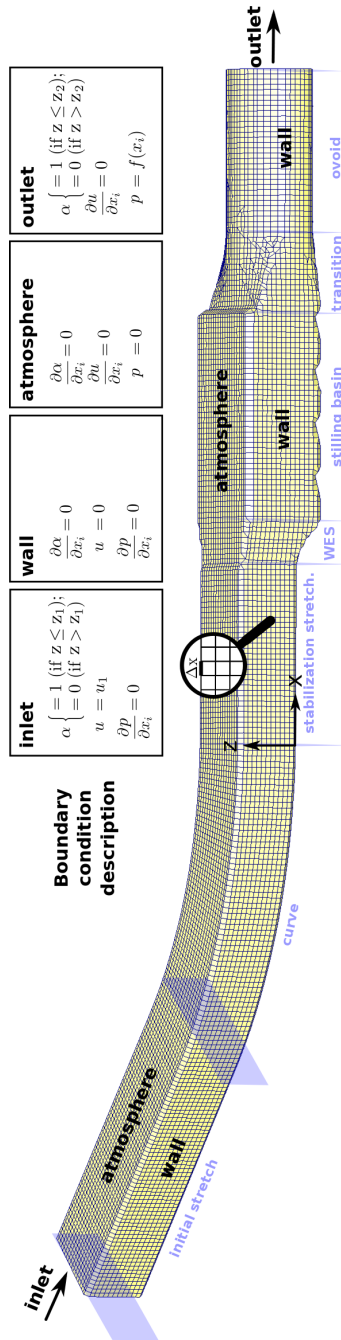
Figure D.2: Mesh example and model boundary conditions.

As regards walls, a no-slip condition is imposed to force the flow to be contained within the channel banks and streambed. In order to save computational resources, it is a common practice in CFD models to implement wall functions. These algorithms by-pass the viscous sub-layer of the boundary layer by imposing a pre-determined velocity profile. Although this can imply a certain accuracy loss, the computational time saving makes in many cases this choice appealing. Besides, as long as the size of mesh elements in contact with solid boundaries is maintained within an appropriate y^+ coordinate range [Schlichting and Gersten, 2000], wall functions do not necessarily compromise the reliability of results.

As the SCS operates in an open air regime and in order to help the model to maintain the mass balance throughout its boundaries, an atmosphere patch is imposed to the domain top. This kind of boundary condition allows the flow to freely enter and live the domain and not using it has proved to cause severe mass conservation problems.

D.2.7 Physical model

In order to validate the numerical model, its results are compared to those obtained using a physical model built ad hoc. As a real scale model was not feasible, a reduction was necessary. To do so,a series of hypotheses that do not bias results excessively were made. The flow under study is likely to be highly tridimensional, so a geometrically distorted model is directly discarded. The water depths imposed have to be those that maintain geometric proportionality with the channel size. The scale 1/20 was found to be the most unfavorable fulfilling the Russell and Chow criterion (which ensures the rough turbulent behavior of the scaled flow).

The size of the flow features that play most important role in a case like this, such as eddy formation and flow detachment, maintain proportionality with flow external dimensions, such as water depth. This allows to scale the model within a certain range without using fluids of different properties, i.e. not fulfilling Reynolds similarity. Nevertheless, given that the flow is essentially driven by gravity, Froude similarity must be strictly respected. This criterion is therefore used to determine the inlet velocity and so the inlet flow rate.

As regards the channel material choice, it was found that the model roughness should as small as possible in order to keep the roughness similarity. The Stenton modified diagram shown that such roughness could only be achieved using materials as smooth as possible. Thus, methyl-methacrylate was used to build the channel banks, which also allows to observe the flow through. In order to reproduce all the streambed geometric singularities, fine grain cement plastered with several covers of plastic smooth paint is used.

Table D.2: Boundary condition comparison: physical model vs. numerical model and real life boundary conditions.

Variable	Numerical model	Physical model
Flow rate (m^3/s)	100	$55.9 \cdot 10^{-3}$
Inlet depth (m)	4.090	0.205
Outlet depth (m)	5.010	0.251

Water depth measurements are conducted using two different methods according to the phenomenon that wants to be captured. Water surface tilt is measured using a multipoint gauge, which allows measuring up to six points per cross section. This way, the flow deviation caused by curves and so the risk of channel bank overflow can be detected. The hydraulic jump water surface profile is more uniform throughout each cross section, but a more abrupt variation in the longitudinal coordinate is expected. For this reason, digital image treatment is used to outline the water surface in the stilling basin. This way, a larger number of points can be obtained by assuming that no significant surface fluctuation occurs within the same cross section.
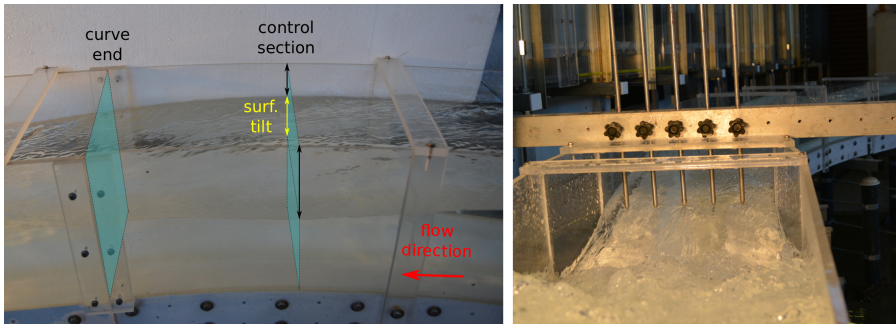
Figure D.3: Water surface tilt in physical model curve stretch (left) and multipoint gauge at spillway crest (right).

D.2.8   Postprocessing

The result postprocessing allows to compare numerical and physical results to determine their reliability and the suitability of the SCS solution design. In order to prevent bank overflow, water surface tilt is measured at four channel cross sections. This will allow to ensure that overflow will not occur at any of the most prone sections, namely: the curve end ($x = 43.31m$), where surface tilt is maximum, and the stabilization stretch ($x = 48.30m$), where it inverts its direction. The water surface tilt is also measured at the spillway crest ($x = 53.31m$) to ensure that the flow has stabilized before reaching the critical flow

section. Water heights are measured at every cross section using five gauge points separated $5cm$ from one another. The rest of the surface is inferred from these points.

As regards the stilling basin, the hydraulic jump water surface profile is measured by digital image treatment at 14 equidistant points throughout the entire stretch, i.e. 1 $point/m$. Ten equidistantly separated snapshots are used to obtain the average water level profile and so be able to be compared to numerical results.

Other relevant variables, such as the streambed shear stresses or velocity profiles, are computed using the numerical model. However, some of these variables cannot be easily measured in the physical model, so they are analyzed only from a qualitative point of view. Indeed, the capability to easily estimate variables like these is one of the main assets of developing, calibrating and validating CFD models in design applications.

D.3   Results

The numerical model results are presented herein. As discussed in the previous section, a mesh sensitivity analysis is conducted. The simulations run demonstrated that no improvement in accuracy is obtained at mesh element sizes below $0.103m$. Besides, when using wall functions, finer meshes not always imply better accuracies, as excessively refined meshes can be resolving boundary layer features that are already modeled, thus introducing certain error in the results. For the sake of simplicity, all numerical results presented below correspond to this mesh size.

The water level numerically computed and experimentally measured at several cross sections is presented in Fig. D.4. Not only the flow surface tilt trends are consistently followed, but also good agreement is found between both sets of data. For some reason, the section expected to be less sensitive to errors, the curve inlet, presents the largest mismatch. However, in the rest of sections, the agreement is practically total. Outward surface tilt is caused by the flow passing through the curve, although both models demonstrated that the proposed bank height is enough to contain it. As expected, this tilt inverts its direction downstream of the curve, in the stabilization region. Nevertheless, the deformation in this stretch is sensitively lower. A gradual decrease of height is observed, which can be explained by the influence of the WES weir section, where critical flow is reached. Indeed, at the latter section, this variable reaches its minimum value. Also at the weir crest, it can be observed how the stabilization stretch accomplishes its purpose, as flow surface is barely skewed. The only observable deformation of surface at this point is a height decrease in the vicinity of the channel banks. This is caused by the section expansion occurred throughout the weir.
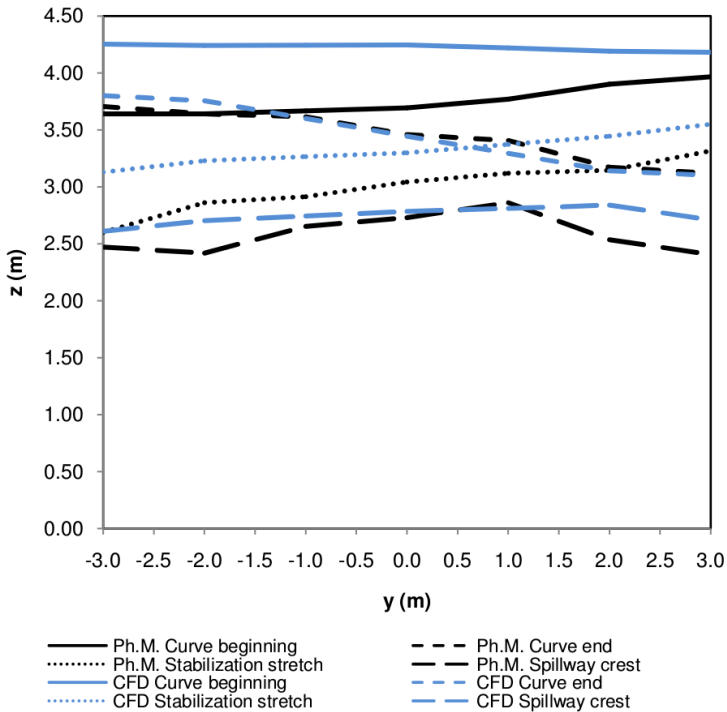
Figure D.4: Water surface tilt comparison between numerical model (CFD) and physical model (Ph.M.) at several cross sections.

As regards the stilling basin, good agreement is also found in the comparison of numerical results and experimental digitally treated images. Fig. D.5 shows the mean water profiles in this stretch according to the turbulence model used compared to the experimental results. On the upper part of the figure, it can be observed how the hydraulic jump occurs right downstream of the weir. This helps to contain the whole flow regime transition within the stilling basin, which was one of the main goals of the new solution design proposed. The sensitivity analysis to turbulence model leads to the conclusion that sensitively different results are obtained according to the model used. Nevertheless, as Fig. D.5 shows, all of them managed to perfectly reproduce the phenomenon and to capture all trends. The coefficient of determination (R^2) of the Standard $k - \varepsilon$, the RNG $k - \varepsilon$ and the SST $k - \omega$ with respect to the physical model results are 0.944, 0.927 and 0.941, respectively. The Standard $k - \varepsilon$ model reproducing best experimental hydraulic jumps is a phenomenon already observed by the authors in the past. However, in previous experiences, SST $k - \omega$ generally did not manage to capture hydraulic jump water profiles as accurately as in this case. The turbulence model used also

implies non-negligible differences in computation time. The authors have found through experience that the Standard $k-\varepsilon$ model tends to be faster in this kind of applications, followed by the RNG $k-\varepsilon$ model and, in the last place, the SST $k-\omega$ model.
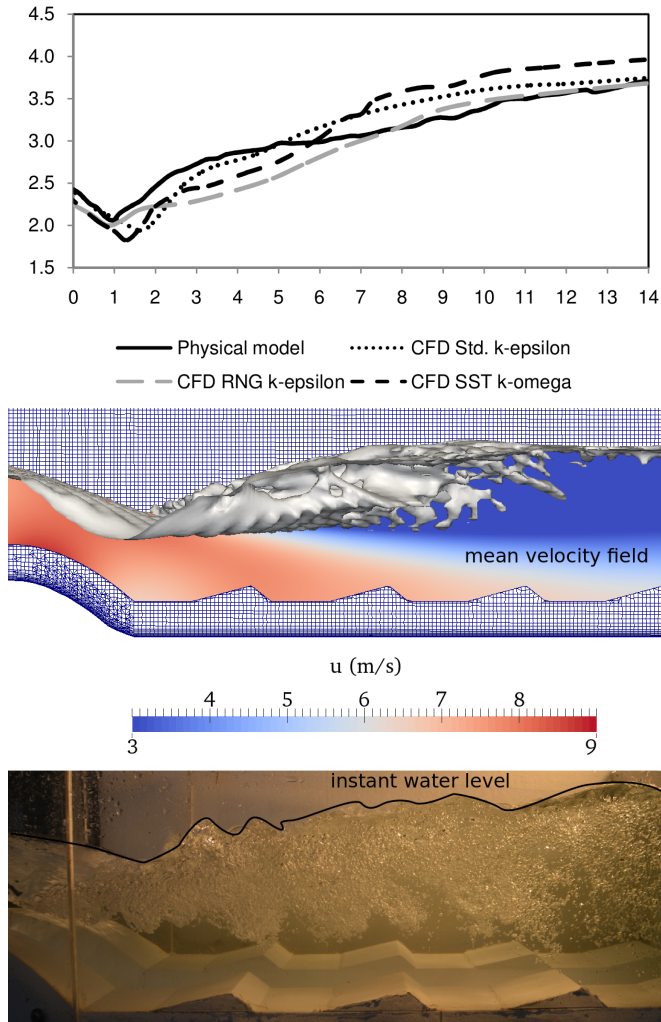

Figure D.5: Hydraulic jump surface profile comparison among different turbulence models at stilling basin (top) and example snapshots: numerical model (center) and physical model (bottom).

Another phenomenon experimentally observed is consistently reproduced by the numerical model: a small flow detachment on the channel banks at the WES weir section. On the left-hand side of Fig. D.6, this process, caused by a sudden flow expansion, is depicted. Areas of negative longitudinal velocity values, where recirculation occurs can be observed due to two reasons, namely: the occurrence of the aforementioned lateral flow detachment and the presence of the hydraulic jump roller.

Flow detachment is an undesirable phenomenon in cases like this and could be avoided by using a smoother transition approach. Nevertheless, in the case under study, this recirculation region remains small and does not seem to be prone to cause problems such as instabilities, fluctuations, etc. Besides, a smoother transition could conflict with pre-existent structures at a urbanistic level.
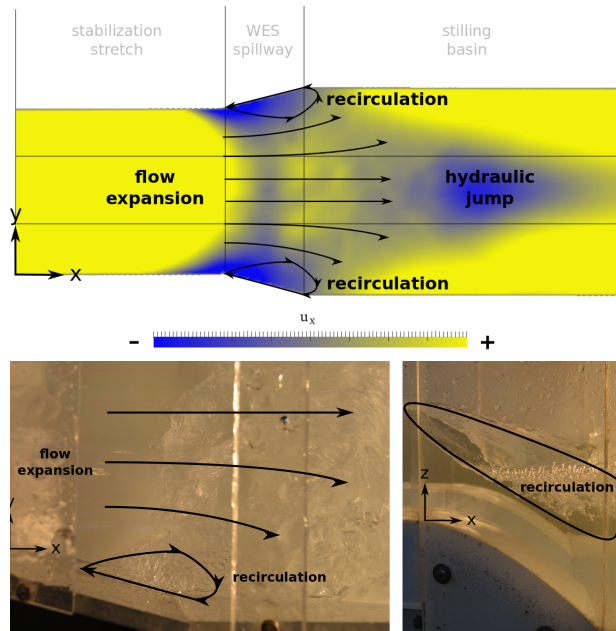

Figure D.6: Recirculation comparison between numerical model (top) and physical model (bottom) at spillway.

Numerical and experimental results demonstrate that the downstream water level $(5.01m)$ is not reached at the end of the stilling basin so, technically, the hydraulic jump would not be confined within this stretch (see Fig. D.5). However, as Fig. D.7 shows, the hydraulic jump aspect most prone to cause damage to the SCS structure, i.e. shear stress, is perfectly controlled and only affects to the tips of the first three macro-roughness elements. An important decrease and stabilization of this variable is observed before the flow reaches the transition section. It is important to remark that, as a wall function is implemented to the CFD model, the exact quantification of shear stresses is uncertain. For this reason, a maximum-minimum is used instead of the actual values yielded by the numerical model.
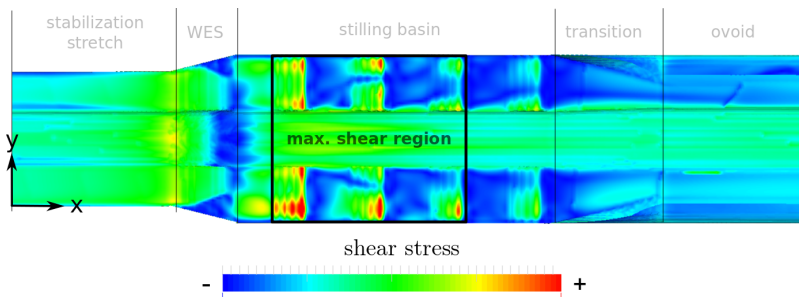

Figure D.7: Shear stresses on streambed at spillway, stilling basin and transition to old channel section.

D.4   Conclusions

The present work deals with the numerical analysis of the South Valencia Sewage Collection System modification. The solution proposed to avoid conflict with the new high-speed railway access to the city is thoroughly analyzed from the hydraulic point of view. The design is highly conditioned by civil engineering and urbanistic issues as it is placed at a densely populated region. For this reason, the channel layout can hardly be modified and so a good hydraulic analysis to deal with the issues detected in preliminary design solutions is crucial.

A fully three-dimensional turbulent CFD model based on the open source platform OpenFOAM is developed for this purpose. The model validation is conducted using a 1/20 scale experimental device built ad hoc. A case study is run using the design flow rate $(100m^3/s)$ as boundary condition. RANS turbulence models are used and the mesh cannot be excessively refined given the size of the whole structure. Despite that, good agreement is found between numerical and experimental results. The variables compared are rather macroscopic, although they are the most relevant ones in the problem under study.

The water surface tilt after a curve section and the effect of the subsequent stabilization stretch is analyzed. It is observed that tilt occurs where expected and always below the channel bank height. Also the stabilization stretch accomplished its role as flow is proved to reach the critical flow section perfectly balanced, which avoids severe potential problems.

In order to ensure appropriate flow restitution conditions to the old SCS layout downstream of the modification analyzed, a hydraulic jump has to be forced at a stilling basin placed after the critical flow section. Its water level profile is numerically computed and compared to experimental results and good agreement is found among both sets of data. Although the whole hydraulic jump is not contained within the stilling basin stricto senso, its position is perfectly stabilized right downstream of the weir. Besides, it is observed that no flow pressurization will occur when reaching the old channel layout and shear stresses, one of the most hazardous effect of hydraulic jumps in hydraulic structures, are proved to be confined within the stilling basin.

Besides the model validation, sensitivity analyses to two of its most relevant parameters, mesh element size and turbulence model, are conducted. Mesh sizes below $0.103m$ do not seem to improve results and make the model unnecessarily slow. As regards turbulence models, the Standard $k-\varepsilon$ proved to be the most accurate in capturing the hydraulic jump profile achieving an accuracy of $R^2 = 0.944$. Anyway, the other two turbulence models tested also managed to reproduce the physics of the phenomenon under study and yielded R^2 values just slightly below that of the Standard $k - \varepsilon$.

Thus, in the light of the results, the model is considered validated and its use can be recommended to analyze the behavior of complex hydraulic structures as this. Besides, the use of relatively coarse meshes and RANS turbulence models allow computation times completely affordable in design cases like this. Also avoiding commercial licenses by using only free open source software allows the application of the model to a wider range of hydraulic engineering cases.

Acknowledgements

Bibliography

F. Ahmed and N. Rajaratnam. Three-dimensional turbulent boundary layers: A review. *Journal of Hydraulic Research*, 35(1):81–98, 1997.

A. Amador. *Comportamiento hidraulico de los aliviaderos escalonados en presas de hormigon compactado.* PhD thesis, Universitat Politecnica de Catalunya, Barcelona (Spain), 2005.

A. Amador, M. Sanchez-Juny, and J. Dolz. Characterization of the nonaerated flow region in a stepped spillway by PIV. *Journal of fluids engineering*, 128(6): 1266–1273, 2006.

S. Andre. *High Velocity Aerated Flows over Stepped Chutes with Macro-Roughness Elements.* PhD thesis, École Polytechnique Fédérale de Lausanne (Switzerland), 2004.

S. Andre and A. Schleiss. High velocity aerated flows on stepped chutes with macro-roughness elements. Technical report, École Polytechnique Fédérale de Lausanne (Switzerland), 2004.

E. J. Arantes. *Caracterização do Escoamento sobre Vertedouros em Degraus via CFD.* PhD thesis, Universidade de São Paulo (Brasil), 2007.

N. Ashgriz and J. Poo. FLAIR: Flux line-segment model for advection and interface reconstruction. *Journal of Computational Physics*, 93(2):449–468, 1991.

A. Attarian, K. Hosseini, H. Abdi, and M. Hosseini. The effect of the step height on energy dissipation in stepped spillways using numerical simulation. *Arabian Journal for Science and Engineering*, 39(4):2587–2594, 2014.

A. Azadeh, M. Saberi, and S. Asadzadeh. An adaptive network based fuzzy inference system–auto regression–analysis of variance algorithm for improvement of oil consumption estimation and policy making: The cases of Canada, United Kingdom, and South Korea. *Applied Mathematical Modelling*, 35(2):581–593, 2011.

163

A. F. Babb and H. C. Aus. Measurements of air in flowing water. *Journal of Hydraulic Division, ASCE*, 107:1615–1630, 1981.

B. A. Bakhmeteff and A. E. Matzke. The hydraulic jump in terms dynamic similarity. *Transactions of the American Society of Civil Engineers*, 101(1):630–647, 1936.

S. Balachandar and J. K. Eaton. Turbulent dispersed multiphase flow. *Annual Review of Fluid Mechanics*, 42:111–133, 2010.

I. Barton. Comparison of SIMPLE- and PISO-type algorithms for transient flows. *International Journal for Numerical Methods in Fluids*, 26(4):459–483, 1998.

A. Bayon and P. A. Lopez-Jimenez. Numerical analysis of hydraulic jumps using OpenFOAM. *Journal of Hydroinformatics*, 17(4):662–678, 2015.

A. Bayon, J. Matos, and P. A. Lopez-Jimenez. Modelado matematico de flujo no aireado en aliviaderos escalonados mediante OpenFOAM. In *IV Jornadas de Ingenieria del Agua, Cordoba (Spain)*, 2015a.

A. Bayon, F. J. Valles-Moran, and P. A. Lopez-Jimenez. Numerical analysis and validation of south valencia sewage collection system diversion. In *36th IAHR World Congress, The Hage (Holland)*, 2015b.

A. Bayon, D. Valero, R. Garcia-Bartual, F. J. Valles-Moran, and P. A. Lopez-Jimenez. Performance assessment of OpenFOAM and flow-3d in the numerical modeling of a low reynolds number hydraulic jump. *Environmental Modelling & Software*, 80:322–335, 2016.

A. Bayon, J. P. Toro, F. A. Bombardelli, and J. Matos. Influence of VOF technique, turbulence model and discretization scheme on the numerical modeling of the non-aerated skimming flow in stepped spillways. *Journal of Hydro-environment Research (accepted)*, 2017.

J. Belanger. *Notes sur l'Hydraulique*. Ecole Royale des Ponts et Chaussees, Paris, France, 1841.

N. D. Bennett, B. F. Croke, G. Guariso, J. H. Guillaume, S. H. Hamilton, A. J. Jakeman, S. Marsili-Libelli, L. T. Newham, J. P. Norton, C. Perrin, and others. Characterising performance of environmental models. *Environmental Modelling & Software*, 40:1–20, 2013.

E. Berberovic. *Investigation of Free-surface Flow Associated with Drop Impact: Numerical Simulations and Theoretical Modeling*. PhD thesis, Technische Universität Darmstadt (Germany), 2010.

E. Berberovic, N. P. van Hinsberg, S. Jakirlic, I. V. Roisman, and C. Tropea. Drop impact onto a liquid layer of finite thickness: Dynamics of the cavity evolution. *Phys. Rev. E*, 79(3):036306, 2009.

G. Bidone. Le remou et sur la propagation des ondes. *Report to Academie Royale des Sciences de Turin*, 12:21–112, 1819.

R. Biswas and R. C. Strawn. Tetrahedral and hexahedral mesh adaptation for CFD problems. *Applied Numerical Mathematics*, 26(1):135–151, 1998.

J. Blazek. *Computational Fluid Dynamics: Principles and Applications*. Elsevier, 2005.

B. Blocken and C. Gualtieri. Ten iterative steps for model development and evaluation applied to computational fluid dynamics for environmental fluid mechanics. *Environmental Modelling & Software*, 33(0):1 – 22, 2012.

B. Blocken, T. Stathopoulos, and J. Carmeliet. CFD simulation of the atmospheric boundary layer: wall function problems. *Atmospheric environment*, 41(2):238–252, 2007.

R. M. Boes and W. H. Hager. Two-phase flow characteristics of stepped spillways. *Journal of Hydraulic Engineering*, 129(9):661–670, 2003.

F. A. Bombardelli. *Turbulence in multiphase models for aeration bubble plumes*. PhD thesis, University of Illinois at Urbana-Champaign (USA), 2004.

F. A. Bombardelli. *Recent Advances on Multi-phase Flows of Environmental Importance*. Springer, 2009.

F. A. Bombardelli. Computational multi-phase fluid dynamics to address flows past hydraulic structures. In *4th IAHR International Symposium on Hydraulic Structures, Porto (Portugal)*, pages 9–11, 2012.

F. A. Bombardelli, C. W. Hirt, M. H. García, B. W. Matthews, C. A. J. Fletcher, A. C. Partridge, and S. Vasquez. Computations of curved free surface water flow on spiral concentrators. *Journal of Hydraulic Engineering*, 127(7):629–631, 2001.

F. A. Bombardelli, I. Meireles, and J. Matos. Laboratory measurements and multi-block numerical simulations of the mean flow and turbulence in the non-aerated skimming flow region of steep stepped spillways. *Environmental Fluid Mechanics*, 11(3):263–288, 2011.

J. E. Borges, N. H. Pereira, J. Matos, and K. H. Frizell. Performance of a combined three-hole conductivity probe for void fraction and velocity measurement in air–water flows. *Experiments in fluids*, 48(1):17–31, 2010.

V. Borue, S. A. Orszag, and I. Staroslesky. Interaction of surface waves with turbulence: direct numerical simulations of turbulent open channel flow. *Jorunal of Fluid Mechanics*, 286:1–23, 1995.

J. Boussinesq. Theorie de l'intumescence liquide, applelee onde solitaire ou de translation, se propageant dans un canal rectangulaire. *Comptes Rendus de l'Academie des Sciences*, 72:755–759, 1871.

J. N. Bradley. *Study of air injection into the flow in the Boulder Dam spillway tunnels, Boulder Canyon Project*. US Bureau of Reclamation, 1945.

P. Bradshaw. Understanding and prediction of turbulent flow. *International journal of heat and fluid flow*, 18(1):45–54, 1996.

D. Brennan. *The numerical simulation of two phase flows in settling tanks*. PhD thesis, Imperial College of Science, Technology and Medicine (UK), 2001.

D. Bung and A. Schlenkhoff. Self-aerated skimming flow on embankment stepped spillways-the effect of additional micro-roughness on energy dissipation and oxygen transfer. In *IAHR European Congress, Edinburgh (United Kingdom)*, 2010.

D. B. Bung. Non-intrusive detection of air-water surface roughness in self-aerated chute flows. *Journal of Hydraulic Research*, 51(3):322–329, 2013.

M. E. Caisley, F. A. Bombardelli, and M. H. Garcia. Hydraulic model study of a canoe chute for low-head dams in Illinois (HES 63). Technical report, Illinois Department of Natural Resources, Office of Water Resources (IDNR WR009820 S98-284), 1999.

R. F. Carvalho. *Acções hidrodinámicas em estruturas hidráulicas: modelação computacional do ressalto hidráulico*. PhD thesis, Universidade de Coimbra (Portugal), 2002.

R. F. Carvalho and A. T. Amador. Physical and numerical investigation of the skimming flow over a stepped spillway. *Advances in Water Resources and Hydraulic Engineering*, pages 1767–1772, 2009.

R. F. Carvalho, C. M. Lemos, and C. M. Ramos. Numerical computation of the flow in hydraulic jump stilling basins. *Journal of Hydraulic Research*, 46(6): 739–752, 2008.

V. Casulli and E. Cattani. Stability, accuracy and efficiency of a semi-implicit method for three-dimensional shallow water flow. *Computers & Mathematics with Applications*, 27(4):99–112, 1994.

I. B. Celik, U. Ghia, P. J. Roache, C. J. Freitas, H. Coleman, and P. E. Raad. Procedure for estimation and reporting of uncertainty due to discretization in CFD applications. *Journal of Fluids Engineering*, 130(7):078001–078001, 2008.

Y. Chachereau and H. Chanson. Free-surface fluctuations and turbulence in hydraulic jumps. *Experimental Thermal and Fluid Science*, 35(6):896–909, 2011.

M. R. Chamani and N. Rajaratnam. Characteristics of skimming flow over stepped spillways. *Journal of Hydraulic Engineering*, 125(4):361–368, 1999.

H. Chanson. Drag reduction in open channel flow by aeration and suspended load. *Journal of Hydraulic Research*, 32(1):87–101, 1994.

H. Chanson. Prediction of the transition nappe/skimming flow on a stepped channel. *Journal of Hydraulic Research*, 34(3):421–429, 1996.

H. Chanson. Boundary shear stress measurements in undular flows: Application to standing wave bed forms. *Water Resources Research*, 36(10):3063–3076, 2000.

H. Chanson. Hydraulic design of stepped spillways and downstream energy dissipators. *Dam Engineering*, 11(4):205–242, 2001.

H. Chanson. The hydraulics of stepped chutes and spillways. *Canadian Journal of Civil Engineering*, 29(4):634–634, 2002.

H. Chanson. Bubbly flow structure in hydraulic jump. *European Journal of Mechanics-B/Fluids*, 26(3):367–384, 2007.

H. Chanson. Hydraulics of aerated flows: qui pro quo? *Journal of Hydraulic Research*, 51(3):223–243, 2013.

H. Chanson. Discussion of "Cavitation potential of flow on stepped spillways" by K. Warren Frizell, Floriana M. Renna, and Jorge Matos. *Journal of Hydraulic Engineering*, 141(5):07014025, 2014.

H. Chanson. Energy dissipation in hydraulic structures. In *IAHR Monograph, CRC Press, Taylor & Francis Group*, 2015.

H. Chanson and T. Brattberg. Experimental study of the air–water shear flow in a hydraulic jump. *International Journal of Multiphase Flow*, 26(4):583–607, 2000.

H. Chanson and R. Carvalho. Hydraulic jumps and stilling basins. *Energy Dissipation in Hydraulic Structures*, page 65, 2015.

H. Chanson and C. Gualtieri. Similitude and scale effects of air entrainment in hydraulic jumps. *Journal of Hydraulic Research*, 46(1):35–44, 2008.

H. Chanson and P. Lubin. Discussion of "Verification and validation of a computational fluid dynamics (CFD) model for air entrainment at spillway aerators" in the Canadian Journal of Civil Engineering 36 (5): 826-838. *Canadian Journal of Civil Engineering*, 37(1):135–138, 2010.

H. Chanson and J. S. Montes. Characteristics of undular hydraulic jumps: Experimental apparatus and flow patterns. *Journal of hydraulic engineering*, 121(2): 129–144, 1995.

H. Chanson, D. Bung, and J. Matos. *Stepped spillways and cascades*. CRC Press, Taylor & Francis Group, Leiden, Netherlands, 2015.

K. Chau, C. Wu, and Y. Li. Comparison of several flood forecasting models in Yangtze River. *Journal of Hydrologic Engineering*, 10(6):485–491, 2005.

M. H. Chaudhry. *Open-channel flow*. Springer Science & Business Media, 2007.

L. Chen and Y. Li. A numerical method for two-phase flows with an interface. *Environmental Modelling & Software*, 13(3):247 – 255, 1998.

Q. Chen, G. Dai, and H. Liu. Volume of fluid model for turbulence numerical simulation of stepped spillway overflow. *Journal of Hydraulic Engineering*, 128 (7):683–688, 2002.

W. Chen and K. Chau. Intelligent manipulation and calibration of parameters for hydrological models. *International journal of environment and pollution*, 28(3): 432–447, 2006.

C. Cheng, K. Chau, Y. Sun, and J. Lin. Long-term prediction of discharges in manwan reservoir using artificial neural network models. In *Advances in Neural Networks–ISNN 2005*, pages 1040–1045. Springer, 2005.

X.-j. Cheng, L. Luo, W. Zhao, and R. Li. Two-phase flow simulation of aeration on stepped spillway. *Progress in Natural Science*, 14(7):626–630, 2004a.

X.-j. Cheng, L. Luo, and W.-q. Zhao. Study of aeration in the water flow over stepped spillway. In *Proceedings of the World Water Congress*, 2004b.

C. Chinnarasri and S. Wongwises. Flow patterns and energy dissipation over various stepped chutes. *Journal of Irrigation and Drainage Engineering*, 132 (1):70–76, 2006.

V. T. Chow. *Open channel hydraulics*. McGraw-Hill Book Company, Inc; New York, 1959.

B. J. Daly. A technique for including surface tension effects in hydrodynamic calculations. *Journal of Computational Physics*, 4(1):97–117, 1969.

D. De Padova, M. Mossa, S. Sibilla, and E. Torti. 3D SPH modelling of hydraulic jump in a very large channel. *Journal of Hydraulic Research*, 51(2):158–173, 2013.

B. Dewals, S. Andre, A. Schleiss, and M. Pirotton. Validation of a quasi-2D model for aerated flows over stepped spillways for mild and steep slopes. In *Proceedings of the 6th International Conference of Hydroinformatics*, volume 1, pages 63–70, 2004.

H. T. Falvey. Air-water flow in hydraulic structures. *NASA STI Recon Technical Report*, 81:26429, 1980.

J. Farhoudi, S. Hosseini, and M. Sedghi-Asl. Application of neuro-fuzzy model to estimate the characteristics of local scour downstream of stilling basins. *Journal of Hydroinformatics*, 12(2):201–211, 2010.

C. Fawer. *Etude de quelques ecoulements permanents a filets courbes*. PhD thesis, École Polytechnique Fédérale de Lausanne (Switzerland), 1937.

S. Felder and H. Chanson. Energy dissipation, flow resistance and gas-liquid interfacial area in skimming flows on moderate-slope stepped spillways. *Environmental fluid mechanics*, 9(4):427–441, 2009.

S. Felder and H. Chanson. Air–water flow properties in step cavity down a stepped chute. *International Journal of Multiphase Flow*, 37(7):732–745, 2011.

S. Felder and H. Chanson. Aeration, flow instabilities, and residual energy on pooled stepped spillways of embankment dams. *Journal of Irrigation and Drainage Engineering*, 139(10):880–887, 2013.

J. H. Ferziger and M. Perić. Turbulent flows. In *Computational Methods for Fluid Dynamics*, pages 265–307. Springer, 2002.

FLOW-3D User Manual. *FLOW-3D User Manual*. Flow Science, 2016.

K. W. Frizell, F. M. Renna, and J. Matos. Cavitation potential of flow on stepped spillways. *Journal of Hydraulic Engineering*, 139(6):630–636, 2012.

K. W. Frizell, F. M. Renna, and J. Matos. Closure to "Cavitation potential of flow on stepped spillways" by K. Warren Frizell, Floriana M. Renna, and Jorge Matos. *Journal of Hydraulic Engineering*, 141(8):07015009, 2015.

M. Giridhar, M. Madaka, A. Ramaraju, and E. Ramakrishna Goud. Analysis of pressures on Nagarjuna Sagar Spillway. *EC Agriculture*, 1:17–28, 2014.

J. F. Gomes. *Campo de pressões: Condições de incipiência à cavitação em vertedouros em degraus com declividade 1V:0.75H*. PhD thesis, Universidade Federal do Rio Grande do Sul, Porto Alegre (Brasil), 2006.

C. A. Gonzalez. *An experimental study of free-surface aeration on embankment stepped chutes*. PhD thesis, University of Queensland, Brisbane (Australia), 2005.

C. A. Gonzalez and H. Chanson. Interactions between cavity flow and main stream skimming flows: an experimental study. *Canadian Journal of Civil Engineering*, 31(1):33–44, 2004.

C. Gualtieri and H. Chanson. Experimental analysis of froude number effect on air entrainment in the hydraulic jump. *Environmental Fluid Mechanics*, 7(3): 217–238, 2007.

C. Gualtieri and H. Chanson. Effect of froude number on bubble clustering in a hydraulic jump. *Journal of Hydraulic Research*, 48(4):504–508, 2010.

W. Hager and R. Sinniger. Flow characteristics of the hydraulic jump in a stilling basin with an abrupt bottom rise. *Journal of Hydraulic Research*, 23(2):101–113, 1985.

W. H. Hager. *Energy dissipators and hydraulic jump*. Springer, 1992.

W. H. Hager and R. Bremen. Classical hydraulic jump: sequent depths. *Journal of Hydraulic Research*, 27(5):565–583, 1989.

F. H. Harlow and J. E. Welch. Numerical calculation of time-dependent viscous incompressible flow of fluid with free surface. *Physics of fluids*, 8(12):2182, 1965.

I. M. Hartanto, L. Beevers, I. Popescu, and N. G. Wright. Application of a coastal modelling code in fluvial environments. *Environmental Modelling & Software*, 26(12):1685 – 1695, 2011.

C. Hirsch. *Numerical computation of internal and external flows: the fundamentals of Computational Fluid Dynamics*. Butterworth-Heinemann, 2007.

C. W. Hirt and B. D. Nichols. Volume of fluid (VOF) method for the dynamics of free boundaries. *Journal of Computational Physics*, 39(1):201–225, 1981.

H. Huang and A. Prosperetti. Effect of grid orthogonality on the solution accuracy of the two-dimensional convection-diffusion equation. *Numerical Heat Transfer*, 26(1):1–20, 1994.

S. Hunt and K. Kadavy. Flow depth and energy coefficient relationships for stepped spillways. In *5th IAHR International Symposium on Hydraulic Structures, Queensland (Australia)*, pages 1–9, 2014.

S. L. Hunt and K. C. Kadavy. Inception point relationship for flat-sloped stepped spillways. *Journal of Hydraulic Engineering*, 137(2):262–266, 2010.

S. M. Husain, J. R. Muhammed, H. U. Karunarathna, and D. E. Reeve. Investigation of pressure variations over stepped spillways using Smooth Particle Hydrodynamics. *Advances in Water Resources*, 66(0):52–69, 2014.

J. M. Hyman. Numerical methods for tracking interfaces. *Physica D: Nonlinear Phenomena*, 12(1):396–407, 1984.

R. I. Issa. Solution of the implicitly discretized fluid flow equations by operator-splitting. *Journal of Computational Physics*, 62:40–65, 1985.

D. Jang, R. Jetli, and S. Acharya. Comparison of the PISO, SIMPLER, and SIM-PLEC algorithms for the treatment of the pressure-velocity coupling in steady flow problems. *Numerical Heat Transfer, Part A: Applications*, 10(3):209–228, 1986.

H. Jasak. *Error analysis and estimation for the finite volume method with applications to fluid flows.* PhD thesis, Imperial College of Science, Technology and Medicine (UK), 1996.

R. Johnson and B. Launder. Discussion of "On the calculation of turbulent heat transport downstream from an abrupt pipe expansion". *Numerical Heat Transfer, Part A Applications*, 5(4):493–496, 1982.

C. Juez, J. Murillo, and P. Garcia-Navarro. Numerical assessment of bed-load discharge formulations for transient flow in 1D and 2D situations. *Journal of Hydroinformatics*, 15(4), 2013.

D. Keyes, A. Ecer, N. Satofuka, P. Fox, and J. Periaux. *Parallel Computational Fluid Dynamics' 99: Towards Teraflops, Optimization and Novel Formulations.* Elsevier, 2000.

J.-J. Kim and J.-J. Baik. A numerical study of the effects of ambient wind direction on flow and dispersion in urban street canyons using the RNG k–ε turbulence model. *Atmospheric Environment*, 38(19):3039–3048, 2004.

S.-E. Kim and F. Boysan. Application of CFD to environmental flows. *Journal of Wind Engineering and Industrial Aerodynamics*, 81(1):145–158, 1999.

A. Lafon and H. Yee. On the numerical treatment of nonlinear source terms in reaction-convection equations. In *AIAA 30th Aerospace Sciences Meeting and Exhibit, Reno, Nevada (USA)*, 1992-01-06.

B. E. Launder and B. I. Sharma. Application of the energy-dissipation model of turbulence to the calculation of flow near a spinning disc. *Letters in Heat and Mass Transfer*, 1(2):131–138, 1974.

J. Leandro, D. B. Bung, and R. Carvalho. Measuring void fraction and velocity fields of a stepped spillway for skimming flow using non-intrusive methods. *Experiments in Fluids*, 55(5):1–17, 2014.

S. Liriano and R. Day. Prediction of scour depth at culvert outlets using neural networks. *Journal of Hydroinformatics*, 3:231–238, 2001.

M. Liu, N. Rajaratnam, and D. Z. Zhu. Turbulence structure of hydraulic jumps of low froude numbers. *Journal of Hydraulic Engineering*, 130(6):511–520, 2004.

X. Liu and M. H. Garcia. Three-dimensional numerical model with free water surface and mesh deformation for local sediment scour. *Journal of Waterway, Port, Coastal, and Ocean Engineering*, 134(4):203–217, 2008.

R. Lobosco, H. Schulz, and A. Simoes. *Analysis of Two Phase Flows on Stepped Spillways, Hydrodynamics - Optimizing Methods and Tools*. University of São Paulo (Brasil), 2011.

D. Long, N. Rajaratnam, P. M. Steffler, and P. R. Smy. Structure of flow in hydraulic jumps. *Journal of Hydraulic Research*, 29(2):207–218, 1991.

P. Lopes, J. Leandro, R. F. Carvalho, and D. B. Bung. Alternating skimming flow over a stepped spillway. *Environmental Fluid Mechanics*, pages 1–20, 2017.

F. Lopez and M. H. Garcia. Mean flow and turbulence structure of open-channel flow through non-emergent vegetation. *Journal of Hydraulic Engineering*, 127 (5):392–402, 2001.

J. Ma, A. A. Oberai, R. T. Lahey Jr, and D. A. Drew. Modeling air entrainment and transport in a hydraulic jump using two-fluid RANS and DES turbulence models. *Heat and Mass Transfer*, 47(8):911–919, 2011.

J. Matos. *Emulsionamento de ar e dissipação de energia do escoamento em descarregadores em degraus*. PhD thesis, Instituto Superior Técnico, Lisboa (Portugal), 1999.

J. Matos and I. Meireles. Hydraulics of stepped weirs and dam spillways: Engineering challenges, labyrinths of research. In *5th IAHR International Symposium on Hydraulic Structures, Queensland (Australia)*, pages 1–30, 2014.

J. Matos, K. H. Frizell, S. Andre, and K. W. Frizell. On the performance of velocity measurement techniques in air-water flows. In *Hydraulic Measurements and Experimental Methods Conference*, 2002.

P. McDonald. The computation of transonic flow through two-dimensional gas turbine cascades. *Paper 71-GT-89, American Society of Mechanical Engineers*, 1971.

I. Meireles. Emulsionamento de ar e dissipação de energia do escoamento em descarregadores em degraus. *Hydraulics of skimming flow and residual energy on stepped spillways) MSc thesis, IST, Lisbon, Portugal*, 2004.

I. Meireles. *Hydraulics of stepped chutes: Experimental-numerical-theoretical Study*. PhD thesis, Universidade de Aveiro (Portugal), 2011a.

I. Meireles and J. Matos. Skimming flow in the nonaerated region of stepped spillways over embankment dams. *Journal of Hydraulic Engineering*, 135(8): 685–689, 2009.

I. Meireles, F. Renna, J. Matos, and F. A. Bombardelli. Skimming, nonaerated flow on stepped spillways over roller compacted concrete dams. *Journal of Hydraulic Engineering*, 138(10):870–877, 2012.

I. C. Meireles, F. A. Bombardelli, and J. Matos. Air entrainment onset in skimming flows on steep stepped spillways: an analysis. *Journal of Hydraulic Research*, 52(3):375–385, 2014.

I. O. d. C. Meireles. *Hydraulics of stepped chutes: experimental-numerical-theoretical study*. PhD thesis, Universidade de Aveiro (Portugal), 2011b.

F. R. Menter. Zonal two equation $k - \omega$ turbulence models for aerodynamic flows. *AIAA paper*, 2906:1993, 1993.

J. A. Moody, J. D. Smith, and B. W. Ragan. Critical shear stress for erosion of cohesive soils subjected to temperatures typical of wildfires. *Journal of Geophysical Research: Earth Surface*, 110, 2005.

M. Mossa. On the oscillating characteristics of hydraulic jumps. *Journal of Hydraulic Research*, 37(4):541–558, 1999.

S. Munta and J. A. Otun. Study of the inception length of flow over stepped spillway models. *Nigerian Journal of Technology*, 33(2):176–183, 2014.

F. Murzyn and H. Chanson. Experimental assessment of scale effects affecting two-phase flow properties in hydraulic jumps. *Experiments in Fluids*, 45(3): 513–521, 2008.

F. Murzyn and H. Chanson. Experimental investigation of bubbly flow and turbulence in hydraulic jumps. *Environmental Fluid Mechanics*, 2(9):143–159, 2009a.

F. Murzyn and H. Chanson. *Two-phase gas-liquid flow properties in the hydraulic jump: Review and perspectives*. Nova Science Publishers, 2009b.

F. Murzyn, D. Mouaze, and J. Chaplin. Optical fibre probe measurements of bubbly flow in hydraulic jumps. *International Journal of Multiphase Flow*, 31 (1):141–154, 2005.

F. Murzyn, D. Mouaze, and J. Chaplin. Air-water interface dynamic and free surface features in hydraulic jumps. *Journal of Hydraulic Research*, 45(5):679–685, 2007.

N. Muttil and K.-w. Chau. Neural network and genetic programming for modelling coastal algal blooms. *International Journal of Environment and Pollution*, 28 (3):223–238, 2006.

R. Nagosa. Direct numerical simulation of vortex structures and turbulence scalar transfer across a free surface in a fully developed turbulence. *Phys. Fluids*, 11: 1581–1595, 1999.

W. F. Noh and P. Woodward. SLIC (Simple Line Interface Calculation). In *Proceedings of the Fifth International Conference on Numerical Methods in Fluid Dynamics, Twente (Holland)*, pages 330–340. Springer, 1976.

M. Oertel and D. B. Bung. Initial stage of two-dimensional dam-break waves: Laboratory versus VOF. *Journal of Hydraulic Research*, 50(1):89–97, 2012.

I. Ohtsu, Y. Yasuda, and M. Takahashi. Flow characteristics of skimming flows in stepped channels. *Journal of hydraulic Engineering*, 130(9):860–869, 2004.

D. Olivari and C. Benocci. *Introduction to Mechanics of Turbulence.* Von Karman Institute for Fluid Dynamics, 2010.

G. Oliveto, V. Comuniello, and T. Bulbule. Time-dependent local scour downstream of positive-step stilling basins. *Journal of Hydraulic Research*, 49(1): 105–112, 2011.

M. H. Omid, M. Omid, and M. E. Varaki. Modelling hydraulic jumps with Artificial Neural Networks. *Proceedings of the ICE-Water Management*, 158(2): 65–70, 2005.

OpenFOAM User Guide. *OpenFOAM: The Open Source CFD Toolbox User Guide.* The Free Software Foundation Inc., 2011.

S. Osher and J. A. Sethian. Fronts propagating with curvature-dependent speed: algorithms based on Hamilton-Jacobi formulations. *Journal of Computational Physics*, 79(1):12–49, 1988.

S. V. Patankar and D. B. Spalding. A calculation procedure for heat, mass and momentum transfer in three-dimensional parabolic flows. *J. of Heat and Mass Transfer*, 15(10):1787–1806, 1972.

A. J. Peterka. The effect of entrained air on cavitation pitting. In *Proceedings of Minnesota International Hydraulic Convention*, pages 507–518. ASCE, 1953.

A. J. Peterka. Hydraulic design of stilling basins and energy dissipators. Technical report, U.S. Bureau of Reclamation, 1984.

M. Pfister. Chute aerators: Steep deflectors and cavity subpressure. *Journal of Hydraulic Engineering*, 137(10):1208–1215, 2011.

M. Pfister and W. H. Hager. Self-entrainment of air on stepped spillways. *International Journal of Multiphase Flow*, 37(2):99–107, 2011.

S. B. Pope. *Turbulent flows.* Cambridge University Press, 2000.

A. Prosperetti and G. Tryggvason. *Computational methods for multiphase flow.* Cambridge University Press, 2009.

N. Rajaratnam. The hydraulic jump as a wall jet. In *Journal of the Hydraulics Division*, volume 91(HY5), pages 107–132, 1965.

F. Renna. *Caratterizzazione fenomenologica del moto di un fluido bifasico lungo scaricatori a gradini.* PhD thesis, Ph. D. thesis, Politecnico di Bari (Italy), 2004.

F. Resch and H. Leutheusser. Reynolds stress measurements in hydraulic jumps. *Journal of Hydraulic Research*, 10(4):409–430, 1972.

P. J. Roache. *Fundamentals of verification and validation*. Hermosa Publ., 2009.

M. A. Rodrigues, L. Padrela, V. Geraldes, J. Santos, H. A. Matos, and E. G. Azevedo. Theophylline polymorphs by atomization of supercritical antisolvent induced suspensions. *The Journal of Supercritical Fluids*, 58(2):303–312, 2011.

J. F. Rodriguez, F. A. Bombardelli, M. H. Garcia, K. M. Frothingham, B. L. Rhoads, and J. D. Abad. High-resolution numerical simulation of flow through a highly sinuous river reach. *Water Resources Management*, 18(3):177–199, 2004.

M. Romagnoli, M. Portapila, and H. Morvan. Simulacion computacional del resalto hidraulico. *Mecanica Computacional*, XXVIII:1661–1672, 2009.

H. Rouse, T. T. Siao, and S. Nagaratnam. Turbulence characteristics of the hydraulic jump. *Transactions of the American Society of Civil Engineers*, 124(1): 926–950, 1959.

K. Roushangar, S. Akhgar, F. Salmasi, and J. Shiri. Modeling energy dissipation over stepped spillways using machine learning approaches. *Journal of Hydrology*, 508:254–265, 2014.

H. Rusche. *Computational fluid dynamics of dispersed two-phase flows at high phase fractions*. PhD thesis, Imperial College of Science, Technology and Medicine (UK), 2002.

A. Saint-Venant. Theorie du mouvement non permanent des eaux, avec application aux crues des rivieres et a l'introduction de marees dans leurs lits. *Comptes rendus des seances de l'Academie des Sciences*, 1871.

M. Sanchez-Juny. *Comportamiento hidráulico de los aliviaderos escalonados en presas de hormigón compactado. Análisis del campo de presiones*. PhD thesis, Universitat Politècnica de Catalunya, 2001.

M. Sanchez-Juny, E. Blade, and J. Dolz. Analysis of pressures on a stepped spillway. *Journal of Hydraulic Research*, 46(3):410–414, 2008.

H. Schlichting and K. Gersten. *Boundary-Layer Theory*. Springer, 2000.

T.-H. Shih, W. W. Liou, A. Shabbir, Z. Yang, and J. Zhu. A new $k - \varepsilon$ eddy viscosity model for high Reynolds number turbulent flows. *Computers & Fluids*, 24(3):227–238, 1995.

P. R. Spalart. Strategies for turbulence modelling and simulations. *International Journal of Heat and Fluid Flow*, 21(3):252–263, 2000.

C. G. Speziale and S. Thangam. Analysis of an RNG based turbulence model for separated flows. *International Journal of Engineering Science*, 30(10):1379–1388, 1992.

B. P. Sweeney. *Converged stepped spillway models in OpenFOAM*. PhD thesis, Kansas State University (USA), 2014.

M. Tabbara, J. Chatila, and R. Awwad. Computational simulation of flow over stepped spillways. *Computers & structures*, 83(27):2215–2224, 2005.

M. Takahashi and I. Ohtsu. Aerated flow characteristics of skimming flow over stepped chutes. *Journal of Hydraulic Research*, 50(4):427–434, 2012.

R. Taormina, K.-w. Chau, and R. Sethi. Artificial Neural Network simulation of hourly groundwater levels in a coastal aquifer system of the Venice lagoon. *Engineering Applications of Artificial Intelligence*, 25(8):1670–1676, 2012.

E. S. Taylor. The skewed boundary layer. *Journal of Basic Engineering, Trans. ASME, Series D*, 81:297–304, 1959.

K. Teuber, T. Broecker, A. Bayon, G. Nutzmann, and R. Hinkelmann. CFD-modelling of free surface flows in closed conduits using the volume of fluid approach. *Progress in Computational Fluid Mechanics (in revision)*, 2017.

S. Thomas, W. Hankey, A. Faghri, and T. Swanson. One-dimensional analysis of the hydrodynamic and thermal characteristics of thin film flows including the hydraulic jump and rotation. *Journal of heat transfer*, 112(3):728–735, 1990.

G. E. Toge. *The significance of Froude number in vertical pipes: a CFD study*. PhD thesis, University of Stavanger (Norway), 2012.

J. P. Toro, F. A. Bombardelli, J. Paik, I. Meireles, and A. Amador. Characterization of turbulence statistics on the non-aerated skimming flow over stepped spillways: a numerical study. *Environmental Fluid Mechanics*, 16(6):1195–1221, 2016.

J. P. Toro, F. A. Bombardelli, and J. Paik. Detached eddy simulation of the nonaerated skimming flow over a stepped spillway. *Journal of Hydraulic Engineering*, 143(9):04017032, 2017.

E. Toth and L. Brandimarte. Prediction of local scour depth at bridge piers under clear-water and live-bed conditions: comparison of literature formulae and Artificial Neural Networks. *Journal of Hydroinformatics*, 13(4), 2011.

O. Ubbink. *Numerical prediction of two fluid systems with sharp interfaces*. PhD thesis, Imperial College of Science, Technology and Medicine (UK), 1997.

D. Valero and D. B. Bung. Hybrid investigation of air transport processes in moderately sloped stepped spillway flows. In *36th IAHR World Congress, The Hage (Holland)*, volume 28, 2015.

D. Valero and R. Garcia-Bartual. Calibration of an air entrainment model for CFD spillway applications. In *Advances in Hydroinformatics*, pages 571–582. Springer, 2016.

F. J. Valles-Moran, I. Escuder-Bueno, I. Andres-Domenech, and C. Benavent-Gascon. Modelos hidráulicos para la evaluación de estructuras fluviales de protección: Cola del embalse de arenós (castellón). *Risk Analysis, Dam Safety, Dam Security and Critical Infrastructure Management*, page 165, 2011.

F. J. Valles-Moran, B. Nacher-Rodriguez, A. Bayon, J. F. Macian-Perez, J. B. M. Segura, and P. A. L. Jimenez. Generacion de resaltos hidraulicos de alto numero de froude a partir de regimenes rapidos emulsionados. una investigacion experimental. In *IV Jornadas de Ingenieria del Agua, Cordoba (Spain)*, pages 18–29, 2015a.

F. J. Valles-Moran, D. Valero, and J. Marco. La aireación forzada del flujo en la rápida como herramienta para la adaptación de los cuencos amortiguadores a mayores caudales de diseño. In *X Jornadas Españolas de Presas, Sevilla (Spain)*, 2015b.

B. Van Leer. Towards the ultimate conservative difference scheme III. upstream-centered finite-difference schemes for ideal compressible flow. *Journal of Computational Physics*, 23(3):263–275, 1977.

B. Van Leer. Flux-vector splitting for the euler equations. In *Eighth international conference on numerical methods in fluid dynamics, Aachen (Germany)*, pages 507–512. Springer, 1982.

T. Von Karman. Mechanische ahnlichkeit und turbulenz. In *Nachrichten von der Gesellschaft der Wissenschaften zu Göttingen, Fachgruppe 1 (Mathematik)*, volume 5, pages 58–76, 1930.

H. Wang and H. Chanson. Experimental study of turbulent fluctuations in hydraulic jumps. *Journal of Hydraulic Engineering*, 141(7):04015010, 2015a.

H. Wang and H. Chanson. Integral turbulent length and time scales in hydraulic jumps: an experimental investigation at large reynolds numbers. In *36th IAHR World Congress, The Hage (Holland)*, pages 1–13. IAHR, 2015b.

H. Wang, S. Felder, and H. Chanson. An experimental study of turbulent two-phase flow in hydraulic jumps and application of a triple decomposition technique. *Experiments in Fluids*, 55(7):1–18, 2014a.

H. Wang, F. Murzyn, and H. Chanson. Total pressure fluctuations and two-phase flow turbulence in hydraulic jumps. *Experiments in Fluids*, 55(11):1–16, 2014b.

J. Warnock. Experiences of the Bureau of Reclamation. *Proc. Amer. Soc. Civil Eng.*, 71(7):1041–1056, 1945.

H. Weller, G. Tabor, H. Jasak, and C. Fureby. A tensorial approach to computational continuum mechanics using object-oriented techniques. *Computers in Physics*, 12:620–631, 1998.

D. C. Wilcox et al. *Turbulence modeling for CFD*, volume 2. DCW industries La Canada, CA, 1998.

A. Witt, J. Gulliver, and L. Shen. Bubble visualization in a simulated hydraulic jump. Technical report, Cornell University Library (USA), 2013.

A. Witt, J. Gulliver, and L. Shen. Simulating air entrainment and vortex dynamics in a hydraulic jump. *International Journal of Multiphase Flow*, 72(0):165–180, 2015.

I. Wood. Air water flows. In *21st IAHR World Congress, Erfurt (Germany)*, pages 18–29, 1985.

I. R. Wood. *Air entrainment in free-surface flows, IAHR Hydraulic Design Manual No.4, Hydraulic Design Considerations*. Balkema Publications, Rotterdam, The Netherlands, 1991.

C. Wu, K. Chau, and Y. Li. Predicting monthly streamflow using data-driven models coupled with data-preprocessing techniques. *Water Resources Research*, 45(8):1–23, 2009.

J.-h. Wu, B. Zhang, and M. A. Fei. Inception point of air entrainment over stepped spillways. *Journal of Hydrodynamics*, 25(1):91–96, 2013.

S. Wu and N. Rajaratnam. Transition from hydraulic jump to open channel flow. *Journal of Hydraulic Engineering*, 122(9):526–528, 1996.

V. Yakhot, S. Orszag, S. Thangam, T. Gatski, and C. Speziale. Development of turbulence models for shear flows by a double expansion technique. *Physics of Fluids A: Fluid Dynamics (1989-1993)*, 4(7):1510–1520, 1992.

C. S. Yih. Stratified flows. *Academic, New York*, 1980.

D. F. Young, B. R. Munson, T. H. Okiishi, and W. W. Huebsch. *A brief introduction to fluid mechanics*. John Wiley & Sons, 2010.

D. L. Youngs. An interface tracking method for a 3D Eulerian hydrodynamics code. *Technical Rep*, 44(92):35–35, 1984.

G. Zhang and H. Chanson. Hydraulics of the developing flow region of stepped spillways. I: Physical modeling and boundary layer development. *Journal of Hydraulic Engineering*, page 04016015, 2016a.

G. Zhang and H. Chanson. Hydraulics of the developing flow region of stepped spillways. II: Pressure and velocity fields. *Journal of Hydraulic Engineering*, page 04016016, 2016b.

G. Zhang and H. Chanson. Gabion stepped spillway: interactions between free-surface, cavity, and seepage flows. *Journal of Hydraulic Engineering*, 142(5): 06016002, 2016c.

G. Zhang, H. Wang, and H. Chanson. Turbulence and aeration in hydraulic jumps: free-surface fluctuation and integral turbulent scale measurements. *Environmental Fluid Mechanics*, 13(2):189–204, 2013.

W. Zhang, M. Liu, D. Z. Zhu, and N. Rajaratnam. Mean and turbulent bubble velocities in free hydraulic jumps for small to intermediate Froude numbers. *Journal of Hydraulic Engineering*, 140(11):04014055, 2014.